Hydrogen Production via Plasma Reformers

by

Christopher J. O'Brien

A.B. in Chemistry
Princeton University, 1994

Submitted to the Department of Mechanical Engineering
in Partial Fulfillment of the Requirements for the Degree of
Master of Science

at the
Massachusetts Institute of Technology
February 1996

Signature of Author _____
Department of Mechanical Engineering
February 7, 1996

Certified by _____
Simone Hochgreb
Assistant Professor of Mechanical Engineering
Thesis Supervisor

Accepted by _____
Ain A. Sonin
Chairman, Department Committee on Graduate Students

Hydrogen Production via Plasma Reformers

by

Christopher J. O'Brien

Submitted to the Department of Mechanical Engineering
on February 8, 1996 in Partial Fulfillment of the
Requirements for the Degree of Master of Science

ABSTRACT

The potential for efficient production of hydrogen-rich gas from hydrocarbon fuels using thermal plasmas has been investigated both analytically and experimentally. Thermodynamic analysis shows that the most efficient production of hydrogen from hydrocarbons can be achieved by partial oxidation (lambda = 0.25); at optimal conditions, the availability of the output fuel mixture is 83 percent of the input availability. Chemical kinetic analyses of the partial oxidation of methane in plasma reactors, using both plug flow reactor and perfectly stirred reactor models, indicates that for residence times of less than 500 milliseconds, the minimum achievable energy input per amount of hydrogen produced ranges from 40 to 50 MJ per kg hydrogen. This corresponds to a thermodynamic efficiency of approximately 75 percent.

An experimental plasma reformer has been constructed and initial tests have been performed using methane as the fuel molecule. The plasmatron has demonstrated startup and response times on the order of hundreds of milliseconds or less and gas heating efficiencies of over 80 percent. Observed hydrogen output is approximately 50 percent of the predicted values; this is presumed to be due to heat losses in the reactor and will be addressed in future reformer designs. The system shows promise for use as a load-following, inline fuel reformer for fuel cells and other power systems.

Thesis Supervisor: Simone Hochgreb
Title: Assistant Professor of Mechanical Engineering

ACKNOWLEDGMENTS

As with any such project, there are countless people (at least, more than I personally can count!) who have been instrumental in making the work presented in this thesis possible. I mention only a few of them here.

Simone Hochgreb has been an inspiration, both as advisor and friend, in my time at MIT. It is hard to overestimate her contribution to my development as an engineer; her guidance and accessibility have made my transition between fields a much easier one. I look forward to working with her in the next few years, and to developing the ideal technique for manufacturing "wow".

Without Leslie Bromberg, Alex Rabinovich, and Dan Cohn at the Plasma Fusion Center, this project would not yet exist. Thanks is due especially to Alex for the plasmatron designs; the "trust me, I know this works" approach is so much more efficient than endless calculations!

If not for Darren and Bill in the PFC machine shop, I would probably still be struggling with a drill press. Their work made it possible to build up a functional laboratory in only a few months, despite the fact that we could break parts as fast as they could make them.

All of us involved in the project thank Neil Rossmeissl and the Department of Energy for funding this work.

My fellow students at the Sloan Automotive Lab have made important contributions to my sanity during the production of this thesis. A few particular thanks: the example of determination and perseverance set by Patia McGrath was something I tried to live up to in the past few months; I have been glad to share an office with her. Brad VanDerWege was always available to listen to my complaints (are you finished yet?). Mike, Leslie and Rachel Norris were very welcoming during my first few months at the lab; they helped to make MIT seem less forbidding.

To my family (Dad, Mom, Katie, Corey, Baron): as usual, your constant support has made all of this easier. Thanks also for giving up most of your time with me during the holidays to this thesis, and for allowing me to continue pursuing a career that won't involve buying a suit!

Most importantly, I need to thank Kristine Jackson for her patience, love and occasional firm reminders that other things can be much more important than work. Without her influence, I doubt that I would be writing this today.

TABLE OF CONTENTS

TABLE OF FIGURES

CHAPTER 1

Introduction

1.1 INTRODUCTION AND MOTIVATION

It is an undisputed fact that the current world energy economy is not a sustainable one. In future energy and power systems, we must meet the goals of decreased use of fossil fuels, higher overall efficiencies and lower chemical emissions levels. This will necessitate not only the advancement and reexamination of existing technologies such as combustion engines and gas turbines, but also the development of newer devices such as fuel cells, ultracapacitors and advanced batteries.

While it is now certain that changes like these will occur, the means by which the transition of such a large infrastructure to a new basis may be made remain an area where much work needs to be done. There are several important requirements for a transitional energy economy, based on the need to support existing power systems, fuels and distribution methods while simultaneously allowing the introduction of new ones. These requirements include fuel flexibility on the part of end-use power systems, fuel conversion and upgrading techniques both to facilitate changing fuel supplies and to reduce distribution costs, and intermediate solutions to the fuel economy and emissions problems of current technologies.

One element of such a transitional infrastructure is the electrification of power systems, which is already underway. Electricity can be produced from a wide variety of fuels at large centralized plants, allowing emissions to be localized and reducing the range of impact of fuel system changes to a small number of plants as opposed to a much larger number of end-use devices. Another idea is the development of a fuel infrastructure based on light fuels such as hydrogen-rich gas, which can be produced either at fuel processing plants or in power systems with integrated fuel reformers and are usable in a wide variety of systems, including fuel cells (compatible with a future electricity-based infrastructure), combustion engines and gas turbines.

This project focuses on one small part of such a transitional system: the reforming of hydrocarbon fuels to hydrogen-rich gas mixtures. Fuel reforming has been studied and practiced in the gas industry for decades; both catalytic and high temperature non-catalytic systems have been employed. However, the current state of technology in this area has many limitations. Most reformers are very large and require long residence times and high pressures for effective operation; catalytic systems have the additional limitation of very poor fuel flexibility. In this work, a novel reforming method based on the use of thermal plasmas is advanced to address these shortcomings. Thermal plasmas, an energetic state of matter

characterized by high degrees of ionization and temperatures of several thousand kelvin, can be generated efficiently through rotated electric arcs; this method is used in the plasmatrons that form the basis of the experimental system presented here. Extremely high temperatures of 2000 to 4000 kelvin are easily accessible with high gas heating efficiencies and a high degree of controllability. The use of such high temperatures allows the acceleration of reforming reactions without the use of a catalyst; this provides a method of decreasing residence times and reactor sizes while retaining the high degree of fuel flexibility associated with thermal methods. Since the plasma is generated by the coupling of electrical energy to gas enthalpy, reformers based on plasmatrons would be entirely consistent with electrical power systems.

A small, fast, and efficient fuel reformer could be employed as an accessory to a fuel cell or other such device in order to alter the efficiency, emissions and fuel flexibility characteristics of the overall power system. Such an addition could serve either to adapt existing technologies to different fuels and emissions requirements or to make newer power systems, which may have intrinsic fuel restrictions, feasible within the existing fuel infrastructure.

1.2 Structure of the Thesis

This thesis presents the initial stages of a study designed to explore the possibilities for plasma reformers, focusing on the production of hydrogen or hydrogen-rich gases from hydrocarbon fuels. The results achieved to date are preliminary, but very promising for future applications of this technology.

The structure of the thesis is as follows: Chapter 2 presents a brief summary of methods of hydrogen production from hydrocarbons, along with a discussion of some of the features of past and present reforming techniques. Chapters 3 and 4 present the results of thermodynamic and chemical kinetic modeling, respectively, considering both the characteristics of the chemical processes themselves and also some of the specific issues presented by the use of plasmatrons in reforming systems. In Chapter 5, the experimental apparatus that has been constructed for the design and study of various plasma reformers is described; in Chapter 6, the initial laboratory results are analyzed. Chapter 7 includes conclusions from the work to date and indications of future directions for this research.

CHAPTER 2

Background and Previous Work

2.1 INTRODUCTION

A considerable amount of work has been done on the production of hydrogen and other fuel gases from hydrocarbon fuels in the gas engineering industry. Unfortunately, relatively few publications in the open literature have resulted from these past efforts. Nevertheless, a brief consideration of the common methods of hydrogen production and the current state of research can provide a basis and motivation for the discussions to follow. This chapter will provide a brief discussion of the range of methods available for hydrogen production, as well as a more detailed background for the processes that will be the focus of the work presented herein.

2.2 HYDROGEN PRODUCTION TECHNIQUES

The methods for hydrogen production from hydrocarbon fuels in the gas industry fall into three major classifications: thermal decomposition, steam reforming and partial oxidation.[i] Most hydrogen and synthesis gas (a mixture of mostly H_2 and CO) production units currently in operation can be described by one or a combination of these three processes. Overviews of commercial applications are available in the literature; a brief discussion of the major features of the three routes will be given here.[1,2]

2.2.1 Thermal Decomposition

Thermal decomposition, also termed cracking or pyrolysis, is the breakdown of hydrocarbon molecules by extreme heating; the major reactions involved are of the type

$$C_nH_{2n+2} \rightleftharpoons nC + (n+1)H_2$$

These reactions are highly endothermic; the required energy inputs to initiate such reactions are determined by the energy required to break an aliphatic C-H bond, approximately 104 kcal/mol (which corresponds to a temperature of 52000 K). This results in extremely long reaction timescales at normal process temperatures; typical timescales for thermal decomposition of butane range from tens to hundreds of seconds at 800 - 1000 K.[3] In order to overcome this

[i] The term *reforming* will be used to refer to partial oxidation as well as steam reforming in the following chapters.

limitation, the process has in a few instances been carried out in plasma reactors, which can achieve temperatures thousands of kelvin higher than traditional fired reactors.[4,5] Another method for accelerating thermal decomposition is to add water or oxygen to the feed gas (oxidative pyrolysis), which allows a small amount of steam reforming or partial oxidation and increases the rate of the overall process, through increased temperatures and radical concentrations.[6] While thermal decomposition has the advantage of relative simplicity and is adaptable to a wide range of input fuels, it requires very high energy densities and is likely to produce soot and other heavy hydrocarbon byproducts which, although they are often valuable in themselves, create problems of separation in integrated power systems.

2.2.2 Steam Reforming

Steam reforming of hydrocarbons is a very common process in industry. Many reactions are involved due to the presence of oxygen in the system, but the overall chemical transformations can be described in general by

$$C_nH_{2n+2} + nH_2O \rightleftharpoons nCO + (2n+1)H_2$$
$$C_nH_{2n+2} + 2nH_2O \rightleftharpoons nCO_2 + (3n+1)H_2$$

These reactions are also highly endothermic, so steam reforming is usually performed with the aid of a catalyst and at high temperatures. The introduction of the catalyst creates problems of cost, catalyst poisoning (for example, by sulfur in the feedstock), and heat transfer to the catalyst material.[2] Catalysts are also in general very fuel-specific, thus limiting the applicability of reformers based on catalyzed reactions. Despite these difficulties, steam reforming has the advantages of inexpensive feed components and the potential for high hydrogen yields (hydrogen is extracted not only from the input fuel, but from the water as well).

2.2.3 Partial Oxidation

Partial oxidation is of a very different character than the former two processes. It consists of the reaction of a hydrocarbon fuel with a small amount of oxygen, leading to H_2 and CO as the major products:

$$C_nH_{2n+2} + {}^n/_2O_2 \rightleftharpoons nCO + (n+1)H_2$$

It is the only exothermic reaction of the group; thus, it may in principle be used to generate useful work. Also, unlike the endothermic processes described above, the energy input required to drive this reaction does not increase proportionally to the throughput; in fact, the reaction may be self-sustaining under certain circumstances. As with the previous two methods, it requires high operating temperatures, but the reaction timescales are considerably smaller. A disadvantage to partial oxidation is the need for oxygen as a feed component; this adds to the cost of the process, either through the cost of supplying pure oxygen or through

diluting the mixture with nitrogen from air, thus requiring greater heat input to attain a given reactor temperature. Partial oxidation is carried out both in catalytic and high-temperature non-catalytic systems.

Partial oxidation is the method considered in this work; this is due to its advantages of extremely high efficiencies (availability out/availability in up to 97 percent), low levels of soot and heavy hydrocarbon byproducts, and short timescales relative to the other methods.[1] The following sections will present some of the work done to date on this specific method of hydrogen production from hydrocarbons, both in catalytic and non-catalytic systems.

2.3 Non-catalytic Partial Oxidation Methods

Very few experimental studies of non-catalytic partial oxidation of hydrocarbons are available in the open literature; due to rapid advances in catalyst technology, most of the work has focused on catalytic systems. A small amount of experimental data from industrial plants is available.[7] As early as 1956, the main features of the process had been identified.[8] The reaction mechanism is generally supposed to consist of two stages – an initial combustion of part of the input fuel followed by conversion of the resulting mixture towards the equilibrium composition, which contains mainly H_2 and CO. The second part of the reaction is relatively slow, which necessitates careful attention to the process parameters in order to achieve equilibrium. Eastman identified some of the important considerations for reaching equilibrium compositions: an increase in pressure accelerates the reaction, but has an adverse effect on the equilibrium levels of H_2 (see Chapter 3). This effect has been overcome in commercial reactors by increasing the oxygen to fuel ratio, which allows more initial oxidation and hence raises the mixture temperature, both increasing the equilibrium H_2 levels and further accelerating the reaction. Due to the long residence times and large reactor volumes in commercial systems, control of heat losses is another important factor; this is in general accomplished by refractory ceramic reactor linings. Over 80 percent conversion of input fuel hydrogen to molecular hydrogen has been achieved through these methods.[8]

A recent numerical study of uncatalyzed partial oxidation was performed by Karim and Zhou, for feed temperatures less than 2000 K and fuel-to-air equivalence ratios of $\phi \leq 3.5$.[9] In this work, a 108-reaction, 28-species chemical mechanism for partial oxidation was developed, which predicted similar behavior to that postulated above. The possible benefit of recirculating product gases to increase initial mixture temperatures and radical concentrations was also examined; it was found that up to a threefold decrease in reaction timescale could be achieved by 15 percent feedback.

An important feature of the uncatalyzed partial oxidation reaction noted in both experimental and numerical studies is that the mixture temperature (for an approximately adiabatic system) peaks near the beginning of the reaction and then decreases to its equilibrium value. This effect is an important consideration for highly temperature-sensitive processes such as NO_x formation.

2.4 Catalytic Partial Oxidation Methods

Catalytic partial oxidation has been the focus of much work lately, in large part due to its potential use in the upgrading of natural gas (i.e. conversion of methane to higher hydrocarbons and oxygenates). A recent review of this work emphasizes the importance of the gas phase reactions (that is, those that do not involve the catalytic surface) to the overall process.[10] This suggests that the mechanism of catalyzed partial oxidation may be quite similar to the non-catalytic process, with the catalytic surface acting mainly as a source of radicals. Naturally, such results vary with different catalyst materials; mechanisms similar to the above have been proposed for catalytic partial oxidation, as well as more complicated ones.[11,12]

A brief description of some characteristic features of catalytic partial oxidation will provide a useful basis for comparison for the results presented in following chapters. For the partial oxidation of methane over rare earth oxide catalysts (a commonly used type), timescales of 15 to 20 seconds for complete methane conversion are observed at reacting temperatures of 800 to 900 K.[13] Output H_2/CO_x ratios are as high as 1.3, with the remaining hydrogen generally appearing in formaldehyde, ethane and water.[13,14] Reported experimental catalyst preheat times are on the order of one hour for operating temperatures of 900 K.

Both the catalytic and thermal partial oxidation methods discussed are characterized by relatively long residence times and slow response to changes in flow rates, limiting their usefulness as integrated parts of power systems. The following numerical and experimental investigations demonstrate the potential of plasma reactors to overcome these limitations, making fuel reforming a much more broadly applicable process.

2.5 REFERENCES

[1] D. Vorum, "Fuel and Synthesis Gases from Gaseous and Light Liquid Hydrocarbons," in C.G. Segeler, ed., Gas Engineer's Handbook (New York, Industrial Press, 1965) Ch. 6.

[2] K.E. Cox and K.D. Williamson, Hydrogen: Its Technology and Implications, Vol. I, "Production Technology" (C.R.C. Press, 1977).

[3] W.L. Nelson, Petroleum Refinery Engineering, 3rd. Eed. (New York: McGraw-Hill, 1940) p. 593.

[4] G.Kaske, L. Kerke, R. Muller, *Hydrogen Energy Progress* **6** p. 1 (1986).

[5] H.-G. Beiers, H. Baumann, D. Bittner, J. Klein, H. Jüntgen, *Fuel* **67** p. 1012 (1988).

[6] V.R. Choudhary, S.T. Choudhary, A.M.Rajput, *AIChE Journal* **37**(6) p. 915 (1991).

[7] R. Mungen and M.B. Kratzer, *Industrial and Engineering Chemistry* **43**(12) p. 2782 (1951).

[8] D. Eastman, *Industrial and Engineering Chemistry* **48**(7) p. 1118 (1956).

[9] G.A. Karim and G. Zhou, *Journal of Energy Resources Technology* **115** p. 307 (1993).

[10] J.C. Mackie, *Catal. Rev. –Sci. Eng.*, **33**(1,2) p. 169 (1991).

[11] P.D.F. Vernon, M.L.H. Green, A.K. Cheetham, A.T. Ashcroft, *Catalysis Letters* **6** p. 181 (1990).

[12] J.A. Lapszewicz, X.-Z. Jiang, *Symposium on Natural Gas Upgrading II, Div. Pet. Chem., ACS*, San Fransisco, p. 252 (1992).

[13] M.M. Koranne, J.G. Goodwin, G. Marcelin, *The Journal of Physical Chemistry* **97** p. 673 (1993).

[14] Y. Matsumura, J.B. Moffat, *Journal of Catalysis* **148** p. 323 (1994).

CHAPTER 3

Thermodynamic Analysis

3.1 INTRODUCTION

A major goal of this project is to produce hydrogen from hydrocarbon fuels. This process involves the transformation of one type of fuel molecule to others; it is of critical importance to retain as much of the fuel energy as possible. In order to design a system that will make the most efficient use of the input fuel energy, it is necessary first to consider the basic thermodynamics of the reforming process, which determine the possible final distributions of the initial energy.

During this analysis, one should keep in mind both the benefits and the limitations of thermodynamic models. Thermodynamics can tell us the *limiting* behavior of the system, such as the maximum useful work that can be extracted from input and output fuels, the bounds on heat release during the reforming process, and the chemical composition of the output gas given infinite time. None of these are values that we are actually likely to see in a real reformer, in which residence times are finite, kinetic effects may outweigh equilibrium effects, and the useful work extracted from the reformed fuel may be significantly lower than the maximum theoretically possible amount. However, thermodynamics allows us to find these limits of system behavior through relatively simple analysis, hence giving us the ability to examine a large parameter space like the one in question here, where the variables include chemical compositions, temperatures, pressures, residence times, process details such as mixing, heating and expansion, and many others, and to find the most productive area or areas on which to focus a more detailed study.

3.2 FUEL REFORMING AS PART OF THE ENERGY CYCLE

As a background for the following analysis, it is important to consider how fuel reforming fits into the overall process of converting energy into useful work. The complete pathway proceeds from the delivery of energy by sunlight to the outputs of heat and work; the portion of this pathway that we need to consider, as shown in Figure 3.1, starts with the energy contained in fuel molecules, and proceeds to the ultimate generation of useful work from that energy. Byproducts released along the way include heat and chemical emissions (which may be desired product molecules or pollutants).

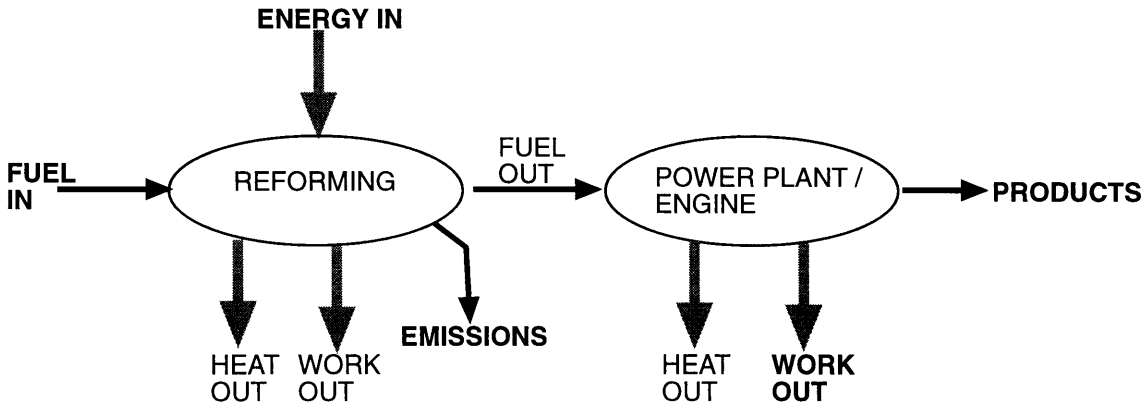

Figure 3.1. Detailed energy consumption pathway with fuel reforming.

From this diagram, we can easily see some of the main issues that will concern us in the analysis to follow. Clearly, an important consideration is the ratio of the chemical and thermal energy contained in the output fuel to the energy in the input fuel. This ratio is essentially the minimum efficiency of the process, presuming that no work done by the system during reforming is captured as useful output work. In general, some parts of the heat release and work generated during reforming are recoverable, i.e. they can still be converted to useful work either within or at the output of the energy pathway shown in Figure 3.1. The amount of recoverable energy determines the maximum efficiency; however, this maximum value is highly process dependent and hence will be affected strongly by small variations in system parameters. The analysis in this section will focus on the energy efficiency under the assumption of no heat or work recovery, which represents a true thermodynamic limit to system performance, and is largely independent of the particular physical characteristics of a given reformer.

An additional issue that we can begin to understand using thermodynamics is the chemical composition of the output gas mixture. Although thermodynamic methods can only predict the *equilibrium* composition of a mixture, it will be shown in Chapter 4 that in many situations the output gas from the reformer will be very near to the equilibrium state. Hence, we can get a rough estimate of how the process parameters affect the output composition without a detailed kinetic analysis, which will be very helpful in focusing on a particular region of the initial parameter space. The thermodynamic efficiency and output composition are closely linked, so the efficiency calculation will necessarily involve constraints related to the desired chemical composition of the reformed gas.

3.3 AVAILABLE ENERGY AND REFORMING EFFICIENCY

In order to determine the energy efficiency of the reforming process, a more precise definition of "energy" is needed. We need to keep track not only of the chemical energy of the fuels, but of the energies involved in heating, expansion, performing work, and mixing, as well.

We also need to determine what part of these energies can be converted into useful work output, and what part is lost during the reforming process.

Thermodynamic analysis concentrates on the energy interactions between a system and its environment. Careful choice of the arbitrary division between system and environment can greatly simplify the analysis. In this case, a useful choice of system is the reacting mixture; that is, the chemical system that initially consists of separated fuel and air, which are mixed and react to form products during the reforming process. Thus, no matter ever crosses the border between system and environment, so all interactions between the two must consist of exchanges of heat and work. The environment is everything that is not included in the system; in this case, the environment can be modeled as a reservoir with a constant temperature T_R and constant pressure p_R that can also exchange volume with the system at no cost. Hence, the environment can receive heat from the system and the system can do work on the environment without changing T_R, and the system may expand against the constant pressure p_R by exchanging volume with the environment. In all cases below, T_R = 298 kelvin and p_R = 1 atmosphere.

A more precise statement of the question we want to answer is: starting from the initial resources of fuel and air, what is the maximum amount of useful work that can be output from the system per unit amount of fuel input, allowing arbitrary heat or work interactions with the environment? The combination of the first and second laws of thermodynamics shows that the maximum amount of work that can be extracted is obtained when all processes are *reversible* (i.e. there are no permanent effects of energy or entropy transfer to the environment) and the final products are in mechanical, thermal and chemical equilibrium with the surroundings. This maximum work is termed the *availability*, Φ. It depends only on the initial and final states and the constraints imposed on the system (e.g. whether progress toward mechanical, thermal or chemical equilibrium is allowed, so that pressure, temperature and chemical potentials are equalized, or whether there are specific constraints on volume, energy or chemical species transfer). The particular constraints that we will consider here are the following: the system is allowed in principle to reach pressure and thermal equilibrium with the environment (i.e. the system reaches T_R and p_R), and the chemical species within the system are allowed to evolve to chemical equilibrium at the final pressure and temperature conditions. In this case, we can

define an *availability function* ψ such that the availability between two states is given by the difference between the values of the availability function evaluated at the states:

$$\Phi_{if} = \psi_i - \psi_f$$

For the conditions described above, the availability function ψ of a system state (denoted by s) is:

$$\psi_s = \sum_j n_j \psi_j = \sum_j n_j (H_j - T_R S_j)$$

in which n_j is the number of moles of species *j*, H_j the molar enthalpy of the species and S_j the molar entropy of the species.

Both H_j and S_j vary with temperature. To take these changes into account, each can be split into two parts; the first is an arbitrary reference value at a particular temperature, H° or S°, and the second gives the difference between the value of H_j or S_j at the specified temperature and the reference. In the standard definitions, the reference values are chosen so that H° is the enthalpy difference between the species and its component elements in their standard states (i.e. their most stable forms at 298 K), denoted $\Delta H°_f$, and S° is such that S_j is zero for all species at zero kelvin:

$$H_j = (H^0 + H(T))_j = (\Delta H_f^0 + H(T))_j$$

$$S_j = (S^0 + S(T))_j = S(T)_j$$

The values of $\Delta H°_f$, H(T) and S(T) for a given species can be found in tables or calculated via polynomial approximations. The values of H_j and S_j at 298 kelvin are listed for species of interest in the reforming process in Table 3.1.

Molecule	$\Delta H°_f$ (kJ/mol)	S(298 K) (kJ/mol.K)	ψ_j(298 K) (kJ/mol)
CH_4	-74.83	0.186	-130.7
O_2	0	0.205	-61.51
H_2	0	0.131	-39.18
CO	-110.5	0.198	-169.9
CO_2	-393.5	0.214	-457.7
H_2O	-383.51	0.189	-298.4

Table 3.1. Thermodynamic properties of selected molecules at standard states

The maximum availability for the initial state of the reforming system (unmixed fuel and air at 298 K and 1 atm, indicated by the subscript i) will be attained when the final state corresponds to thermal and pressure equilibrium with the environment (i.e. T = 298 K and p =

1 atmosphere), and chemical equilibrium within the system itself. At this equilibrium state, denoted by the subscript 0, the availability function ψ_0 of the system is minimized, given the constraints imposed by T_R, p_R, and the mixture composition. (If $T > T_R$ or $p > p_R$, the system can still do work, so Φ will not be minimized.) Hence, a final state at ψ_0 will give the maximum availability for any initial state of the specified system.

We can now quantify the energies involved in the energy consumption pathway of Figure 2. The energy of the input fuel corresponds to the availability of the transition between the initial (i) and equilibrium (0) states:

$$\Phi_{i0} = \psi_i - \psi_0 = \sum_{j_i} n_{j_i}(H_{j_i} - T_R S_{j_i}) - \sum_{j_0} n_{j_0}(H_{j_0} - T_R S_{j_0})$$

where the summation over j_i indicates summation over all chemical species in the initial state, and j_0 indicates the equilibrium state species. The energy contained in the output fuel is the availability between the reformed state, given the subscript r, and the equilibrium state:

$$\Phi_{r0} = \psi_r - \psi_0 = \sum_{j_r} n_{j_r}(H_{j_r} - T_R S_{j_r}) - \sum_{j_0} n_{j_0}(H_{j_0} - T_R S_{j_0})$$

Finally, the energy that could be recovered as work from the reforming itself is the availability of a process that takes the system from the initial state to the reformed state:

$$\Phi_{ir} = \psi_i - \psi_r = \sum_{j_i} n_{j_i}(H_{j_i} - T_R S_{j_i}) - \sum_{j_r} n_{j_r}(H_{j_r} - T_R S_{j_r})$$

In the current analysis, we assume that this energy is "lost" to the environment.

To completely define the efficiency of reforming, we must also consider energy inputs to and losses from the system. Energy input during the reforming process (such as the electrical work input by a plasmatron, W_{in}) can be added to the initial availability; that is, the total energy input to the reformer is the sum of the availability of the fuel/air mixture and the energy added as electrical work during the process. Energy "losses" during the reforming correspond to irreversible heat or work transfer to the environment; thus, the availabilities described above correspond to a situation with minimized losses.

Using the above definitions, the thermodynamic efficiency ε of the reforming process is given by

$$\varepsilon = \frac{\Phi_{r0}}{\Phi_{i0} + W_{in}}$$

Hence, the problem of determining the efficiency of the system is reduced to determining the value of ψ for the initial, reformed, and equilibrium states (which requires the pressure, temperature and chemical composition of each state) and the minimum work or energy input required to move the system from the initial state to the reformed state.

The above energy relationships are shown diagrammatically in Figure 3.2. Several important points regarding the relationship between Φ_{i0} and Φ_{r0} may be noted here. The assumptions made above require that in the reformed state, the system contains the same atoms as it does in the initial state (i.e. no mass crosses the border between system and environment) and the pressure is unchanged. The chemical species distribution and temperature of the reformed state will in general be different from those of the initial state, and these will determine the availability function of the reformed mixture. Since there may be an energy input during reforming, it is possible that ψ_r will be greater than ψ_i.

The preceding analysis applies to any set of initial, reformed and equilibrium states of the system as defined above, with transitions occurring at constant pressure. The variables that remain are the chemical compositions and temperatures of the initial, reformed and equilibrium states, the input energy, and the constraints placed on the path that takes the system from the initial to the reformed state. In the following sections, the effects of changes of these variables on the efficiency and other system parameters are considered.

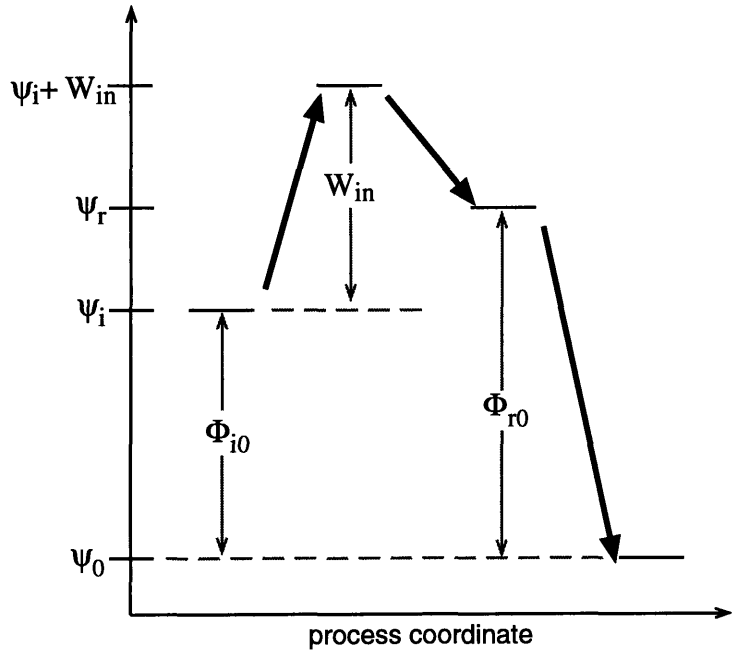

Figure 3.2. Availability relationships for the states of the reforming process

3.4 ANALYSIS OF THE INITIAL PARAMETER SPACE.

Despite the assumptions and restrictions made above, the parameter space left to investigate is still extremely large. However, a few additional assumptions can be made in order to allow a useful analysis of this space without much further loss of generality. By specifying that the input mixture consists of a (gaseous) hydrocarbon fuel in air, we limit the

chemical composition of the system. Since nitrogen and oxygen concentrations are proportional to each other, the chemical composition (scaled by the amount of carbon in the system) may be characterized by the hydrogen to carbon and oxygen to carbon ratios.

Some restrictions on the initial, reformed and equilibrium states will complete the assumptions. A generalized reforming process can be a useful guide in deciding what limitations to place on the states. For a hydrocarbon fuel in air, the maximum availability is achieved through complete combustion; this is therefore the most common process used to release energy from hydrocarbon fuels. Hence, it is reasonable to define the initial state as separated fuel and air at the stoichiometric ratio for combustion, in thermal and pressure equilibrium with the environment. Likewise, the equilibrium state can be defined as equilibrium combustion products (CO_2 and H_2O), again in thermal and pressure equilibrium with the environment. Thus, only the reformed state remains to be defined. To do this, we may model the reforming process as follows (see Figure 3.3 for a schematic representation of the states): the fuel and some portion of the air are injected into the reformer, where the energy input W_{in} is added to the resulting mixture. The heated gas then evolves to equilibrium adiabatically and at constant pressure (i.e. $\Delta H = 0$). Although the equilibrium composition technically is only reached at infinite time, it will be shown in Chapter 4 that for most of the reactions under consideration, the major products concentrations are likely to be very close to equilibrium levels after only a short time (typically much less than a second under the conditions we will examine). This defines a reformed state consisting of two parts: the first is a mixture containing all of the fuel mass and some part of the air mass from the initial state, at a pressure of p_R and at the "reformed temperature" T_r, with a chemical composition corresponding to equilibrium at this temperature and pressure; the second part is the remaining air mass from the initial state, still at T_R and p_R.

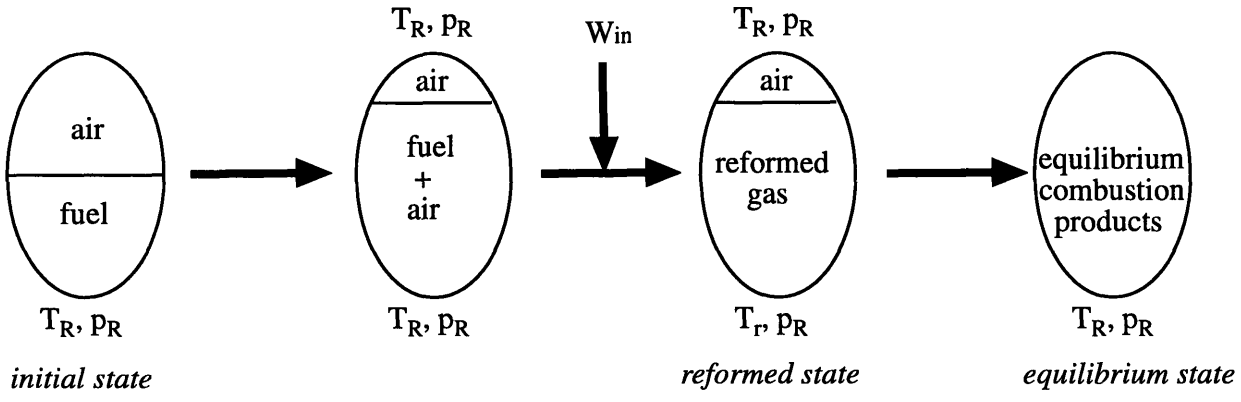

Figure 3.3. States of the plasma fuel reforming system (horizontal line represents a physical separation of gases).

Defining the three states as above reduces the variable system parameters to the H:C ratio of the input fuel, the O:C ratio of the portion of the gas that passes through the reformer (the overall O:C ratio is stoichiometric for combustion), and the reformed temperature T_r. A complete set of values for these parameters will allow the calculation of ψ_i, ψ_r, and ψ_0.

Since the reforming process is assumed to occur adiabatically and at constant pressure, the reformed gas and the gas mixture input to the reformer after the plasma heating must have the same enthalpy. Hence, the minimum required work input W_{in} is simply the enthalpy difference between the reformed state and the initial state (the reserved air has constant enthalpy and thus does not affect W_{in} for the purposes of this calculation).

With the parameter space thus reduced to a manageable form, we may consider the effects of the parameter values on important aspects of reforming, such as the reformed state availability and H_2 production levels. The first areas to examine are how the chemical composition of the reformed state and the availabilities vary as a function of the hydrogen to carbon and oxygen to carbon ratios of the gas entering the reformer and T_r.

The availability functions of the initial state (ψ_i) and equilibrium state (ψ_0) are functions of the H:C ratio of the fuel for a given T_R and p_R. For sake of simplicity, the input fuel is taken as a mixture of carbon and hydrogen, with a specified H:C ratio, in chemical equilibrium at T_R (at H:C = 1, the mixture is mostly acetylene, at H:C = 4, mostly methane). Figure 3.4 shows the variations in ψ_i and ψ_0 (in units of kJ per mole of carbon in the fuel) with H:C for T_R = 298 K and p_R = 1 atm. The availability Φ_{i0} is also given in this figure. Ideally, the availability of the product gas will be very close to Φ_{i0} at the H:C ratio used in the reforming process.

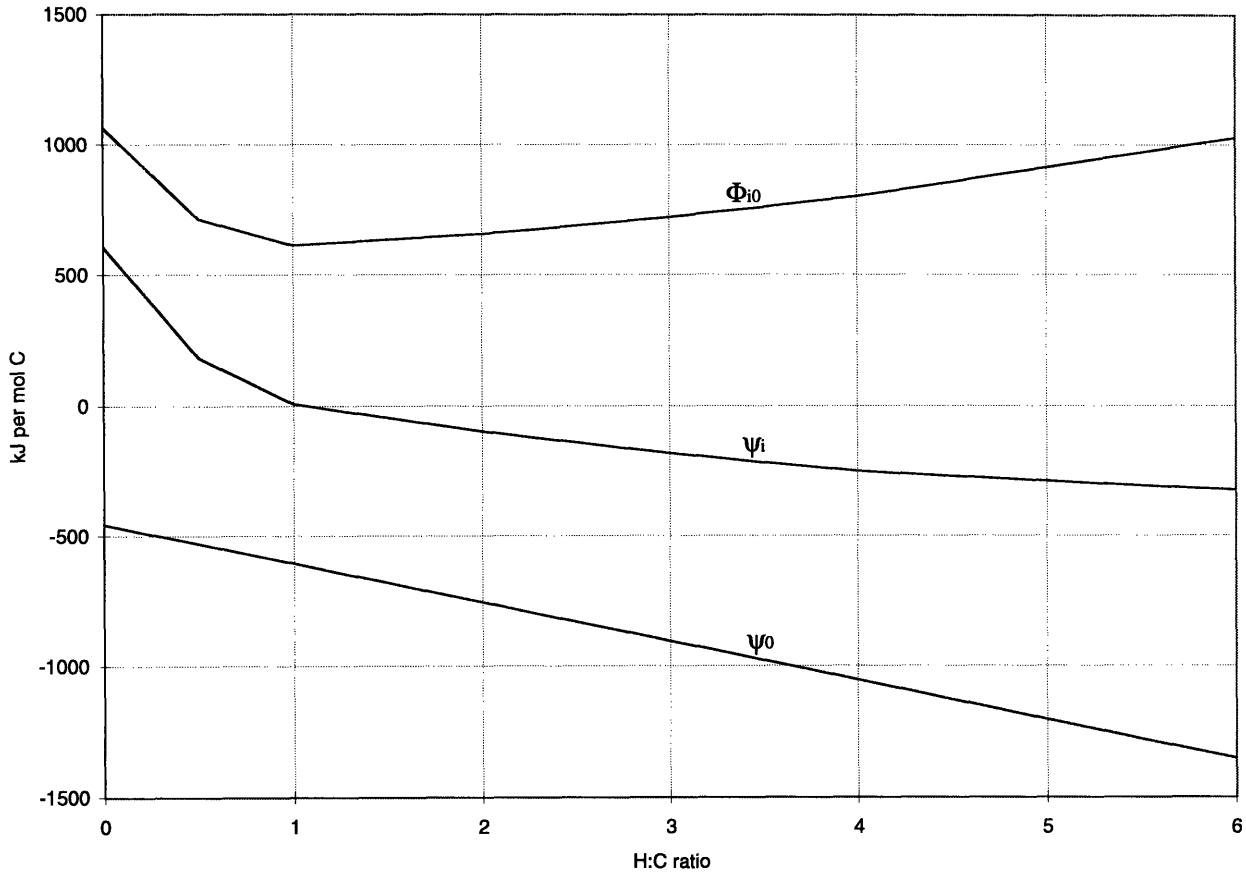

Figure 3.4. Initial and equilibrium state availability functions and Φ_{i0} with T_R = 298 K and p_R = 1 atm.

Figures 3.5 through 3.14 show how the chemical composition of the reformed state varies with H:C and O:C for T_r = 298 K and T_r = 1500 K at p_R = 1 atm. All species concentrations are given relative to the molar amount of carbon in the system. The equilibrium calculations were carried out by the element potential method, using a CHEMKIN interface to the STANJAN equilibrium code.[1,2] A description of the calculations is included in Appendix A.

A comparison of Figures 3.5 and 3.10 shows that H_2 production is greatly favored by the increase in T_r. At 298 K, there is essentially no H_2 production at H:C ratios less than 4:1 (the maximum achievable ratio with hydrocarbon fuels); that is, none of the hydrogen from the input fuel will be converted to molecular hydrogen at this temperature. At 1500 K, up to 100% of the hydrogen from the input fuel is converted to H_2, depending strongly on the O:C ratio. Thus, a high T_r is essential for hydrogen production. As can be seen from the rest of the figures in this series, increasing T_r also increases the availability of the reformed state with respect to the equilibrium state. At 298 K, the reformed state composition corresponds essentially to partial combustion (limited by the amount of oxygen in the reformer), resulting in a very low availability. At the higher temperature of 1500 K, very small amounts of the equilibrium products H_2O and CO_2 are present in the output mixture for lower O:C ratios, resulting in higher

availability. The larger availability at higher temperature is mostly due to the associated difference in chemical composition, rather than the increase in thermal energy.

Given that a high T_r is preferred, Figures 3.10 through 3.14 allow an examination of the trends in output composition in those conditions. As is seen in Figure 3.10, the maximum H_2 production occurs at an O:C ratio of 1:1, corresponding to the conversion of almost all the hydrogen of the input fuel to H_2. Given a hydrocarbon fuel in air, the limit on the H:C ratio is 4:1 (which corresponds to methane as the fuel molecule).[i] This suggests that at high temperature and atmospheric pressure, the optimum input chemical composition to the reformer for hydrogen production is H:O:C = 4:1:1 (for fuels other than methane, saturated hydrocarbons should be used for maximum H_2 production, with O:C = 1:1). The following figures show the amounts of various other compounds at equilibrium for the same space of conditions. CO production is maximized at O:C = 1 and is relatively insensitive to H:C. CH_4 decreases rapidly with increasing O:C, and is negligible for O:C $\geq$ 1:1. Water increases with both O:C and H:C, and is at negligible levels for O:C $\leq$ 1:1. CO_2 levels increase rapidly with O:C and decrease slowly with H:C. Once a critical O:C ratio is reached for a given H:C ratio, (roughly O:C = 0.5*(H:C) + 2, the stoichiometric ratio for combustion), the output H_2O and CO_2 levels correspond to complete combustion of the input fuel.

Figure 3.15 indicates the variation of Φ_{r0} with the H:C and O:C ratios, for T_r = 1500 K, p_R = 1 atm and T_R = 298 K. In order to maximize the thermodynamic efficiency of the reforming process, Φ_{r0} should be as large as possible. As should be expected, positive availabilities are only found for O:C ratios lower than stoichiometric combustion; the availability increases with increasing H:C ratio. Thus, combining the goals of maximum H_2 production and high efficiency leads to a particular region of the parameter space, defined by an O:C ratio near 1:1, as high an H:C ratio as possible, and high T_r.

[i] The continuing increase in H_2 production beyond H:C = 4:1 suggests the consideration of other input mixtures, such as fuel, air and water (i.e. steam reforming), which could allow an H:C ratio greater than 4:1.

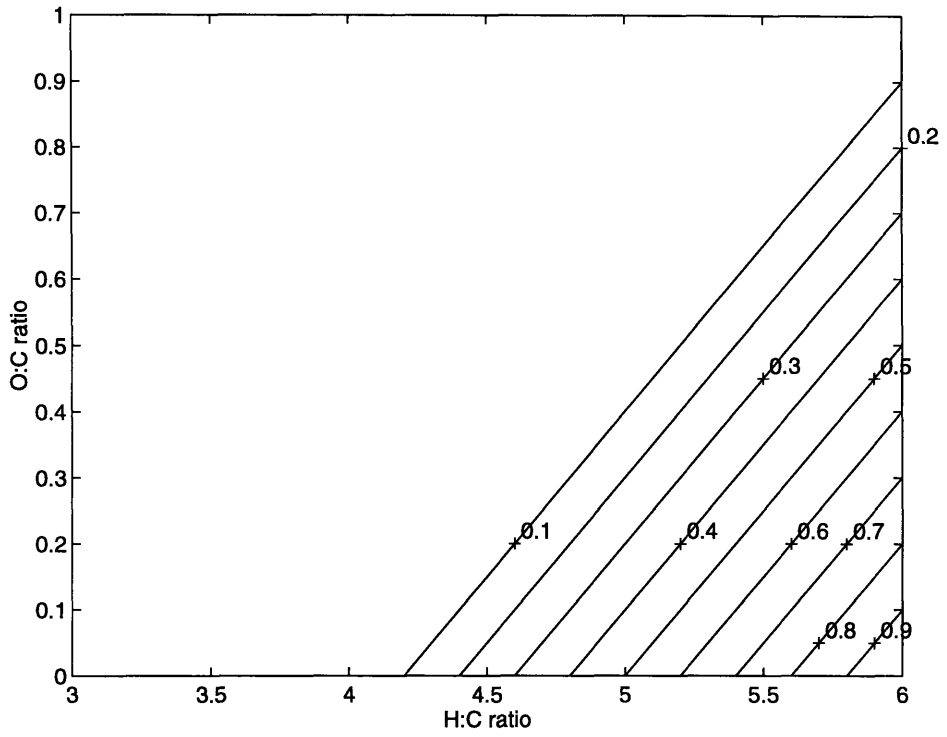

Figure 3.5. H_2 production as a function of H:C and O:C ratios at 298 K, 1 atmosphere

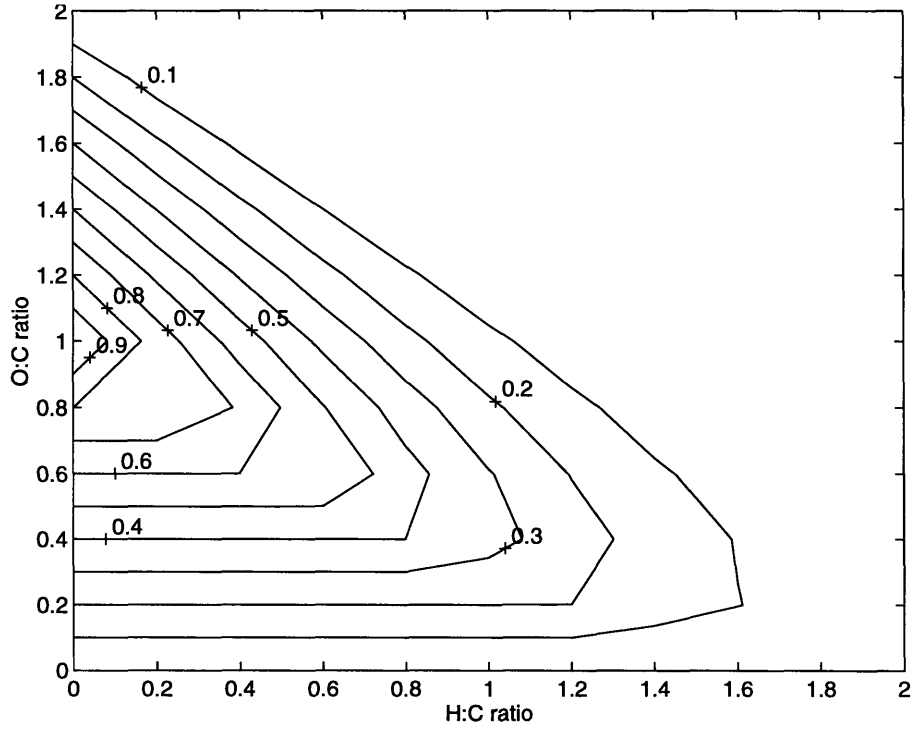

Figure 3.6. CO production as a function of H:C and O:C ratios at 298 K, 1 atmosphere

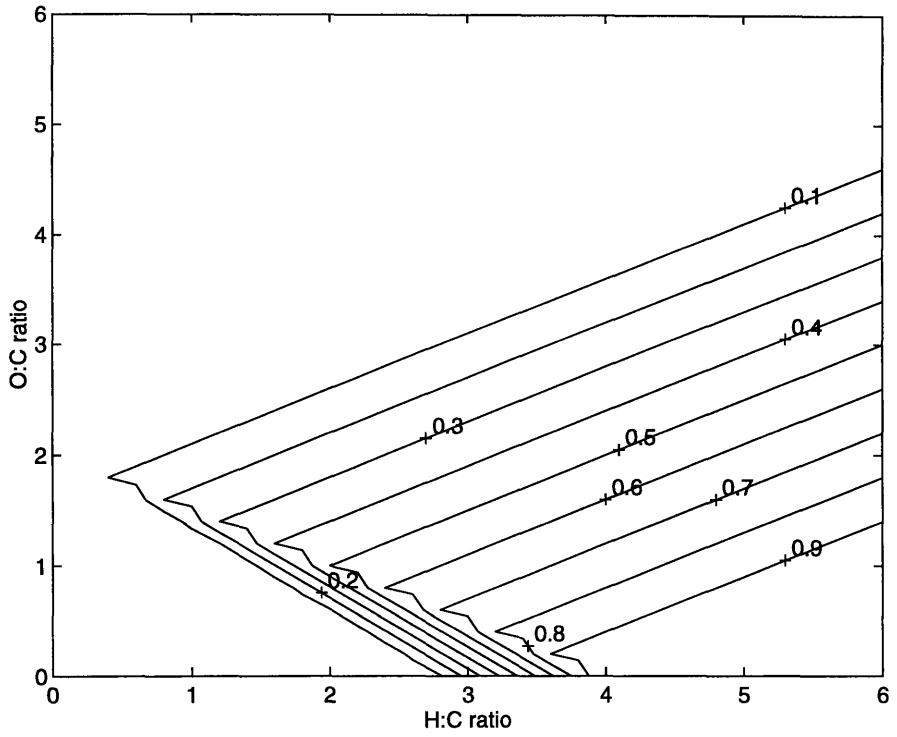

Figure 3.7. CH_4 production as a function of H:C and O:C ratios at 298 K, 1 atmosphere

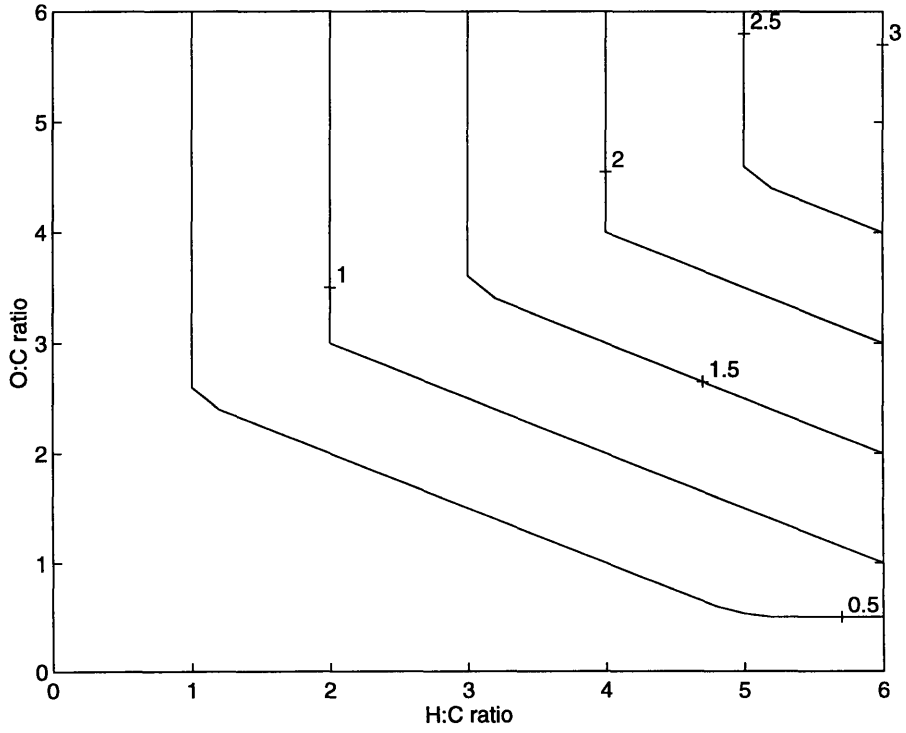

Figure 3.8. H_2O production as a function of H:C and O:C ratios at 298 K, 1 atmosphere

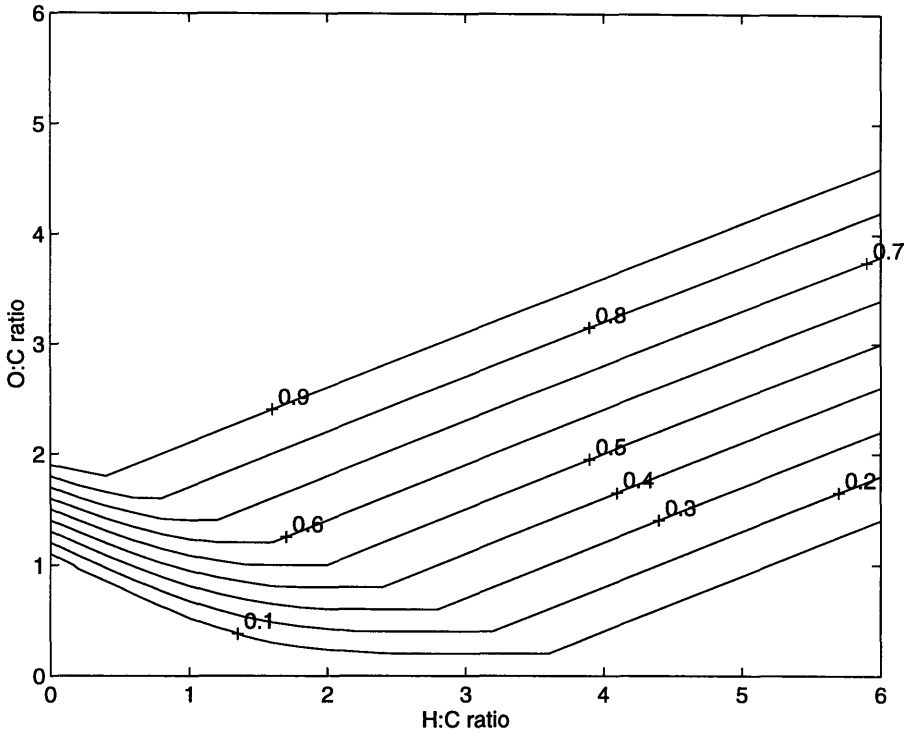

Figure 3.9. CO_2 production as a function of H:C and O:C ratios at 298 K, 1 atmosphere

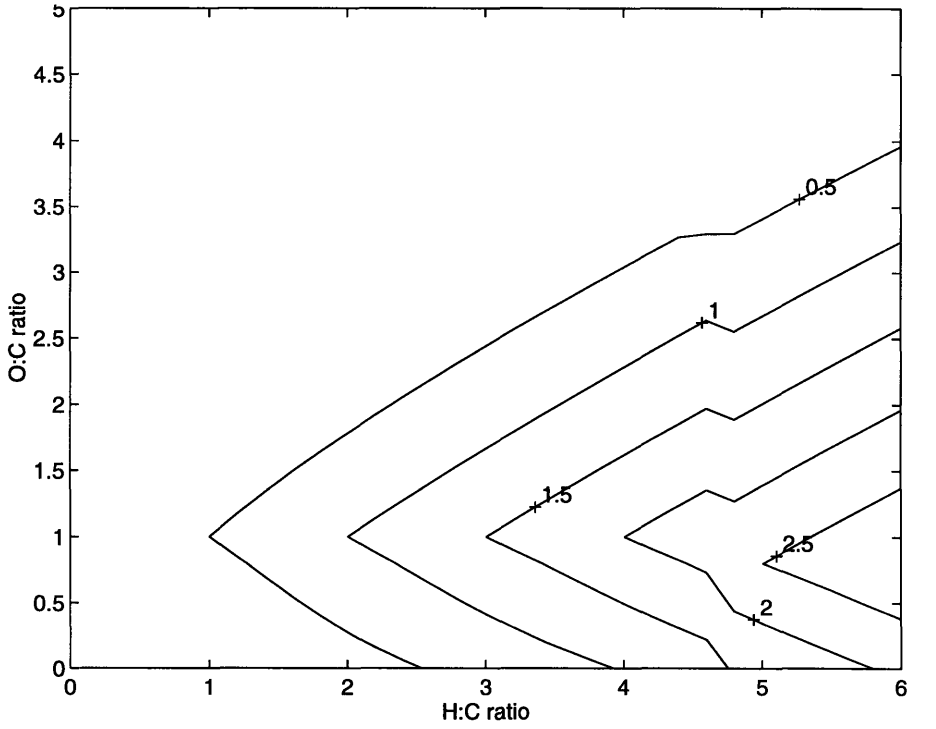

Figure 3.10. H_2 production as a function of H:C and O:C ratios at 1500 K, 1 atmosphere

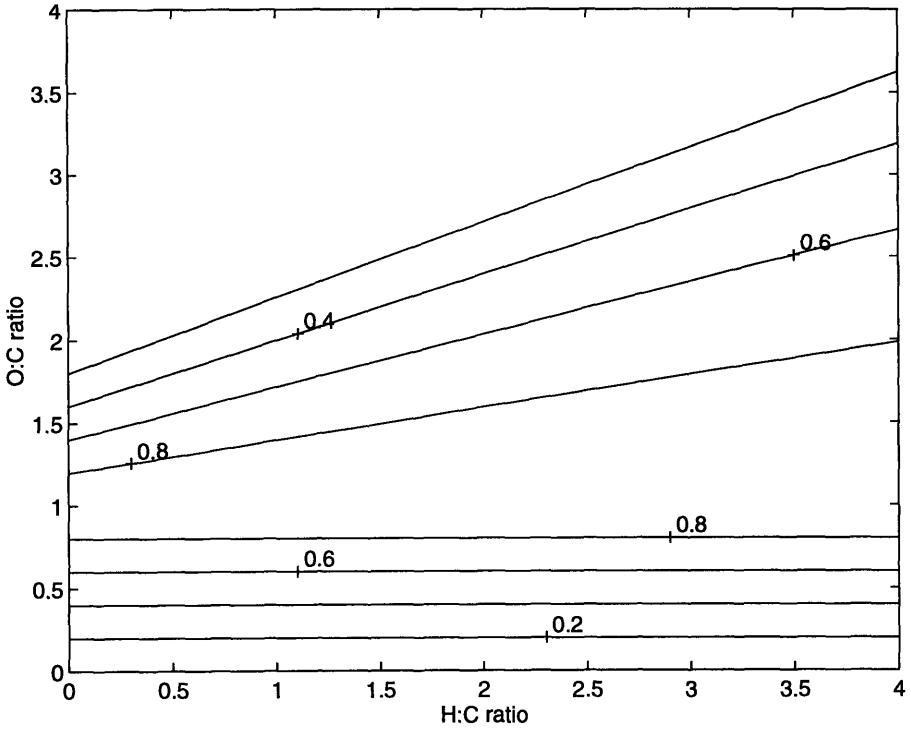

Figure 3.11. CO production as a function of H:C and O:C ratios at 1500 K, 1 atmosphere

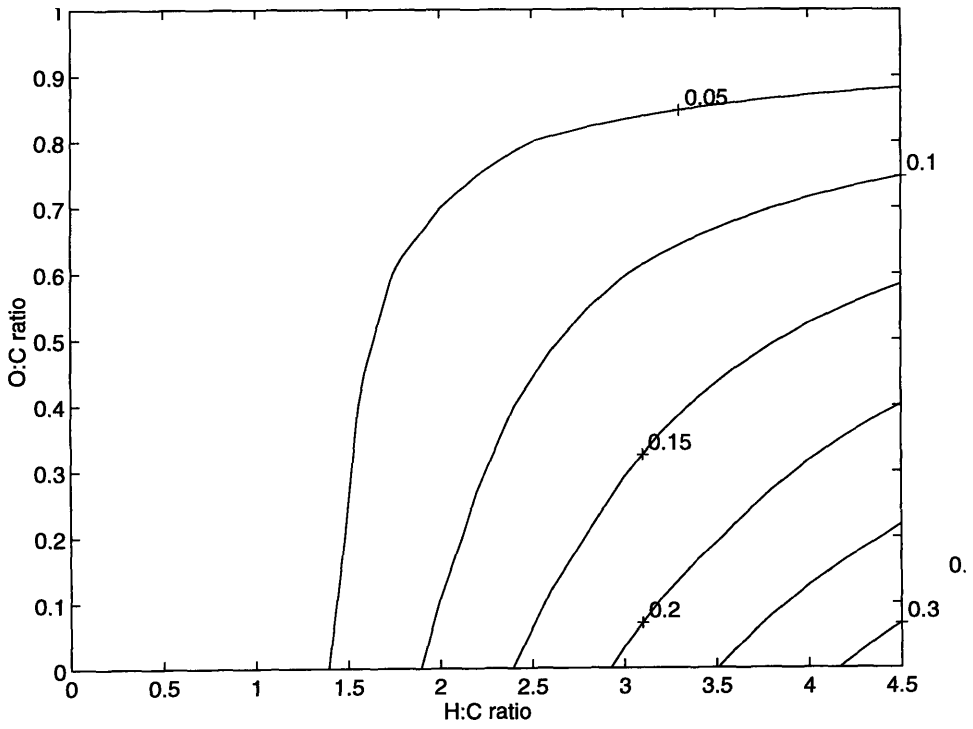

Figure 3.12. CH_4 production as a function of H:C and O:C ratios at 1500 K, 1 atmosphere

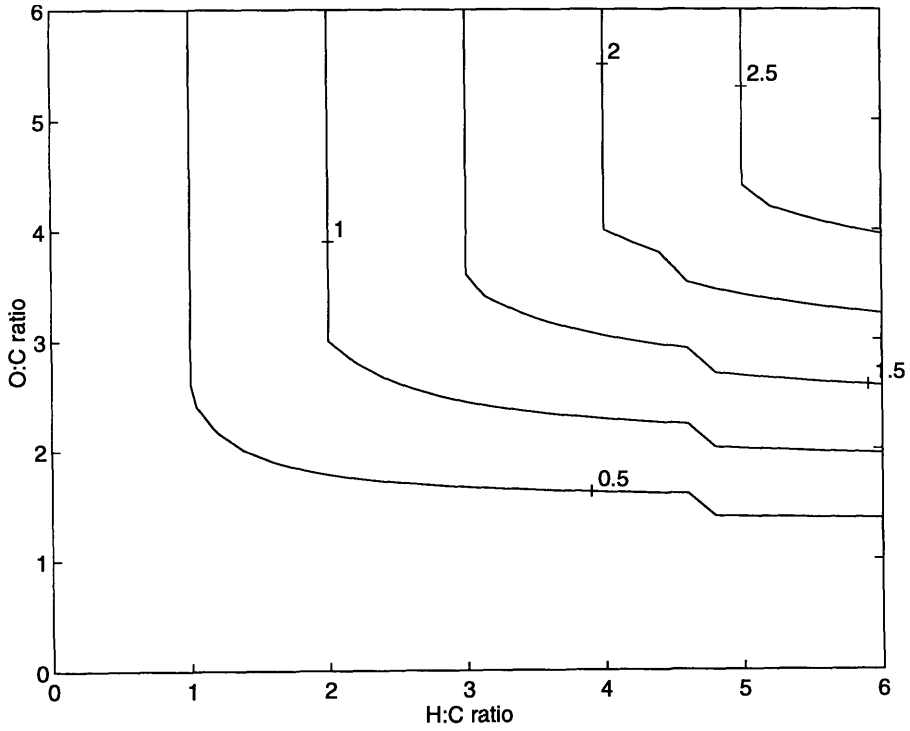

Figure 3.13. H_2O production as a function of H:C and O:C ratios at 1500 K, 1 atmosphere

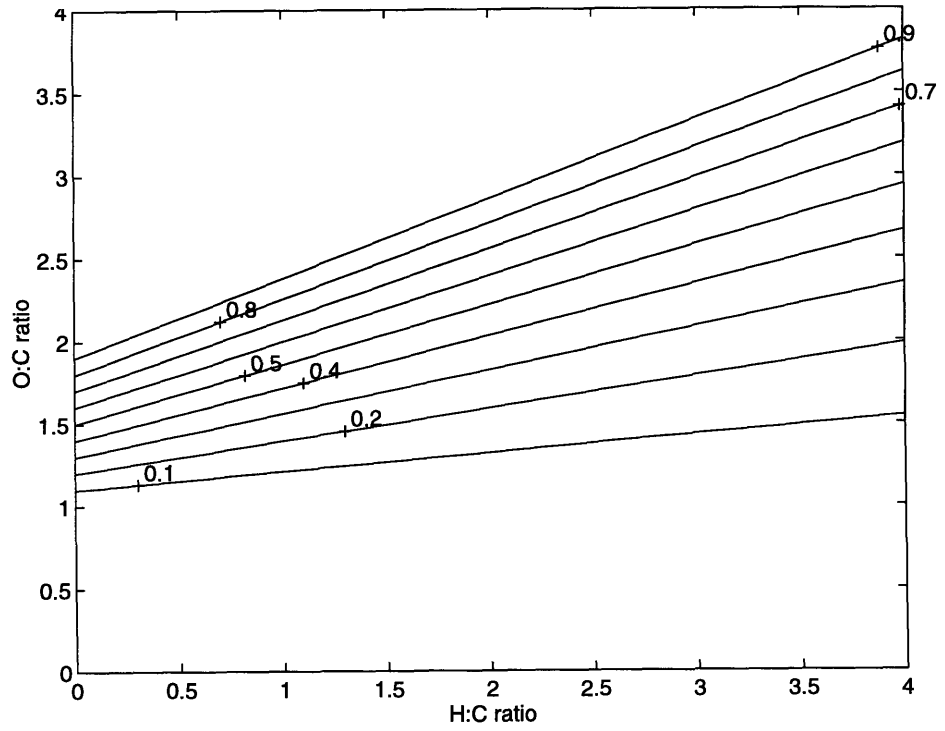

Figure 3.14. CO_2 production as a function of H:C and O:C ratios at 1500 K, 1 atmosphere

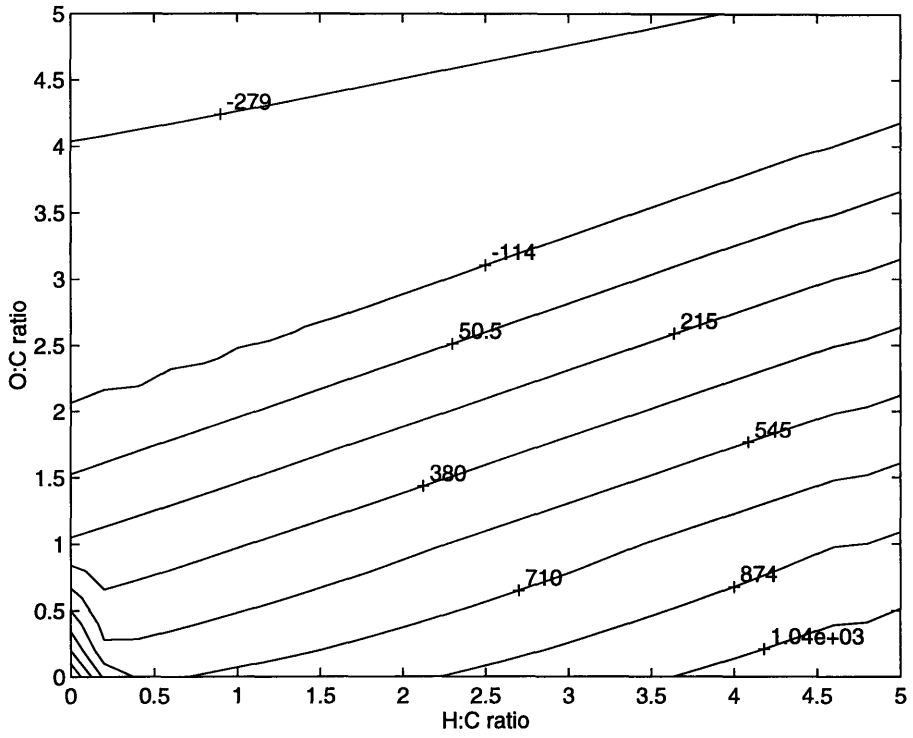

Figure 3.15. Φ_{r0} (kJ/mol C) as a function of H:C and O:C ratios at T_r = 1500 K, T_R = 298 K, p_R = 1 atm.

This region corresponds to a particular reaction, namely *partial oxidation* (see Chapter 2). For methane, the partial oxidation reaction can be written as

$$CH_4 + 1/2\ O_2 \rightarrow 2\ H_2 + CO$$

Examination of Figures 3.10 through 3.14 shows that the above expression accurately describes the transition from initial to reformed states for H:O:C ratio of 4:1:1 and T_r = 1500 K. If the partial oxidation reaction is performed with a hydrocarbon fuel in air, it can be characterized by an air-to-fuel equivalence ratio λ, defined as

$$\lambda = \frac{\dfrac{n_{air}}{n_{fuel}}}{\left(\dfrac{n_{air}}{n_{fuel}}\right)_{\substack{stoichiometric \\ combustion}}}$$

For methane in air, $\lambda = 0.25$.

For this particular reaction, we can now examine more thoroughly the effects of the reformed state temperature and p_R on the composition of the reformed state. (Up to this point we have assumed that p_R = 1 atm. However, the reforming process could potentially be performed at an arbitrary constant pressure, so it is useful to examine the effect that this has on

the reformer output.) Figure 3.16 shows the variation of chemical composition of the reformed state with T_r for $\lambda = 0.25$ and $p_R = 1$ atm. As T_r increases, the mole fractions of H_2 and CO increase towards values of 0.67 and 0.33, while all other species decrease to zero. The rate of this variation with T_r indicates that for maximum H_2 production T_r should be greater than 1200 K, but there is little gain in hydrogen output from increasing T_r much further. Figure 3.17 shows the variation of the reformed state composition at $T_r = 1500$ K as p_R increases from zero to 50 atmospheres. One can see from this graph that in order to optimize H_2 production, the pressure should be kept as low as possible.[ii] Atmospheric pressure is thus the most sensible choice, since it is the lowest pressure that can be achieved without expending energy to draw a vacuum.

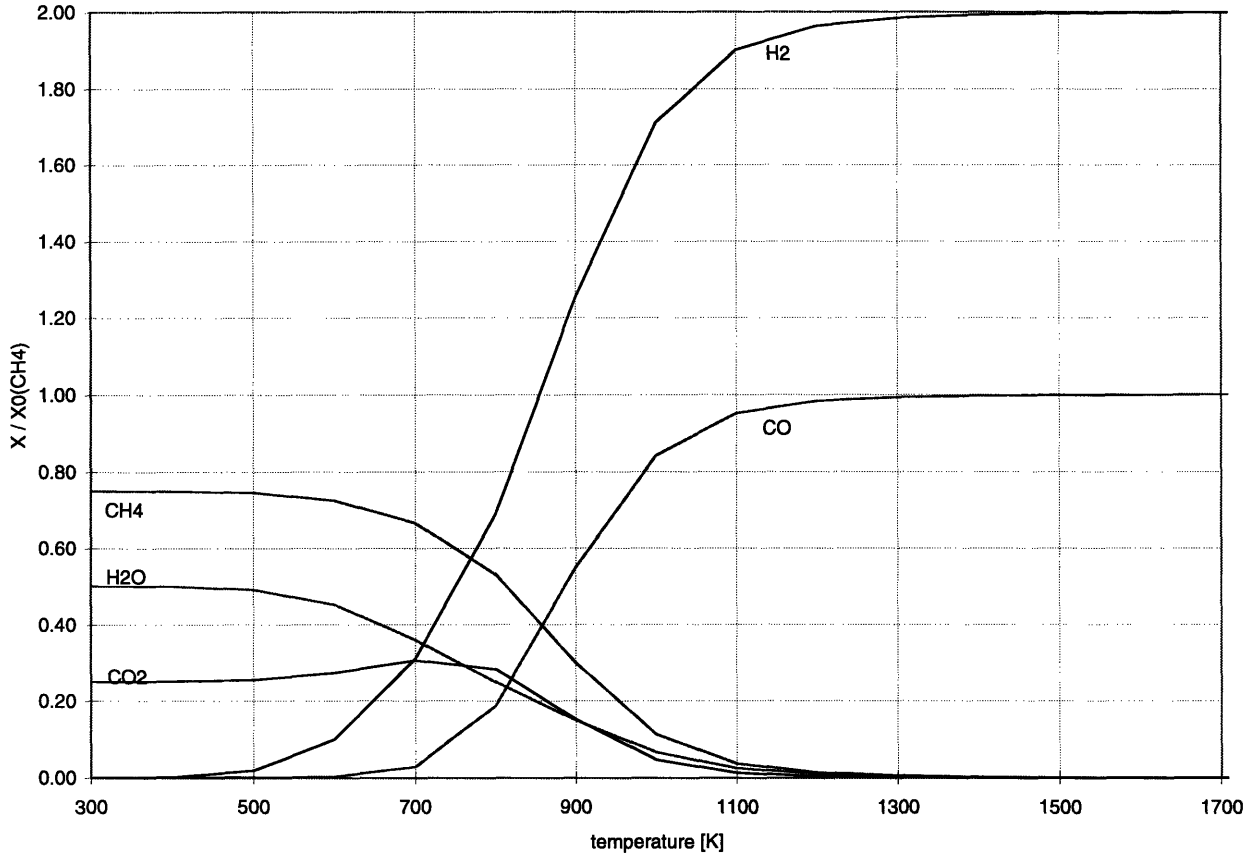

Figure 3.16. Chemical composition of the reformed state as a function of T_r at p = 1 atm.

[ii] A simple physical explanation of this effect is that the production of H_2 and CO from methane and air results in an increase in the total number of molecules. Since the energy of the system at a given pressure increases with the number of molecules, higher pressures act against the production of H_2 and CO.

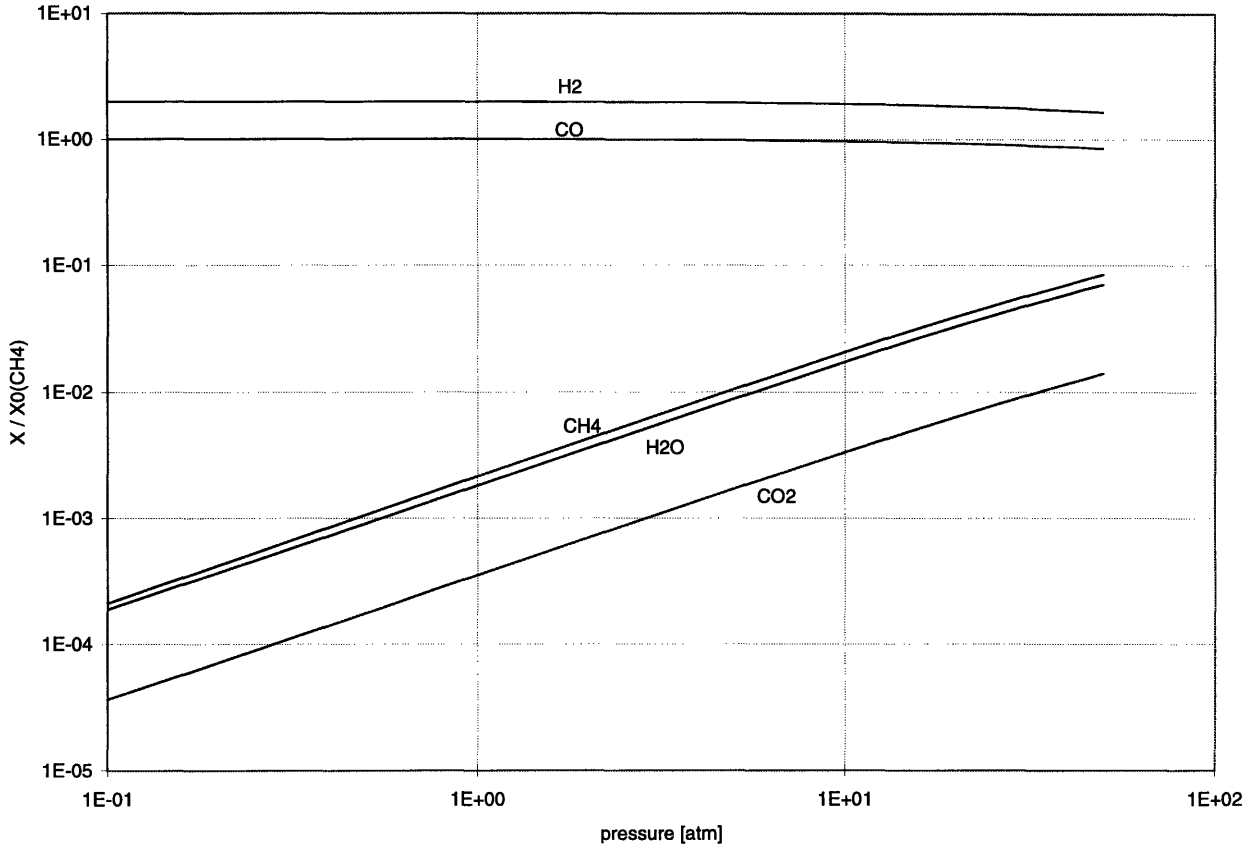

Figure 3.17. Chemical composition of the reformed state as a function of pressure at T_r = 1500 K (log plot).

This relatively quick thermodynamic analysis has allowed us to choose a reasonable set of operating conditions for the reforming system in order to maximize H_2 production while keeping the thermodynamic efficiency as high as possible, assuming that the reformed mixture reaches near equilibrium conditions at the operating temperature and pressure. If H_2 production is the most important design criterion, then the reformer should operate at temperatures on the order of 1200 K and at atmospheric pressure, with a air-to-fuel ratio of $\lambda = 0.25$ (for methane as the fuel molecule). If raising the efficiency becomes more important, λ should be decreased. The same information also allows a quick assessment of the effects of other design criteria on the operating conditions. For example, if it were necessary to minimize CO production, one can see from figures 11 to 15 that lowering the O:C ratio (i.e. decreasing λ) could accomplish this at the expense of lower methane conversion, whereas raising the O:C ratio would lower CO production and H_2 production while increasing output CO_2 levels.

3.5 THERMODYNAMIC EFFICIENCY OF THE REFORMING PROCESS

The reforming parameters determined in the previous section provide the necessary information to calculate the minimum efficiency of the reformer. At T_R = 298 K and p_R = 1 atm, the availabilities Φ_{i0} and Φ_{r0} can be calculated as functions of T_r; these values are given in Figure 3.18. The minimum work input W_{in} required to take the system from the initial state to the reformed state is also included in this figure. Note that for reformed temperatures below 900 K, W_{in} is negative. This indicates that the system could in principle do work while moving from the initial to the reformed state; in order to be consistent with the rest of the analysis, we assume that this work is not recoverable, and hence should be ignored.

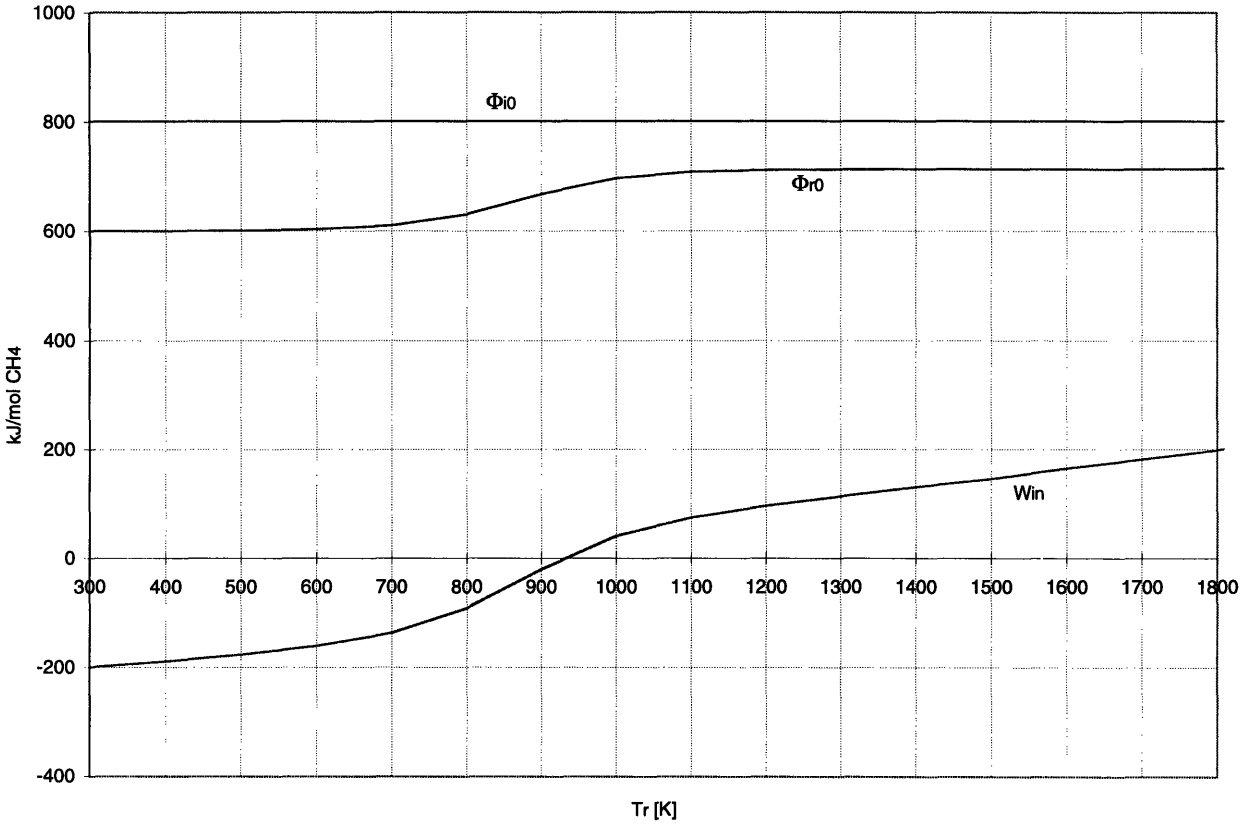

Figure 3.18. Availabilities and minimum work input for the reformer with T_R = 298 K, p_R = 1 atm, λ = 0.25

Figure 3.19 shows the thermodynamic efficiency ε of the reformer as defined above as a function of T_r, calculated from the availabilities in Figure 3.18. The features of the efficiency profile can be explained in physical terms. At 300 K, ε is 75 percent; this is due to the fact that the reformed state in this case corresponds simply to combustion of 25 percent of the fuel with 25 percent of the air (see Figure 3.16), leaving the rest of the fuel and air available for further combustion. The maximum efficiency of 83 percent occurs at 900 K, the maximum reformed

state temperature for which $W_{in} \leq 0$. This is the maximum value of T_r for which the reaction will occur spontaneously, and since Φ_{r0} increases with T_r, it gives the largest reformed state availability of the set of spontaneous processes. Given sufficient time under adiabatic, constant pressure conditions, the system will automatically move to this state. After this temperature, Φ_{r0} reaches an approximately constant value, whereas W_{in} is continually increasing, resulting in decreasing efficiency values. Considering Figures 3.16 and 3.19, it is evident that the thermodynamically ideal range of reformed temperatures T_r is from 900 K (maximum ε) to 1200 K (maximum H_2 production), corresponding to energy inputs W_{in} between zero and 96 kJ/mol CH_4. These values represent the limits of performance that may be achieved with a reformer defined by the assumptions made in this chapter. In a real situation, in which infinite times are not available, the energy costs of reforming will not only reflect these thermodynamic limits, but also will include the cost imposed by the kinetics of the chemical processes involved in bringing the system to a near-equilibrium state within a specified timescale. These effects will be considered in the following chapter.

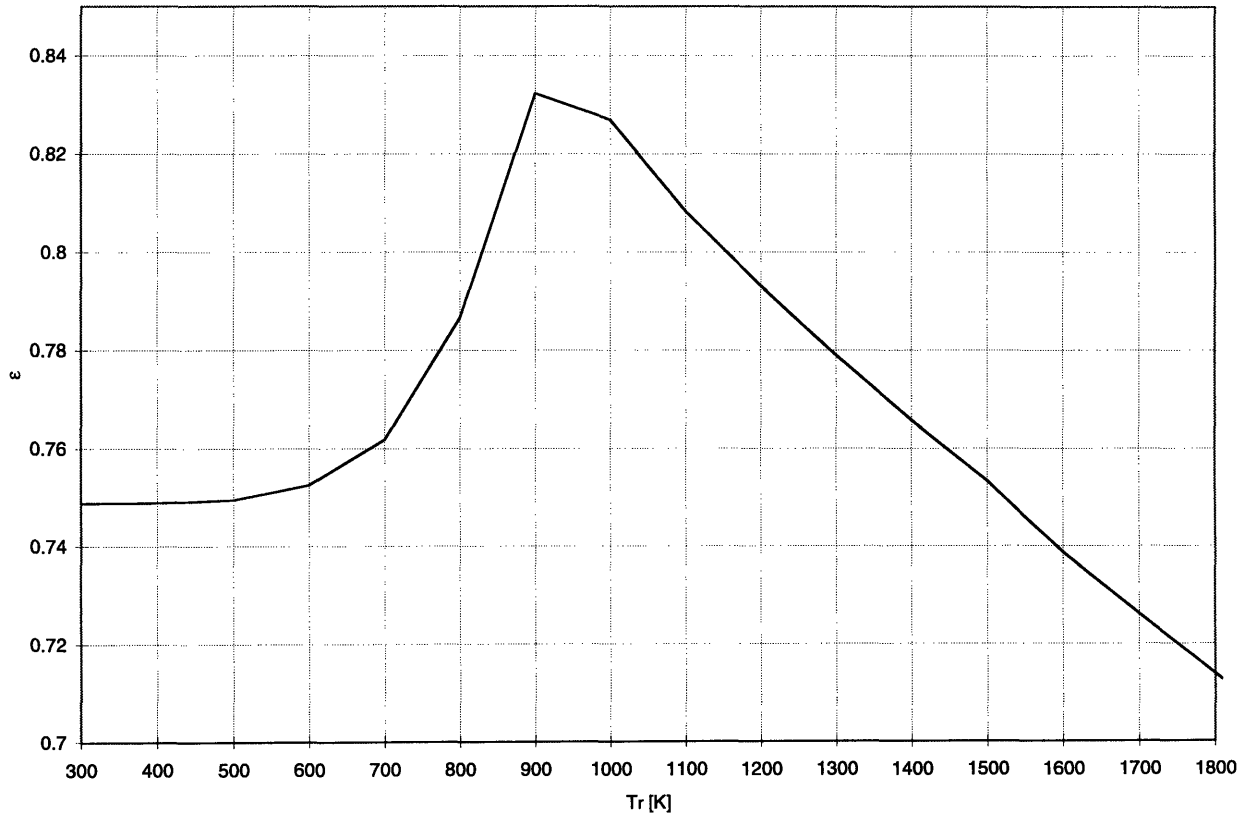

Figure 3.19. Thermodynamic efficiency of the reformer with T_R = 298 K, p_R = 1 atm, and λ = 0.25

3.6 REFERENCES

[1] R.J. Kee, F. M. Rupley, J.A. Miller, "CHEMKIN-II: A FORTRAN Chemical Kinetics Package for the Analysis of Gas Phase Chemical Kinetics," Sandia National Laboratories Report SAND89-8009 (1989).

[2] W.C. Reynolds, "The Element Potential Method for Chemical Equilibrium Analysis: Implementation in the Interactive Program STANJAN," Department of Mechanical Engineering, Stanford University (1986).

CHAPTER 4

Chemical Kinetic Analysis

4.1 INTRODUCTION

The preceding thermodynamic analysis defines the limiting behavior of the reformer, and the basic information on efficiency and H_2 production that it provides suggests focusing on a system with the following specific parameters: a hydrocarbon fuel, preferably with a high H:C ratio, is supplied to the reformer along with air at $\lambda = 0.25$ (the air-to-fuel ratio for partial oxidation). The electrical work supplied by the plasmatron supplies the energy necessary to heat the mixture to a level where the chemical equilibrium of the fuel-air mixture favors H_2 and CO. The thermodynamic efficiency is 83 % at optimal conditions for methane fuel, presuming no recovery of heat released and work done during reforming. Given an infinite residence time in the reformer, this is a reasonably accurate analysis. However, since residence times in the real system are far less than infinite (typically $\tau_r \leq 500$ ms), the thermodynamic efficiency is an upper limit on realistically achievable efficiencies, and we must consider kinetic effects in order to be able to predict the actual behavior of the reformer.

The chemical kinetic calculations in this section have two goals: first, by examining in detail the time evolution of the reacting system with a given energy input, we can begin to understand the quantitative effects of a finite residence time on the reformer output and efficiency. Secondly, by studying the relation between the reaction kinetics and the physical constraints imposed by the reformer itself, we can develop a computational model of the physical system that can reproduce certain characteristics of the experimental system; this type of model can be useful as a predictive design tool.

These two analyses are presented in the following sections: in section 4.2, the evolution of a mixture reacting adiabatically at constant pressure (i.e. at constant enthalpy) is considered. This analysis gives the product distribution as a function of residence time, and thus the minimum time required for conversion to the equilibrium composition. In section 4.3, the minimum energy requirements for the ignition of the reaction within the reformer and the energy cost of H_2 production are considered for a simple physical model of the plasma reformer. These minimum energy requirements are quite different from the thermodynamic minimum energy input discussed in the previous section; they are associated with the energy required to overcome the reaction energy barrier, and reflect the energy cost of performing the reaction within a finite time.

4.2 PLUG-FLOW REACTION PROGRESS CALCULATIONS

A basic question that we would like to answer with kinetic calculations is the following: Given the reforming system as described above, with a specified power input from the plasmatron and air/fuel flow rate, how do the chemical composition and temperature of the mixture evolve with time? Thermodynamic analysis has indicated where the chemical system can go; kinetics can describe the specific path by which it will get there. It will allow us to capture such characteristics as ignition temperatures and delay times and incomplete reforming.

We begin with an air/fuel mixture and a certain electrical work rate imposed on it by the plasmatron. This situation can be characterized by the ratio of electrical power to total fuel and air flow rate (or simply fuel flow rate at a fixed λ), which gives the amount of work input per unit mass of methane, for example. This ratio of power to flow, ζ, is the most important system parameter in the following analyses.

The transformation of the reactants (air and fuel) to partial oxidation products is investigated assuming that the reactants are instantaneously raised to the temperature corresponding to the energy input per unit mass of reactant, and that the reaction then proceeds adiabatically and at constant pressure. We consider the time evolution of a fixed quantity of gas, which could be envisioned as a control volume that moves through the reformer, exchanging neither heat nor mass with neighboring volumes. The gas is well-mixed within the volume. This model, referred to as an adiabatic plug flow reactor (PFR), allows us to examine the effects of input energy on the time evolution of the reacting chemical system, in the absence of heat losses, mixing and other complications. Thus, the conclusions drawn from this analysis are related to the dynamics of the chemical system itself, as opposed to other factors such as reactor characteristics. The fuel considered is methane, with a air-to-fuel ratio of $\lambda = 0.25$ and a specified ζ. The chemical reaction mechanism used to model the oxidation of methane, GRI-MECH, was developed for the natural gas industry and includes 177 reversible reactions involving 31 chemical species, from the initial decomposition of methane to the formation of final products.[1]

The dynamics of the system reacting according to the specified mechanism can be reduced to a set of ordinary differential equations. A chemical reaction of the form

$$n_1 S_1 + n_2 S_2 + n_3 S_3 + \ldots \rightarrow n_1' S_1 + n_2' S_2 + n_3' S_3 + \ldots \qquad (1)$$

where S_k represents a particular chemical species and n_k is a molar amount, can be written as the algebraic summation

$$\sum_k \nu_{jk} S_k = 0 \tag{2}$$

in which ν_{jk} is the *net stoichiometric coefficient* of species k for reaction j, given by $n_k' - n_k$. (Thus ν_{jk} is negative for reactants and positive for products). The time evolution of each species is given by

$$\frac{dY_k}{dt} = \frac{M_k \hat{w}_k}{\rho} \tag{3}$$

where Y_k is the mass fraction of species k, M_k is the molecular weight of that species (kg/mol), ρ is the overall mixture density (kg/m^3), and $\hat{w}_k$, the molar rate of production of species k (mol/m^{3}s), is given by

$$\hat{w}_k = \sum_j \nu_{jk} \hat{R}_j \tag{4}$$

in which $\hat{R}_j$ is the rate of reaction j in mol/m^{3}s. The temperature of the mixture during the reaction is calculated using the energy equation

$$\frac{dT}{dt} = -\frac{1}{\rho c_p} \sum_k M_k \hat{w}_k h_k \tag{5}$$

where T is the mixture temperature, c_p the mass-average mixture specific heat at constant pressure, and h_k the total enthalpy per unit mass of species k at mixture conditions. The negative sign accounts for the fact that if the enthalpy of the mixture formed is lower than that of the initial mixture, the energy released is converted into thermal energy.

The CHEMKIN set of subroutines was used to integrate the stiff system of ODEs resulting from equations (3) and (5).[2] The initial conditions are given by the stoichiometry of the mixture ($\lambda = 0.25$) and the initial enthalpy of the mixture, here given by the enthalpy of the reactants at standard conditions (298 K, 1 atm), plus the energy added by the plasma (specified by ζ).

Figures 4.1 - 4.3 show the time evolution of major species concentrations and temperature for p = 1 atm, $\lambda = 0.25$, and $\zeta = 7.5$, 10 and 15 MJ/kg CH_4, corresponding to initial temperatures of 1200, 1500 and 1800 kelvin, respectively. These plots cover the important range of ζ for the residence times under consideration. All species concentrations are normalized by the initial amount of CH_4. The most obvious feature in each of these plots is a rapid change in concentrations over a relatively short period of time, accompanied by a sharp increase in temperature. This is caused by the slow buildup of key chemical species, particularly radicals, which upon reaching critical concentrations initiate rapid chain reactions,

thus creating the observed 'ignition' of the mixture. Both the period of time over which the rapid changes occur and the delay until they begin decrease as ζ increases. The combination of this effect with a finite residence time defines an ignition energy ζ_i (or temperature T_i), that is, the energy input per mole of CH_4 that is necessary for ignition to occur within the residence time. Figure 4.4 shows the decrease of ignition delay time with ζ, or conversely, ζ_i as a function of residence time.

A second feature of the three plots is that the species concentrations do not go immediately to equilibrium levels after ignition. Directly after the ignition event, there are significant amounts of CO_2, H_2O and C_2H_2 present, at levels which are not consistent with the equilibrium composition. Afterwards, the composition slowly moves to equilibrium levels. This behavior is consistent with the two-stage mechanisms for partial oxidation discussed in Chapter 2. Hence, if ζ is very near to ζ_i for a given residence time, we can expect to find water, carbon dioxide and acetylene in the output mixture. This two-part mechanism creates two separate energy input criteria; one for the reaction to begin within the residence time, and one for reaching the equilibrium product distribution during τ_r.

The conclusions that we can draw from Figures 4.1 - 4.3 are that for the expected residence times $\tau_r \leq 500$ ms, ignition energies on the order of $\zeta_i = 7.5$ MJ/kg CH_4 will be required for minimal conversion, corresponding to pre-ignition temperatures of roughly T_i = 1200 K, but much higher energies, $\zeta = 15$ MJ/kg CH_4, will be required to reach the desired product composition within the available residence time. This energy is provided in the form of electrical work from the plasmatron.

The optimal energy input should fall somewhere between the values noted above, at the point where the efficiency gain due to increasing H_2 production is offset by the escalating input power requirements. Figure 4.5 shows the energy cost of H_2 production C, in MJ of input energy per kilogram of H_2 output, as a function of ζ, for residence times of 100 to 500 ms. It can be seen from the figure that for this entire range of residence times, the optimal value of ζ for H_2 production falls between 11 and 13 MJ/kg CH_4, corresponding to energy costs of 52 - 59 MJ/kg H_2. The value of C associated with the optimal condition increases slightly with decreasing τ_r; however, for higher ζ values, this effect is smaller. Hence, this model suggests that the ideal operating conditions for the reformer for residence times of hundreds of milliseconds are characterized by ζ in the range 11 - 13 MJ/kg CH_4.

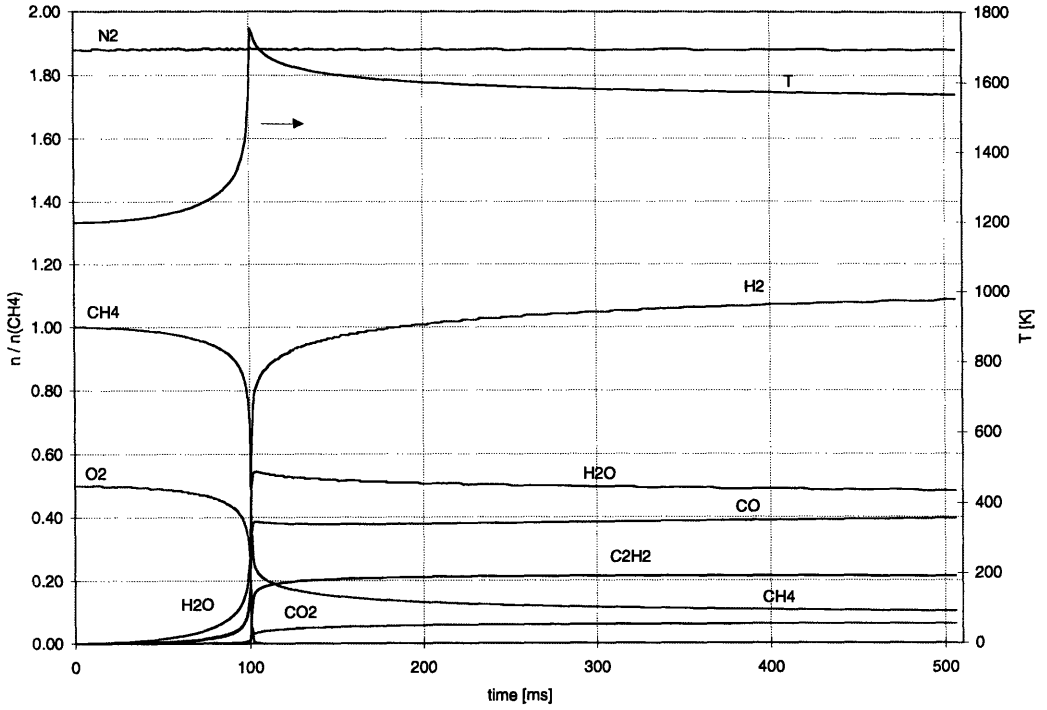

Figure 4.1. Species concentrations (relative to input CH4) and temperature versus time at p=1 atm, ζ=7.5 MJ/kg CH_4

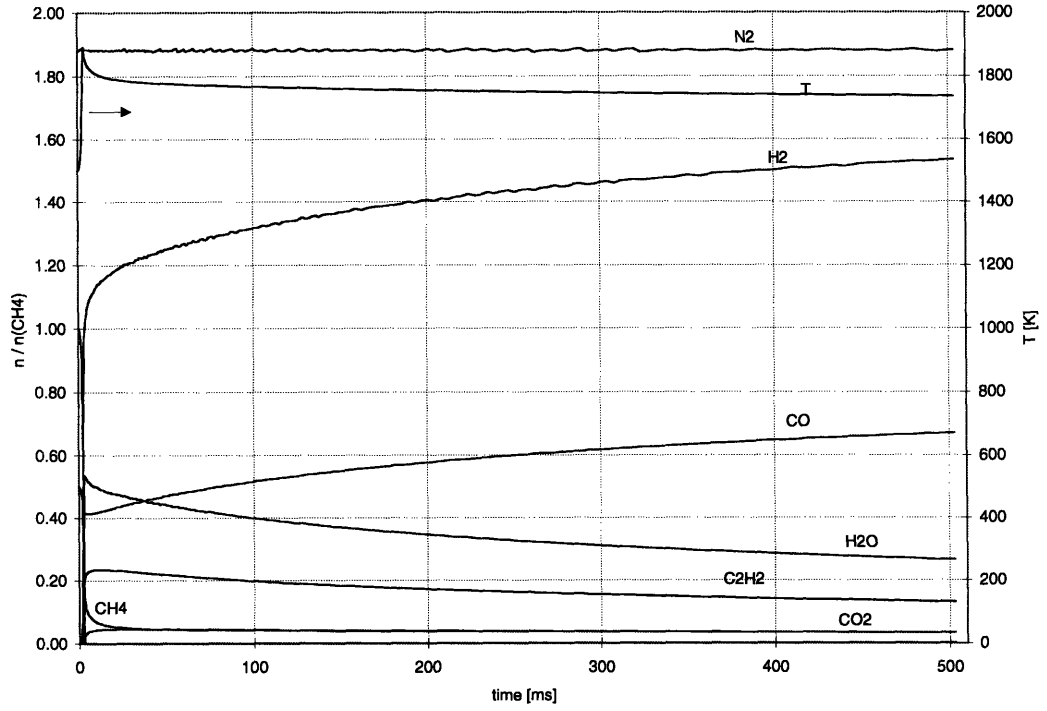

Figure 4.2. Species concentrations (relative to input CH_4) and temperature versus time at p=1 atm, ζ=10 MJ/kg CH_4

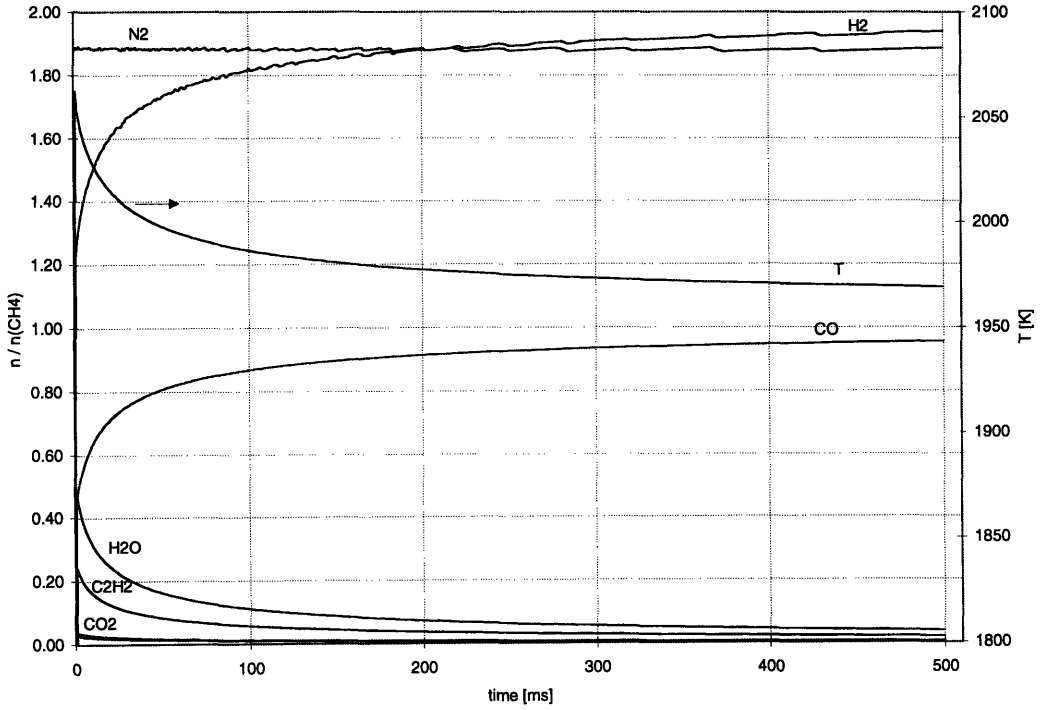

Figure 4.3. Species concentrations (relative to input CH_4) and temperature versus time at p=1 atm, ζ=15 MJ/kg CH_4

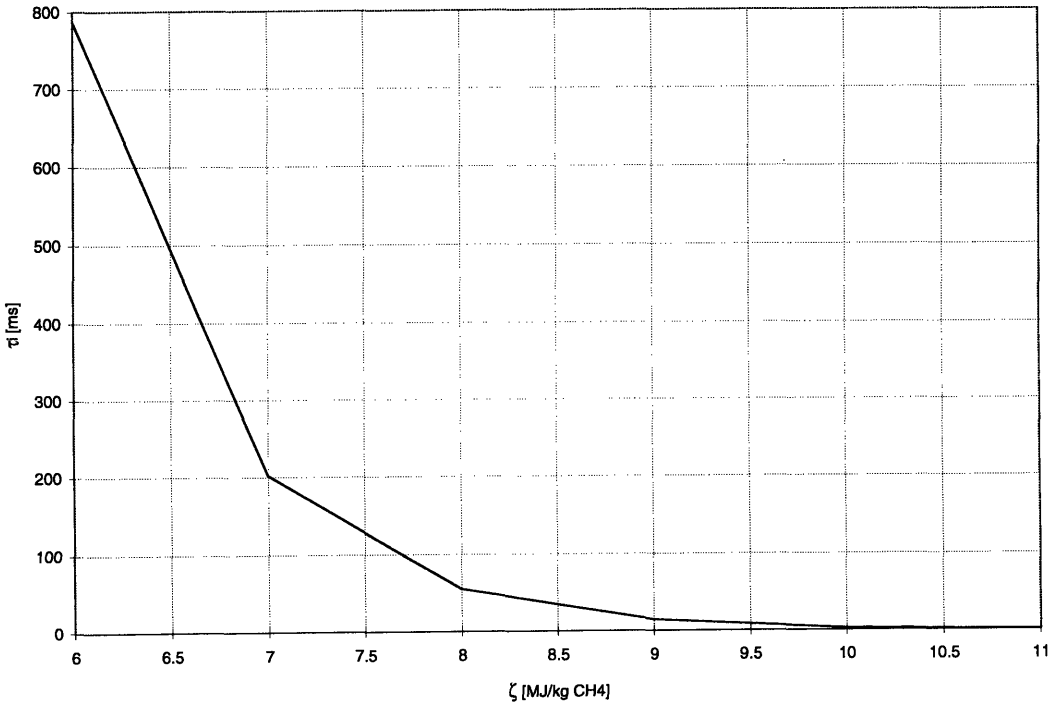

Figure 4.4. Ignition delay time versus ζ for the plug flow reactor model; p = 1 atm, λ = 0.25.

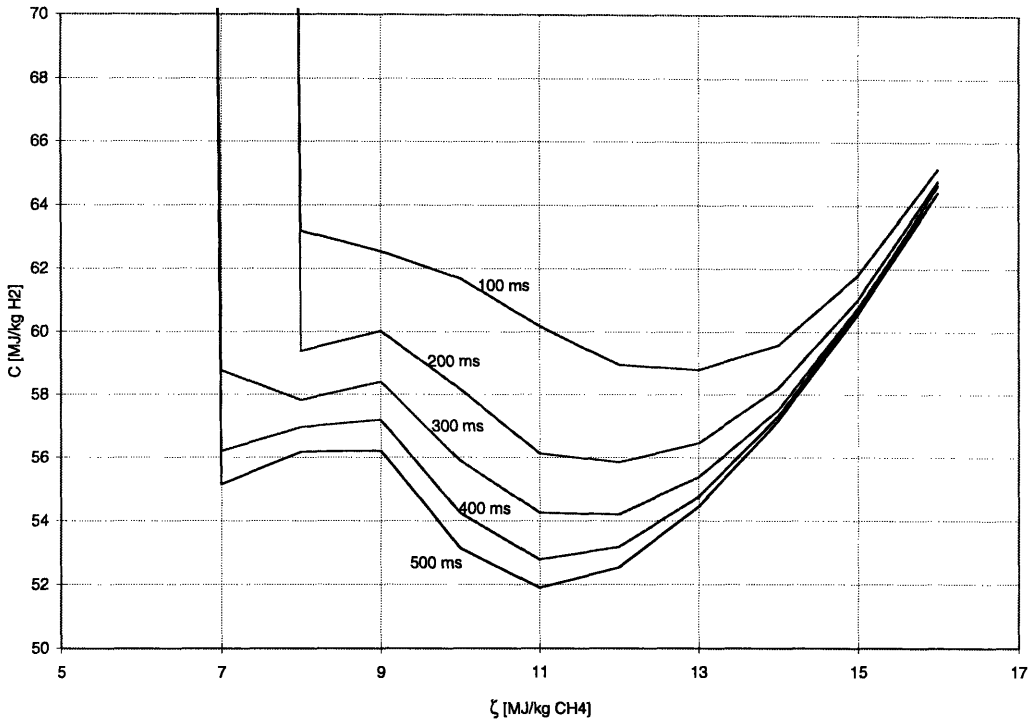

Figure 4.5. Energy cost of H_2 production versus ζ for the plug flow reactor model; p = 1 atm, $\lambda = 0.25$.

4.3 PERFECTLY STIRRED REACTOR MODEL OF THE PLASMA REFORMER

The preceding calculations apply to gas mixture flows at constant enthalpy in a plug flow reactor. This gives insight into a particular limiting case, in which a certain volume of gas flowing through the reactor does not interact with neighboring volumes. In order to provide a more detailed account of the mass and energy transfers occurring in the reformer, and to understand the limiting conditions and the optimal conditions under which the actual device can operate, a more physical picture of the reforming process is necessary.

Figure 4.6 shows a simplified model of the plasma reformer. Mixed fuel and air (at $\lambda =$ 0.25) flow through the plasmatron, in which electrical work causes a power flow into the gas stream. Immediately after the plasma heating, the mixture passes through a highly turbulent reactor of a specified volume, in which the part of the reaction in which we are interested occurs. As the reacting mixture moves through the volume, there may be heat losses to the walls. The exit of the volume can be considered to be a sampling point or the inlet to a further processing or power stage.

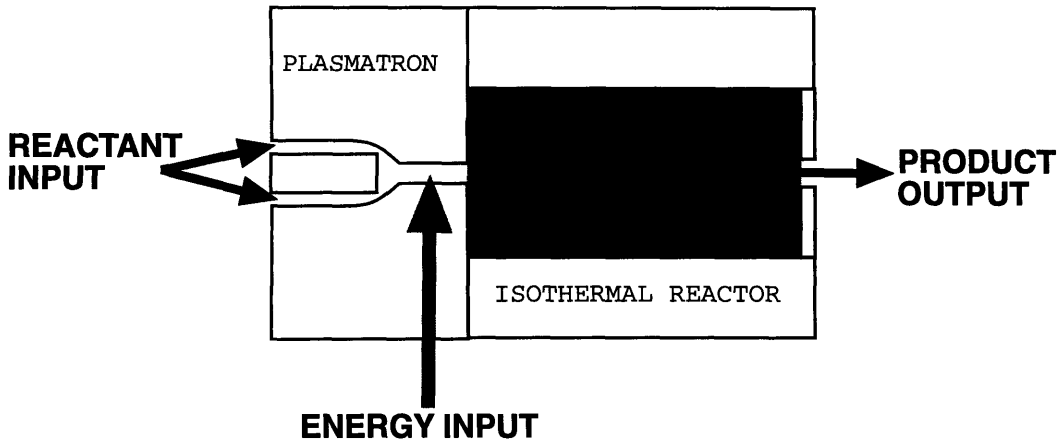

Figure 4.6 Simple model of the plasma reformer.

In order to simplify the analysis, as well as to provide a limiting case for the ignition behavior of the device, perfect mixing is assumed for the reacting volume within the reformer. (Note that this and the plug flow calculations assume opposite extremes of mixing along the reactor coordinate, although both are spatially uniform in some sense.) This assumption implies that the timescale for mixing by turbulent diffusion τ_m, is much smaller than that of chemical reaction τ_{reac}; i.e. the Damkohler number

$$Da = \frac{\tau_m}{\tau_{reac}} \tag{6}$$

is very small. Perfect mixing also implies that there is only one temperature within the volume, which must be the same as the temperature of the exiting gas. The volume thus contains an homogeneous mixture of products and reactants, so that the species distribution in the output flow must be the same as that within the reactor.

This collection of assumptions is referred to as a perfectly-stirred reactor (PSR) model. Connections between this model and the preceding kinetic analysis can easily be found. The ratio of the electrical work rate (power) of the plasmatron to the flow rate of fuel is ζ, as above. The reactor volume divided by the fuel flow rate gives τ_r. However, this model can capture different aspects of the reactor dynamics than those that were examined using the plug flow calculations, and it has the advantage that its parameters correspond to easily adjustable characteristics of an actual device. PSR models are applied frequently to combustion systems, and have recently been shown to compare well with experiments in catalytic reforming systems.[3]

This analysis focuses on the *steady states* of the reformer. These are the starting points for understanding the full dynamic behavior of the system. At a particular steady state,

characterized by a fuel/air flow rate and plasmatron power, or simply ζ, reaction and flow are balanced, and heat release matches heat losses from the reactor, so the output gas mixture should have a well-defined temperature and chemical composition that do not change in time. This not only simplifies the calculations, but it is a good approximation to realistic operating conditions of the reformer (i.e. changes in input power and flow rate will be slow compared to system dynamics, so the reformer will always be in pseudo-steady state operation). Thus, the PSR model will allow calculation of the efficiency and H_2 production cost of the reformer, based on a model that closely approximates the actual device.

The variables governing the behavior of the reactor in this model are T_0, the temperature of the gas mixture immediately after plasma heating, and the residence time τ_r, given by the reactor volume divided by the *total* flow rate. The parameters that are actually varied are ζ and the reactor volume, as would be the case in an experimental system.

In order to allow a more intuitive analysis, it is assumed that the reaction within the volume is characterized by a single rate equation, so that it can be expressed as

$$\nu_f X_f + \nu_o X_o \xrightarrow{\hat{R}_r} \nu_p X_p \tag{7}$$

where ν_k is the net molar stoichiometric coefficient of species k, X_k is the mole fraction of that species, $\hat{R}_r$ is the reaction rate in molar units, and the subscripts f, o, and p stand for fuel, oxidizer and products, respectively. The unidirectional arrow in this expression indicates that the reverse reaction is very much slower than the forward reaction.

To find the heat release and rate of change of reactant concentrations in the mixture, the following Arrhenius expression for the rate of reaction is used:

$$\hat{R}_r = \rho^n A e^{-\frac{T_a}{T}} \frac{Y_f^{n_f} Y_o^{n_o}}{M_f^{n_f} M_o^{n_o}} \tag{8}$$

In the above expression, A, T_a, n_f and n_o are empirically determined coefficients, and $n = n_f + n_o$. T_a (in kelvin) is a indication of the energy required for reaction, whereas the A and n_k factors relate to the likelihood of reacting collisions between molecules in the mixture. These empirical coefficients are obtained experimentally or through reduction of chemistry models and must be chosen to be appropriate for the particular system under consideration.[4]

The mass rate of consumption of a particular reactant species is given by

$$w_k = -\rho \frac{dY_k}{dt} = \nu_k M_k \hat{R}_r \tag{9}$$

The units of w_k are kg of species k per cubic meter per second.

A further simplification can be made if it is known that the reaction is occurring at close to stoichiometric conditions (i.e. $\lambda = 0.25$). In this case, the molar rates of consumption of fuel and oxidizer are related by the mass stoichiometric ratio ϕ:

$$\frac{w_f}{w_o} = \phi = \frac{M_f \nu_f}{M_o \nu_o} \tag{10}$$

Using equations (9) and (10), a relation can be found between Y_f and Y_o:

$$\frac{w_f}{w_o} = \frac{dY_f}{dY_o} = \phi \tag{11}$$

Integrating the above, noting that $Y_{f,0} = \phi Y_{o,0}$, gives the following:

$$Y_o = \frac{1}{\phi} Y_f \tag{12}$$

Combining equations (8), (9) and (12) gives an expression for the mass rate of species production at near-stoichiometric conditions that depends only on T, ρ, and Y_f:

$$w_k = M_k \nu_k A e^{-\frac{T_a}{T}} \rho^{n_f + n_o} \frac{Y_f^{n_f + n_o}}{\phi^{n_o} M_f^{n_f} M_o^{n_o}} = k_k(\rho, T) \frac{Y_f^n}{\phi^{n_o}} \tag{13}$$

By making the further assumption that the mass-average specific heat of the mixture is a constant (a good assumption for dilute mixtures, such as those where air is used as the "oxidizer"), the mass fraction of fuel can be related to the temperature of the mixture:

$$c_p(T - T_0) = \frac{\Delta H_r}{\nu_f M_f}(Y_f - Y_{f,0}) = \Delta H_{r,f}(Y_f - Y_{f,0}) \tag{14}$$

where $\Delta H_{r,f}$ is the enthalpy of reaction per unit mass of fuel, in J/kg (this quantity is negative for an exothermic reaction), and T_0 is the initial temperature of the mixture in K. Since $\Delta H_{r,f}$ is a constant for a particular reaction, the above equation describes a linear relationship between T and Y_f. If all the fuel is consumed, Y_f in equation (14) becomes zero, and the "burned mixture temperature" T_b can be defined as:

$$T_b = T_0 - \frac{\Delta H_{r,f} Y_{f,0}}{c_p} \tag{15}$$

Note that for constant c_p, T_b is a constant that is independent of the reaction kinetics. Combining equations (14) and (15) leads to the relation

$$\frac{Y_f}{Y_{f,0}} = \frac{T_b - T}{T_b - T_0} \tag{16}$$

Substituting equation (16) into equation (13) leads to an expression for the mass rate of consumption of fuel per unit reactor volume that depends only on reactor temperature and mixture density (or pressure):

$$w_f = \frac{k_f(\rho,T)}{\phi^{n_0}}\left(\frac{T_b - T}{T_b - T_0}\right)^n Y_{f,0}^n = \frac{M_f \nu_f A}{M_f^{n_f} M_o^{n_o} \phi^{n_0}} \rho^n e^{-\frac{T_a}{T}} \left(\frac{T_b - T}{T_b - T_0}\right)^n Y_{f,0}^n \tag{17}$$

The units of this rate are kilograms of fuel per cubic meter per second.

The heat release rate of the reaction at a given temperature and pressure within the reactor is obtained by multiplying the above by the reactor volume and the enthalpy of reaction per unit mass of fuel:

$$\dot{Q}_r = V \Delta H_{r,f} w_f \tag{18}$$

where $\dot{Q}_r$ is the rate of heat release in J/s and V is the reactor volume in m^3. Note that $\dot{Q}_r$ has been chosen to be positive for an exothermic reaction proceeding in the "forward" direction.

The reaction heat release rate as a function of reactor temperature at a given pressure is shown graphically in Figure 4.7 (for hypothetical reaction conditions). It is helpful at this point to note the important qualitative features of this curve. At low temperatures, the heat release is almost zero, but as temperatures begin to increase, the heating rate increases exponentially. However, as temperatures increase further, $\dot{Q}_r$ passes through a maximum and then falls to zero at T_b. This phenomenon is a result of the trade-off of energy between mixture enthalpy and heat release. The reaction is the only source of energy release in the reactor volume. This energy goes to two places; part of it must heat the incoming reactant flow to the reactor temperature, and the remaining part comprises $\dot{Q}_r$. However, as was shown in equation (15) above, raising the temperature of a given amount of fuel/air mixture to T_b requires *all* of the heat released by the reaction of that mixture. Hence, at a reactor temperature of T_b, all the energy of the incoming mixture is used to maintain the temperature within the volume, and none is left as $\dot{Q}_r$.

There are two means by which energy may leave the reactor volume. The first is due to the fact that the gas flow leaves the reactor with a higher temperature than it had upon entering, so that more thermal energy leaves than enters the volume. With a constant c_p, the rate of energy leaving the volume with the flow is linearly related to the reactor temperature and can be expressed as

$$\dot{Q}_f = -\dot{m} c_p (T - T_0) \tag{19}$$

where $\dot{m}$ is the total mass flow rate through the volume in kg/s, and $\dot{Q}_f$ is the rate of heat loss in J/s. Note that since $\dot{Q}_f$ corresponds to energy removed from the volume, its sign is opposite from that of $\dot{Q}_r$, which represents energy added to the volume. The magnitude of this energy loss (for some c_p and mass flow rate) as a function of temperature is included in Figure 4.7.

An additional energy loss term $\dot{Q}_l$ can account for losses to the vessel walls. If we model the heat transfer to the walls as being characterized by a heat transfer coefficient κ, we have

$$\dot{Q}_l = -\kappa(T - T_0) \tag{20}$$

which has the same form as equation (19). A representative plot of $\dot{Q}_l$ is also included in Figure 4.7.

The remaining factor to be considered is the heating of the input gas mixture by the plasmatron. We can model this process by assuming that the electrical power supplied by the plasmatron will be transferred to the gas mixture as enthalpy with some efficiency η, which may be determined experimentally for a given plasmatron (see results section). We can make the further assumption that the gas heating occurs before the reaction begins. This corresponds well to the actual experimental arrangement, in which only the air passes through the arc, and the fuel is injected immediately thereafter. Thus, no reaction can occur until after the heating of the air, and since fuel is less than 20 percent of the mixture by mass, it is reasonable to assume that the temperature change upon fuel injection will be both small and rapid. Given these assumptions, the temperature of the gas mixture at the entrance to the reactor volume, T_0, is given implicitly by

$$\eta \frac{P}{\dot{m}} = \int_{T^0}^{T_0} c_p(T)dT \tag{21}$$

where η is the efficiency of the plasmatron, P the electrical power supplied, and T^0 = 298 K. Under the assumption of constant c_p, we can solve for T_0:

$$T_0 = T^0 + \frac{\eta P}{c_p \dot{m}} \tag{22}$$

Note that modeling the plasma heating in this way allows T_0 to be found explicitly knowing only the power and flow inputs and the plasmatron efficiency, which greatly simplifies the calculation, since T_0 is an important parameter in all three of the $\dot{Q}$ curves in Figure 4.7. The $\dot{Q}_f$ and $\dot{Q}_l$ lines always pass through zero at $T = T_0$, although their slopes are unaffected by variations in T_0. More importantly, the entire character of the $\dot{Q}_r$ curve changes with T_0; for example, if T_0 is high enough, the reaction heat release may start at a high level and decrease monotonically in the range T_0 to T_b.

The three curves shown in Figure 4.7 contain sufficient information for an analysis of the system behavior at and near steady states. The questions that we need to answer are the following: given pressure, flow and power conditions and reactor size, at what temperature or temperatures will steady states be achieved in the reactor, and how does the system behave near these steady state conditions?

At steady state, since the temperature within the volume is constant, the heat release from reaction must exactly balance the losses, so that the net heating rate in the reactor is

$$\dot{Q}_{net} = \left|\dot{Q}_r\right| - \left|\dot{Q}_f\right| - \left|\dot{Q}_l\right| = 0 \tag{23}$$

Graphically, this corresponds to an intersection point between the $\dot{Q}_r$ curve and the line

$$\left|\dot{Q}_f\right| + \left|\dot{Q}_l\right| = (\kappa + \dot{m}c_p)(T - T_0) \tag{24}$$

which is also included in Figure 4.7. One can see from this graphical representation that there may be multiple temperatures at which the system is in steady state, due to the shape of the $\dot{Q}_r$ curve. The number of intersections is limited by the geometries of the two curves to lie in the range from one to three. The nature of the system behavior near an intersection is determined by the position of that intersection in relation to the maximum of the $\dot{Q}_r$ curve. An examination of the possible types of intersections will show that only a few distinct varieties can exist.

Figure 4.7 shows three intersection points, the largest number that can exist for a given set of conditions. Figure 4.8 is a plot of $\dot{Q}_{net}$ within the reactor volume for the same conditions. As mentioned above, the points where $\dot{Q}_{net}$ crosses zero are the steady state temperatures. When $\dot{Q}_{net}$ is positive, the mixture temperature within the reactor will increase with time, and when $\dot{Q}_{net}$ is negative, the temperature will decrease. Given this information, we can see that both the lowest and highest steady state temperatures represent *stable* states; that is, a small increase in temperature will result in a negative $\dot{Q}_{net}$, and a small decrease will give a positive $\dot{Q}_{net}$, so that the temperature will return to the steady-state value. The middle steady state temperature is an *unstable* state; if the temperature is perturbed in either direction, it will continue to move away from the steady-state temperature. Thus, we can see that at these conditions with *any* initial temperature in the volume, the system will move in time to one of the two stable steady states, and will remain there unless some external disturbance is applied.

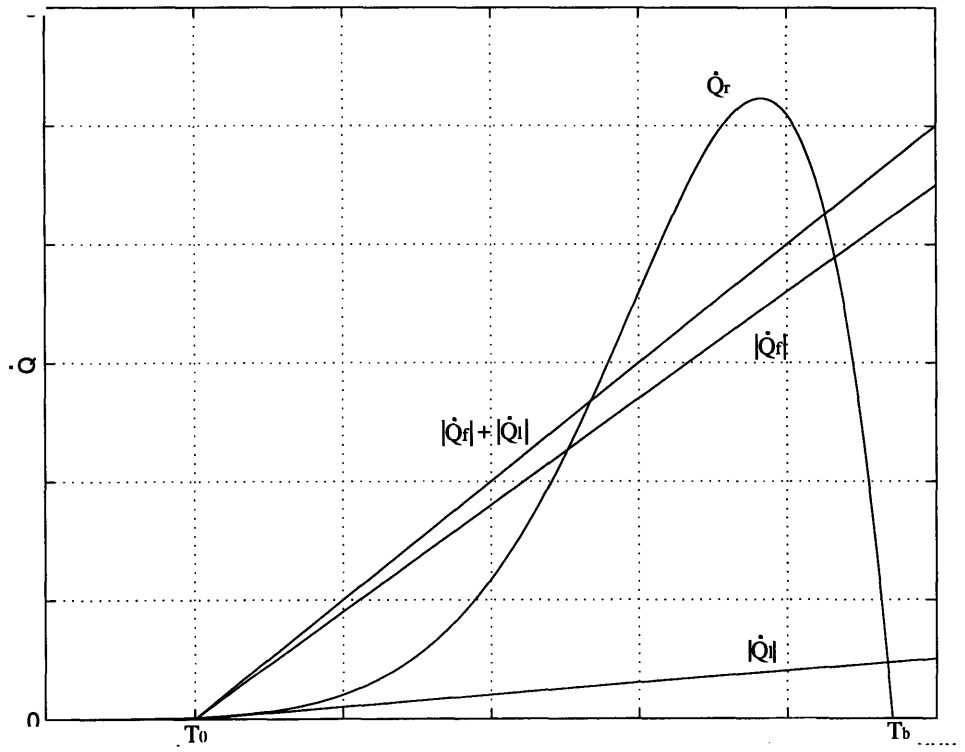

Figure 4.7. Heat release ($\dot{Q}_r$) and heat loss ($\dot{Q}_f, \dot{Q}_l$) rates (arbitrary units) for a perfectly stirred reactor model.

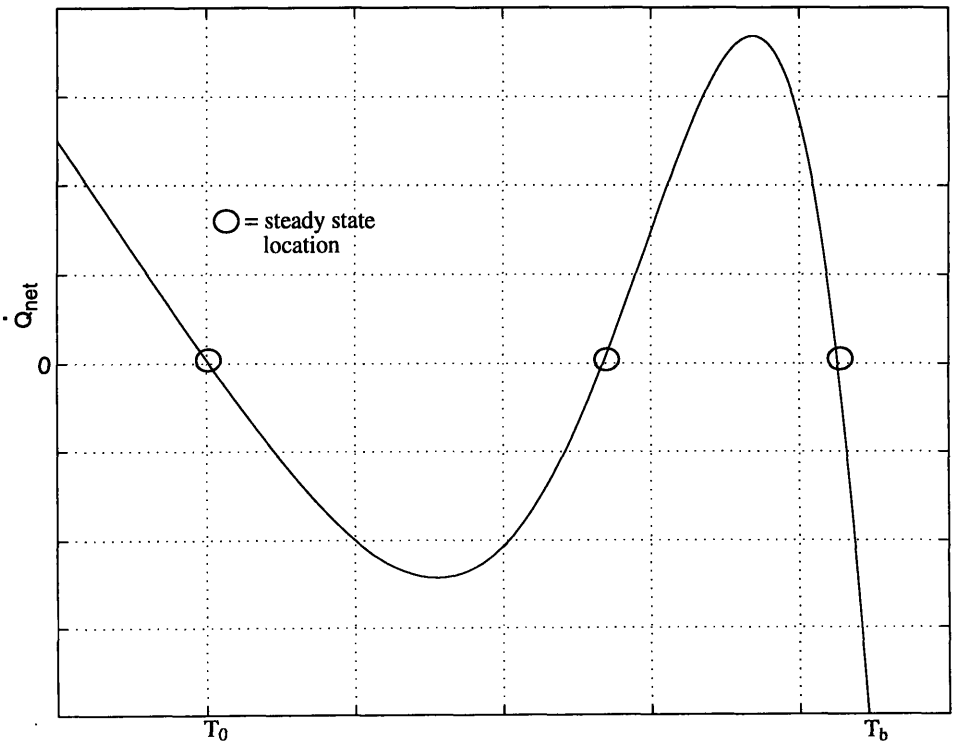

Figure 4.8. Net heating rate $\dot{Q}_{net}$ for the perfectly stirred reactor of Figure 4.7.

There are only two other possible types of intersection, which are both of key importance to the system behavior. These correspond to tangencies between the reaction heat release and heat loss curves. The two situations are shown in Figure 4.9. In the first case, the two curves are tangent at a low temperature. The corresponding plot of $\dot{Q}_{net}$ shows that perturbing the temperature in either direction will cause a temperature increase. Hence, this system will always end up at the high-temperature steady state. In the second case, the tangency occurs near the maximum of $\dot{Q}_r$, and perturbations in either direction will result in a negative $\dot{Q}_{net}$. This system, in contrast to the previous one, will always end up at the lower temperature steady state.

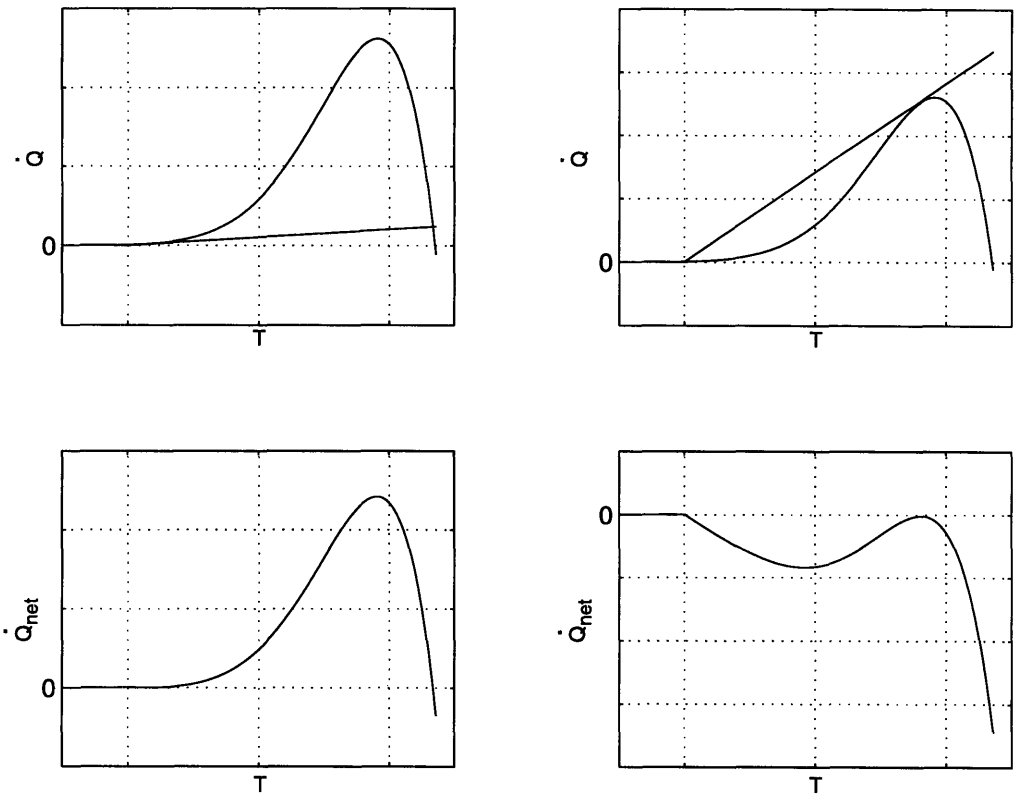

Figure 4.9. Tangency conditions for the perfectly stirred reactor model.

The steady states described allow us to determine some features of the dynamic nature of the reforming process. Since high reactor temperatures correspond to low values of Y_f in the reactor, the high-temperature steady states correspond to high levels of conversion. The low-temperature steady states, in contrast, describe modes of operation at which conversion is very poor (percent conversion in this model varies linearly with reactor temperature, as described in Equation (16)). Thus, we can say that our goal is to design a system which will operate at a

high-temperature steady state, and that will remain at this state in the presence of perturbations. The most significant design parameters (given that the fuel-air ratio is fixed at $\lambda = 0.25$) are ζ and τ_r, which are determined by the electrical power, total flow rate, and reactor volume. The effect of increasing ζ is to raise the inlet temperature, as given in equation (21), whereas τ_r clearly will determine the extent to which the reaction can proceed within the reactor.

One way to look at variations in ζ is to consider variations in total mass flow rate of fuel/air mixture at constant plasma power (presuming $\dot{Q}_l$ to be small compared to $\dot{Q}_f$). Under these conditions, the shape of the $\dot{Q}_r$ curve does not vary greatly, whereas the slope of $\dot{Q}_f$ is proportional to the mass flow rate. As the mass flow rate is increased from zero, several important features of the dynamic behavior of the system are encountered. At very low flow rates, there is only one available steady state, which is stable and occurs at temperatures near T_b. As the flow rate is increased, it eventually reaches the level where the lower-temperature tangency of $\dot{Q}_r$ and $\dot{Q}_f$ occurs. This is the highest flow rate at which the system *must* end up at the high-temperature steady state. Thus, it corresponds to an ignition flow rate, and the power-to-flow ratio under these conditions is ζ_i. For all flow rates between this point and the higher-temperature tangency, three steady states are available, as in Figure 4.7, and the system may operate at either high or low temperatures. The flow rate at which the high-temperature tangency occurs is the highest flow rate for which high-temperature operation *may* occur, although the high-temperature steady state is unstable; as such, it is referred to as the *blowout* or *extinction* flow rate, and the power-to-flow ratio is the minimum possible value for sustaining reaction, ζ_{min}. If the flow rate is increased so that ζ falls below ζ_{min}, it must be decreased until ζ reaches ζ_i to reignite the reformer.

The values of ζ_i and ζ_{min} will also depend on the reactor volume (which determines τ_r). Although it is a small effect, ζ_i and ζ_{min} both decrease with increasing volume.

From the above, we can see the main requirement for a reformer with our desired characteristics is that it must operate at ζ not less than ζ_{min} (for a given reactor volume). If the device is to retain a high rate of reforming (high temperature operation) in the presence of perturbations, it must either operate at a ζ of at least ζ_i or be able to move to ζ_i in the event of extinction.

This PSR model has been applied to the plasma reformer for a range of values of ζ and for a range of reactor volumes. The empirical reaction rate parameters used were $A = 4E9\ s^{-1}$, $T_a = 24400$ K, $n_f = -0.3$, and $n_o = 1.3$.[5] For $\lambda = 0.25$, $\psi = 1.11$ and $Y_{f,0} = 0.19$. All other parameters can be determined *a priori*. The major simplifying assumptions were the single-step reaction mechanism and constant mass-average c_p. The plasmatron heating efficiency η was

taken to be one, so all power values correspond to power reaching the gas as input enthalpy. It was also assumed that losses to the walls ($\dot{Q}_l$) were very small compared to flow heat losses ($\dot{Q}_f$).

The results are expressed in the following manner: ζ is given in units of MJ per kilogram of CH_4 (since λ is fixed, the mass of methane is proportional to the total input mass), and is varied over a range that corresponds to the capabilities of the experimental units currently in operation (power reaching the gas stream between 0 and 1.5 kW and CH_4 mass flow rates from 0 to 0.2 g/s). The reactor volume was varied from 1.0 to 1E-6 m^3 (the experimental reactor has a volume of roughly 1E-4 m^3).

Figure 4.10 shows the variation of the temperature of the highest temperature steady state, T_h, with ζ for a reactor volume of 1E-4 m^3. Note that increasing ζ corresponds to a lower total mass flow rate for a given input power, or higher power for a fixed flow rate. The features observed in the curve may be explained as follows: The first part of the curve corresponds to heating of the gas mixture by the plasma that is insufficient to ignite the reaction (i.e. T_0 is increasing, and T_h is very near T_0). Hence, the variation of T_h with ζ is linear, with a slope roughly proportional to c_p. ζ_{min} for this system occurs at approximately 7 MJ/kg CH_4. This accounts for the nonlinear portion of the curve, which is due to the heat release from the reaction. This is essentially a residence time effect; at ζ_{min}, the mixture ignites, but there is not sufficient time for the reaction to proceed very far within the reactor. Thus, little of the reaction heat release is available to increase the temperature within the reactor volume. As ζ increases, however, the reaction proceeds faster, and more heat is released within the volume. Thus, in this section of the curve, we see the combined effects of an increase in T_0 due to larger ζ (a linear effect) and a greater amount of reaction heat release, resulting in the observed nonlinear profile. After this region of the curve, the reaction proceeds essentially to completion (i.e. equilibrium product distribution) in the reactor, and the observed linear increase in T_h is once again entirely due to the increase in T_0 with ζ. Note that the temperature increase due to reaction is quite small compared to the plasma heating effect. It is clear from this plot alone that the optimal ζ for the reformer with this reactor volume should not occur at ζ_{min}, but at a higher value of ζ where more of the heat of reaction is being utilized.

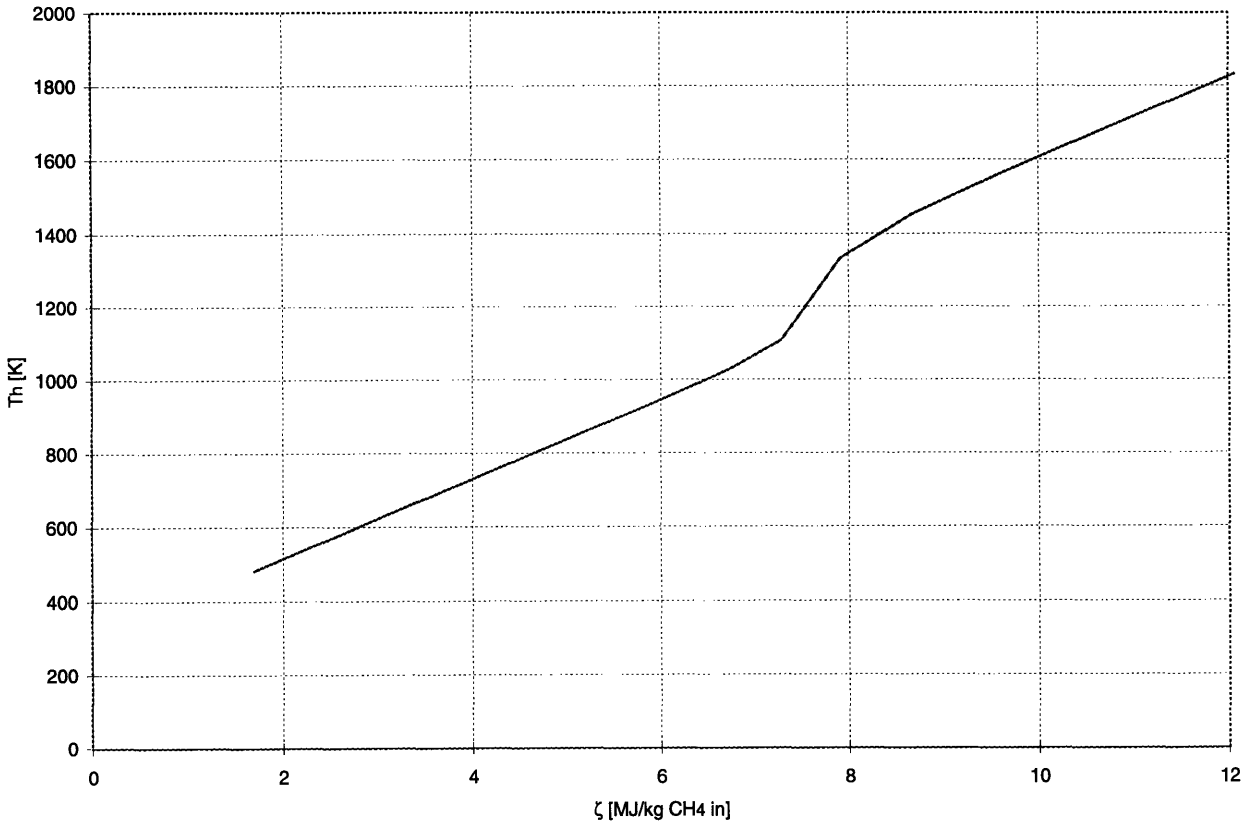

Figure 4.10. Variation of T_h with ζ for reactor volume of 1E-4 m3 (0.1 L)

The degree of conversion of CH_4, or extent of reforming, allows a more precise definition of ζ_{min}. Figure 4.11 shows the residual amount of CH_4 (as a percentage of the input amount) in the gas mixture at the outlet of the reformer as a function of ζ (again for a reactor volume of 1E-4 m^3). This plot assumes operation at the highest-temperature steady state available. The CH_4 level decreases from its input level to nearly zero within a small range of ζ (approximately 5 MJ/kg CH_4). Since these calculations assume a one-step reaction mechanism, the residual CH_4 level is directly related to the production of H_2. The output H_2 concentration (normalized by CH_4 input) is also shown in Figure 4.11. ζ_{min}, identified above with the blowout value of ζ, is essentially a measure of the energy required to support the reaction within the reformer. For the sake of consistency, ζ_{min} may be defined (somewhat arbitrarily) as the value of ζ where the CH_4 concentration drops below 90 percent of its initial value; in this case, ζ_{min} = 6.9 MJ/kg CH_4.

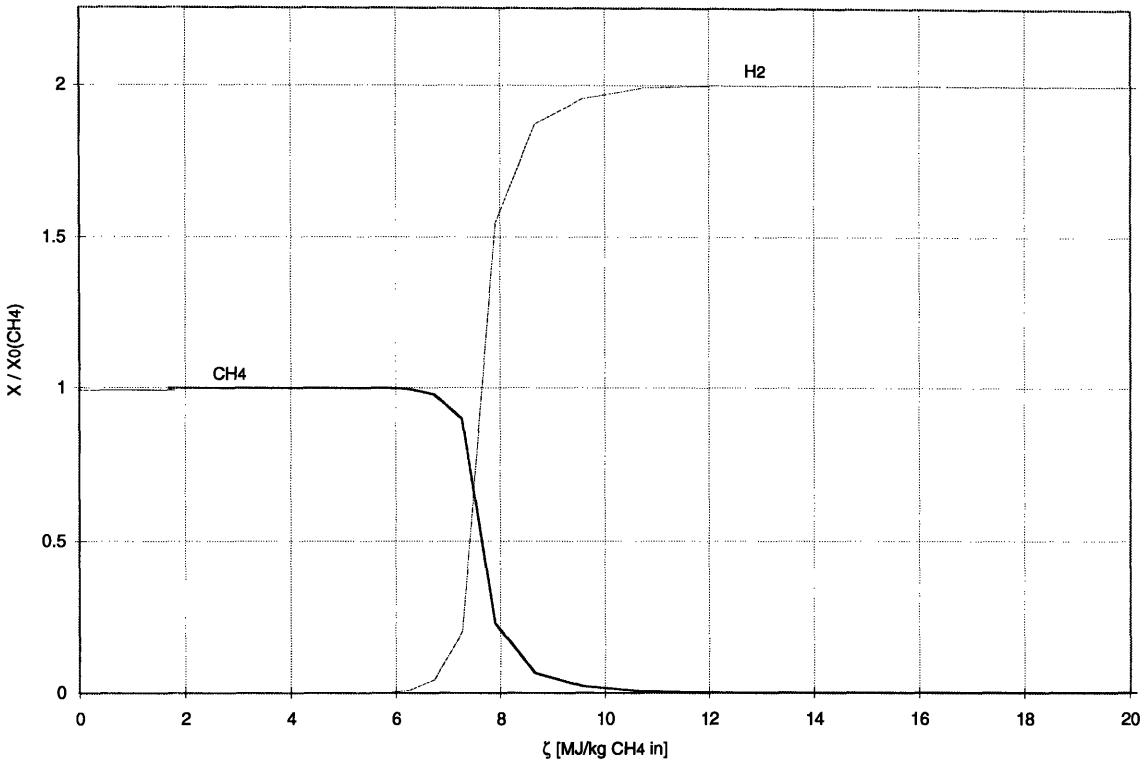

Figure 4.11. Variation of output CH_4 and H_2 levels relative to initial CH_4 with ζ for reactor volume of 1E-4 m^3

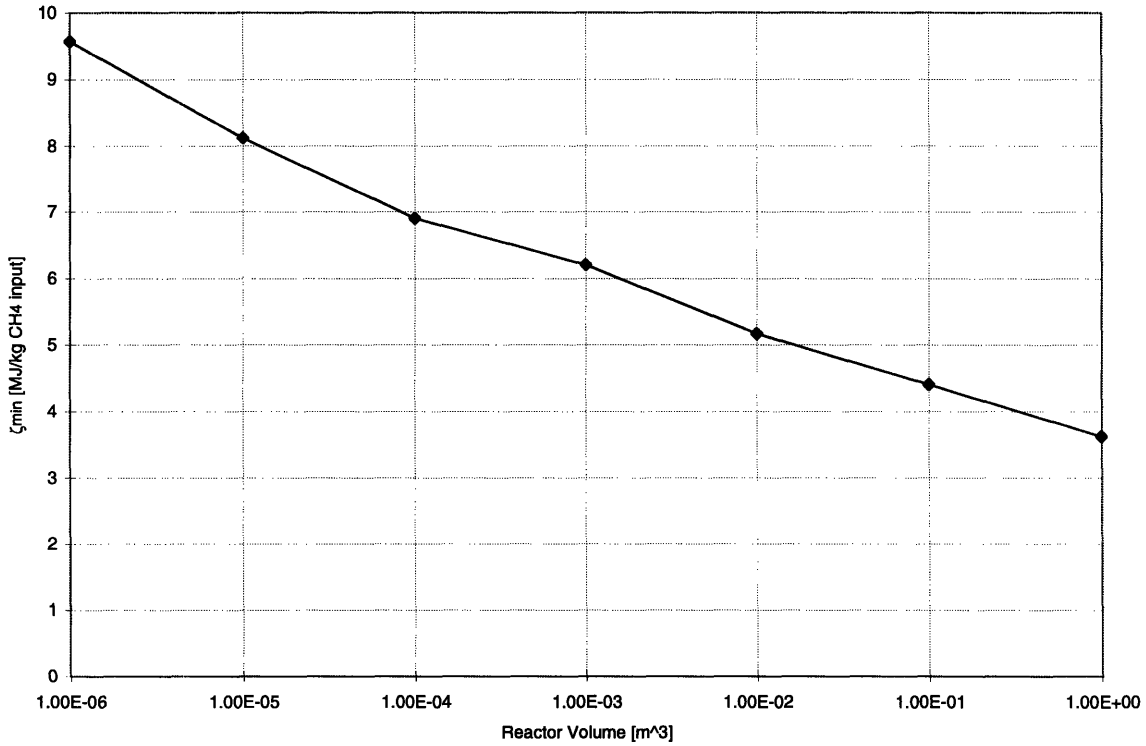

Figure 4.12. ζ_{min} as a function of reactor volume (abscissa scale is logarithmic)

The effect of changes in volume on ζ_{min} is shown in Figure 4.12. Note that this effect is very small; a change of an order of magnitude in volume corresponds to a change of approximately 1 MJ/kg CH_4 in ζ_{min}. Thus, in forming a physical model of the reformer, the accuracy of the reactor volume is not a critical factor, which is useful since this volume may be difficult to define in a real system.

The results given in the preceding figures allow us to define the "energy cost" of reforming, C, as the amount of energy input to the reformer per unit mass of H_2 produced, as was done with the plug flow reactor model. The variation of this energy cost with ζ is given in Figure 4.13. According to this model, the optimal operating condition for H_2 production for a reactor volume of 1E-4 m^3 is at the minimum of the curve, C_{opt} = 37 MJ/kg H_2, which corresponds to ζ_{opt} = 8.9 MJ/kg CH_4 at the input to the reformer. This value of ζ_{opt} gives a reactor temperature T_h = 1500 K. According to the thermodynamic analysis of the previous chapter, this temperature should correspond to a thermodynamic efficiency of 76 percent. Since at ζ_{opt} the output composition will be close to the equilibrium composition, the same energy efficiency should apply to the kinetic process. Figure 4.14 shows the variation of ζ_{opt} and C_{opt} with reactor volume.

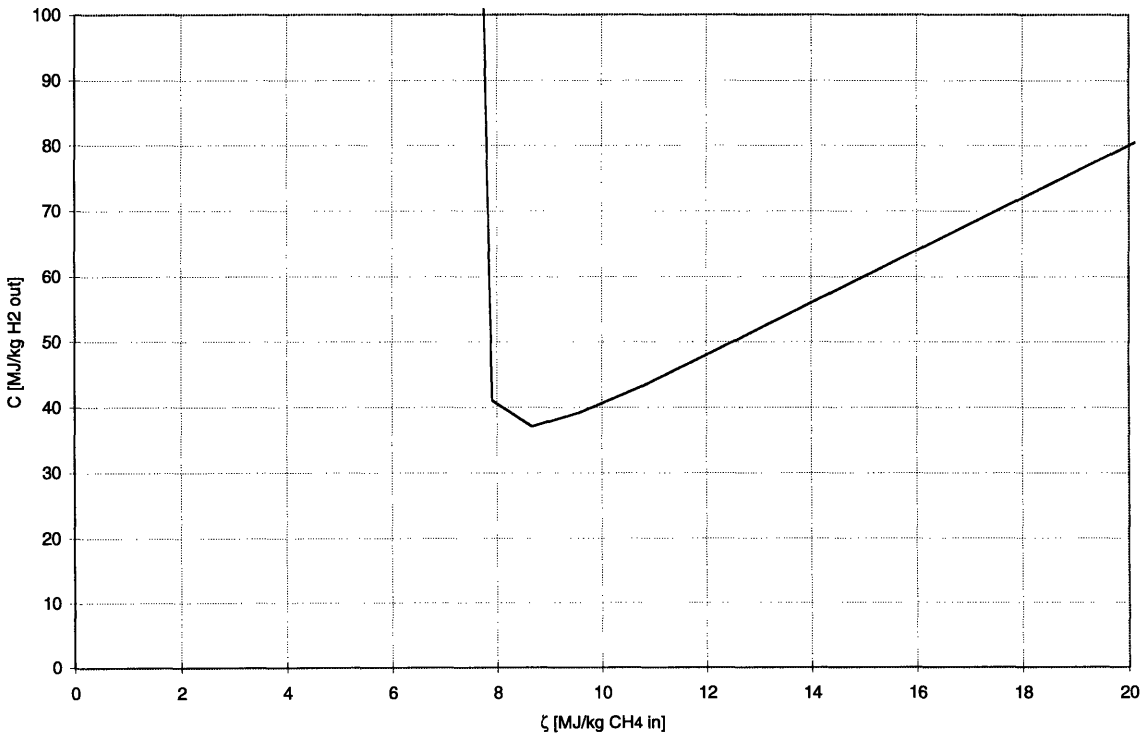

Figure 4.13. Variation of energy cost of H_2 production (C) with ζ for reactor volume of 1E-4 m^3

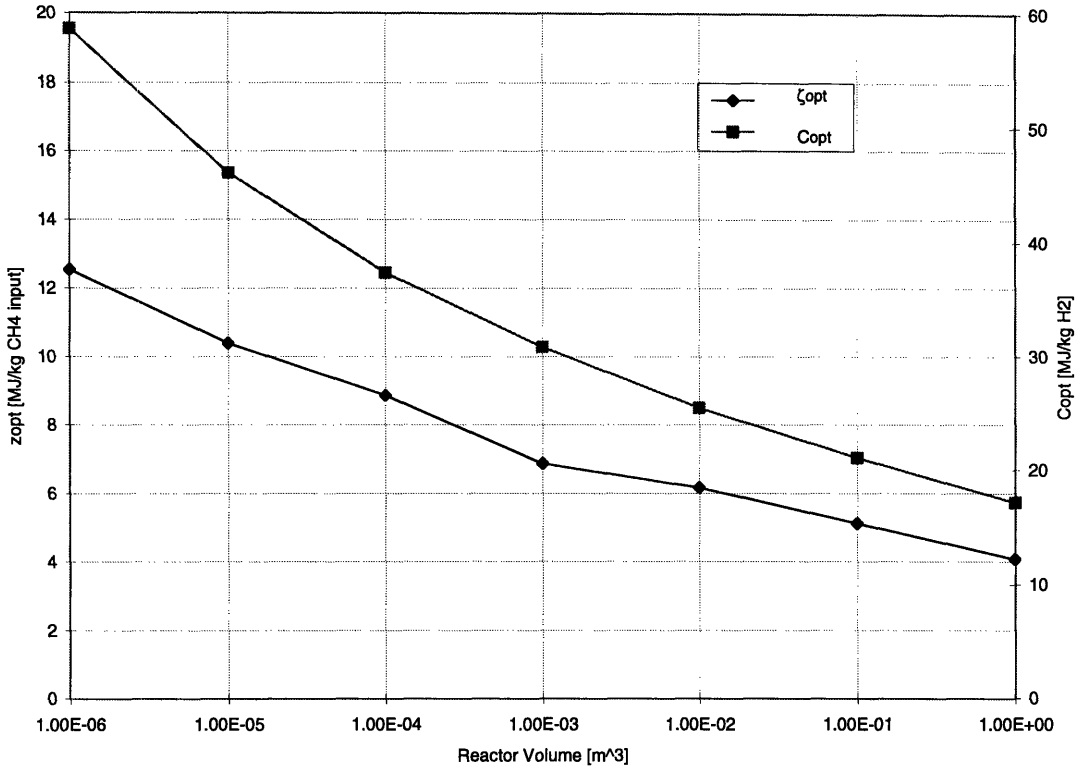

Figure 4.14. Variation of ζ_{opt} and C_{opt} with reactor volume

Since the above results are based on a physical model of the reformer, they may be used as an aid in reformer design and scaling. As will be described in the following sections, the results of this model show quantitative agreement with experimental observations, which suggests that the assumptions made in the derivations above are reasonable approximations to the actual physical system.

4.4 Conclusions

The two models discussed in this chapter represent opposing assumptions for mixing in the reactor; the plug flow calculations correspond to purely local mixing, while the perfectly stirred reactor assumes homogeneous mixing throughout the reactor. Hence, areas where the predictions of the two models are in close agreement point to system characteristics that are relatively independent of the type of mixing in the reformer. Until the character of the mixing is measured experimentally, it is these results that are the most useful as guides for reactor design.

Such an area of agreement is found in the predictions of optimal energy inputs and energy costs for H_2 production made by the two models. Both models predict that ζ_{opt} will be close to 10 MJ/kg CH_4, with C between 40 and 50 MJ/kg H_2. This supplies us with a useful

design parameter for the plasmatron; different combinations of power and flow rates that lie in this region can be explored in order to optimize the gas heating.

It is also useful to examine the results of the kinetic models in light of the thermodynamic analysis of Chapter 3. As discussed, the optimum thermodynamic efficiency of 83% occurs at zero energy input, since the partial oxidation reaction is exothermic. The models in this chapter help to quantify the price one has to pay to drive the reaction towards equilibrium within a finite residence time, or equivalently, inside a reactor of finite size. For both models, the loss in efficiency is less than ten percent.

Perhaps the most important use of these models is to identify the most important system parameters and potential difficulties. The plug flow calculations point to the importance of the residence time for H_2 production; most of the H_2 comes from a slow process, making this a critical issue. An important consideration that goes along with larger residence times is the minimization of heat loss from the reacting mixture. The perfectly stirred reactor model highlights the issues of ignition and extinction; which become very important when operating near the optimal energy input level, where extinction is possible through small power or flow fluctuations. These areas that are emphasized by the two models are important guides for experimentation and further numerical modeling.

4.5 REFERENCES

[1] M. Frenklach, H. Wang, C.T. Bowman, R.K. Hansen, G.P. Smith, D. Golden, W. Gardiner, V. Lissianski, "GRI-MECH," Gas Research Institute report, in press (1995).

[2] R.J. Kee, F. M. Rupley, J.A. Miller, "CHEMKIN-II: A FORTRAN Chemical Kinetics Package for the Analysis of Gas Phase Chemical Kinetics," Sandia National Laboratories Report SAND89-8009 (1989).

[3] B.F. Gray, J.F. Griffiths and G.A. Foulds *Natural Gas Conversion II* (The Netherlands, Elsevier Science) p. 13 (1994).

[4] N. Peters, B. Rogg (eds.) Reduced Kinetic Mechanisms for Applications in Combustion Systems (Berlin, New York: Springer-Verlag, 1993).

[5] C.K. Westbrook, F.L. Dryer, *Combustion Science and Technology* **27** p. 31 (1981).

CHAPTER 5

Experimental Apparatus

5.1 INTRODUCTION

A laboratory has been constructed for the study of fuel reforming in small-scale plasma reactors. The equipment has been designed so as to provide a versatile experimental and diagnostic apparatus for the study of plasma-assisted chemical reactions, allowing for a range of different plasmatron and reactor designs.

5.2 THERMAL ARC PLASMATRON

A schematic diagram of the plasmatron used for the experiments discussed in this work is shown in Figure 5.1. The device is based on a commercial plasma cutting system (Thermal Dynamics Pak Master 25). The power supply consists of an adjustable current-regulated source capable of an open-circuit voltage of 400 V and a radiofrequency oscillator circuit that is used for ignition of the arc. The oscillator output reaches approximately 5000 volts peak-to-peak. The working gas for the plasmatron (air, nitrogen or argon) is supplied through an internal regulator in the power supply; a single line serves both to carry the working gas to the air gap in the plasmatron and to connect the cathode to the negative terminal of the power supply. The unit has been modified to operate at two current ranges; the first allows current adjustment from 5 to 8 amperes at an arc voltage drop of approximately 160 volts; the second gives adjustable current from 14 to 20 amperes at a voltage drop of 100 to 130 volts.

The plasmatron itself consists of a commercial cathode, also from the plasma cutting system, a water-cooled anode and an insulator. The cathode is a steel rod with a zirconium insert at the tip (Thermal Dynamics 5-0250); curved channels are carved into the tip of the rod in order to induce swirl in the working gas. The copper anode is cooled by water flow through four channels approximately 1 mm in diameter; a large central channel (approximately 1 cm diameter) carries the gas flows. A step in the diameter of the central channel creates a recirculation zone that stabilizes the arc length. The gap between cathode and anode is maintained by a G10 insulator. When the radiofrequency voltage oscillation is imposed between the cathode and anode, the arc ignites at the point of smallest separation between the electrodes; the stream of ionized gas is then carried out past the step in the channel by the flow of the working gas. Once the arc is established, it is driven by a DC current from the power supply. The swirl of the flow causes the root of the arc to move about rapidly on the cathode and anode surfaces, thus preventing damage to the materials from the high energy densities in the arc and decreasing heat loss rates. The gas in the arc is in a thermal plasma state, with both

ionization temperatures and thermal temperatures on the order of 10,000 K. Although the response time of the device has yet to be measured, the timescale for arc ignition is less than one second over the full range of operating conditions.

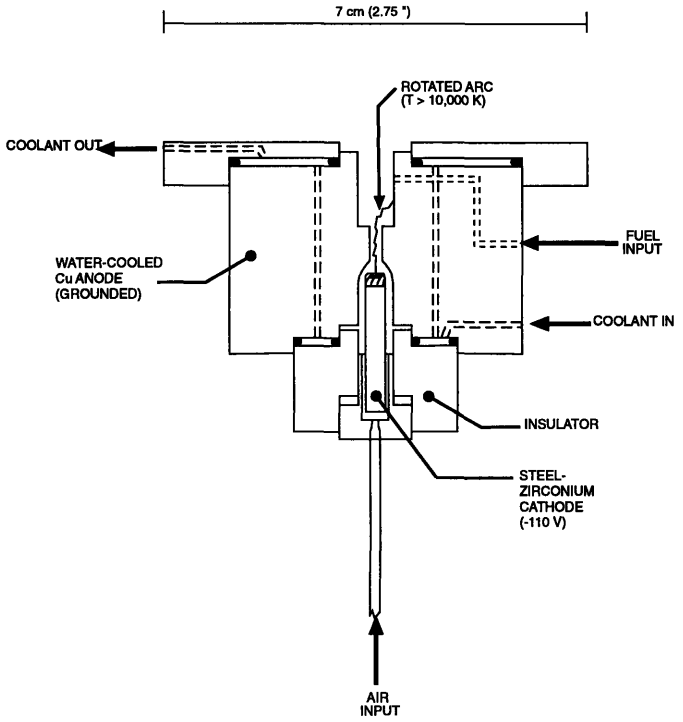

Figure 5.1. Schematic diagram of the research plasmatron (bar indicates size; internal dimensions not to scale).

Reactants may be injected at two axial positions in the plasmatron. The first is a one-point injection port located just downstream of the location of the arc root on the anode (shown in Figure 5.1); the second provides two-point injection, and is located at the outlet of the anode channel. Several flow configurations are possible, including an inert working gas with premixed reactant injection, air as a working gas with pure fuel injection, and air as the working gas with premixed air and fuel injection. These options allow independent variation of the air-to-fuel ratio, gas heating rate and plasma characteristics.

The plasmatron operates at powers of 1 to 2 kW, with air flow rates less than 0.5 g/s. Gas flow at the plasmatron outlet is relatively turbulent, with Re $\approx$ 2600. Calculated output gas temperatures range from 1000 K to over 4000 K.

The facility is easily adaptable to varying plasmatron designs; two additional units have been tested to date. The first operates from 500 W to 2 kW at low flow rates (0.1 to 0.2 g/s air) in a laminar flow regime (Re $\approx$ 500); the second can function at up to 10 kW and uses higher flow rates (>1 g/s air, Re $\approx$ 5100).

5.3 PLASMATRON DIAGNOSTICS

Figure 5.2 is a schematic of the diagnostic apparatus associated with the plasmatron itself. Gases used as the plasmatron working gas include air (BOC Gases, industrial grade), nitrogen (BOC, Grade 5) and argon (Matheson Gas Products, Grade 2.2). All gas flows are monitored by rotameters (Omega models FL-3840C and FL-3839G); flow rates up to 1.5 g/s of air at STP can be supplied to the plasmatron, and up to 0.2 g/s of methane and 0.3 g/s of air to the injection port. A single pressure transducer and digital meter (Setra Systems, models 205.2 (100 psia) and DATUM-2000) are employed to monitor the pressure at all flow meters through a solenoid valve system. Gas flows from the two reactant flowmeters are premixed by flowing through a long mixing tube before reaching the plasmatron injection point; 30-micron filters are used as flame arrestors on both ends of the mixing tube.

Cooling water flow to the anode is monitored by a rotameter (Omega, FL-1016); additional rotameters are available to provide coolant flows to the reactor and to the cathode in cooled-cathode plasmatron designs. The coolant temperatures at all inlet and outlet ports are monitored by type K thermocouples (Omega model GKMQSS-062G) immersed in the water flow.

The arc voltage is measured by a digital meter (Omega DP460-V) connected to a 1000:1 voltage divider with an equivalent impedance of approximately 150 MΩ and a low-pass filter to protect the meter from the oscillator voltage. The total power reaching the meter is less than 0.25 W during oscillator operation and less than 1 mW when an arc is established in the plasmatron. Current is measured by a 2.5 milliohm shunt (Omega DCS1000-40) located in the ground return line from the anode and a digital panel meter (Omega DP18-DS).

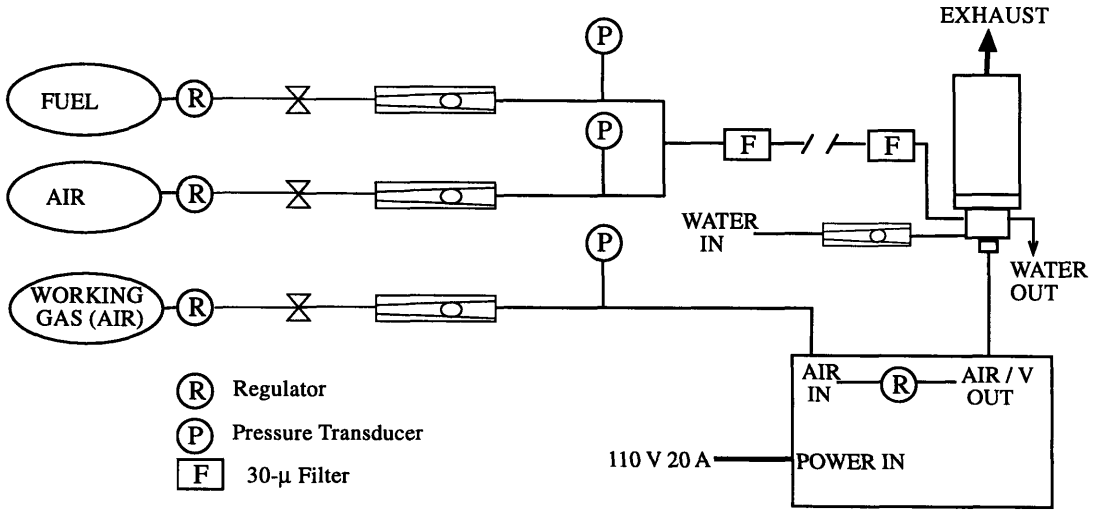

Figure 5.2. Schematic diagram of the plasma fuel reformer apparatus.

5.4 Gas Chromatography Diagnostics

Figure 5.3 indicates the arrangement of the gas chromatography diagnostic system for species concentrations. The gas chromatograph (GC) used (MTI model M200) consists of a sample loop, vacuum pump, and two columns, each with an injector valve and thermal conductivity detector (TCD). The first column is a Molecular Sieve 5A PLOT using argon (BOC, Grade 5.0) at 25 psi as the carrier gas, and is capable of separating H_2, O_2, N_2, CO and CH_4. The second column, a PoraPLOT U, uses helium at 25 psi as the carrier gas (BOC, Grade 5.0) and can resolve composite air, CH_4, CO_2, and some higher hydrocarbons, notably acetylene (C_2H_2), ethylene (C_2H_6) and propane (C_3H_8). Gas samples are provided directly from the reactor by means of a water-cooled sampling probe, shown schematically in Figure 5.3. The probe consists of a 0.5 mm inner diameter fused nickel tube, one end of which is soldered into the side of a copper tube. Water flows through the outer tube counter to the flow direction in the nickel tube, so as to quench the sampled gas as quickly as possible. The reactor section shown in Figure 5.3 is designed to provide a large number of GC sampling points. At each of four axial locations, spaced approximately 2 cm apart, the sampler may be inserted in either of two orientations at 90° to each other. The sampler inlet can be moved to any position along the diameter of the reactor. This arrangement allows the measurement of both axial and radial concentration variations, with the slight disadvantage that the sampler/reactor unit must be disassembled in order to change the axial sampling location. The GC system has been calibrated using a gas mixture of 20.2 volume percent H_2, 20.0 percent CH_4, 10.0 percent CO, 10.0 percent CO_2, and 39.8 percent N_2 (Matheson Gas Products).

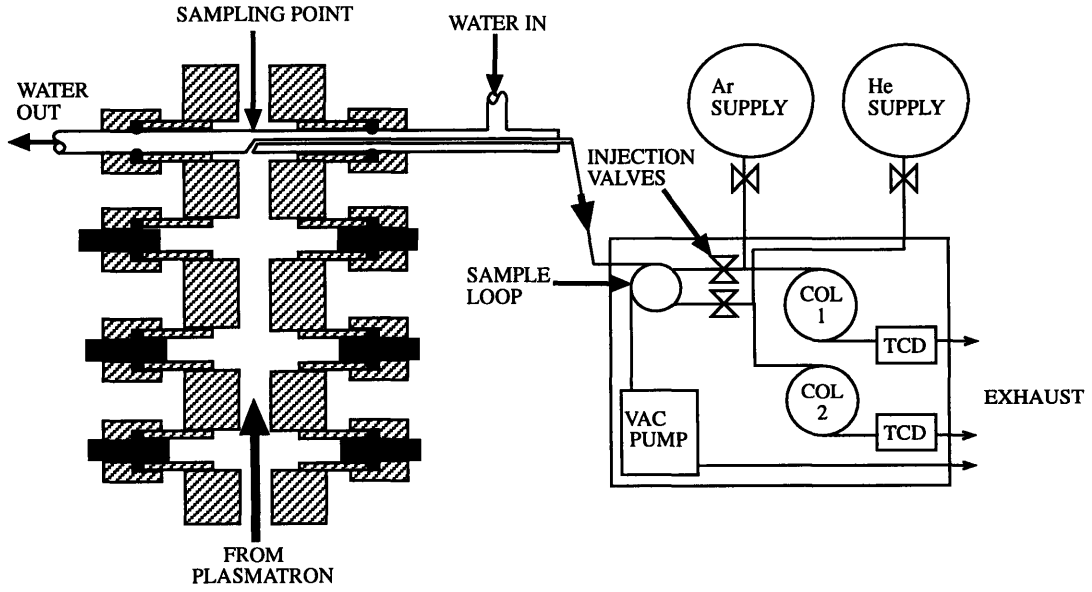

Figure 5.3. Sampler and instrumentation for gas chromatography diagnostics.

5.5 FT-IR DIAGNOSTICS

A system is currently under development to measure both species concentrations and temperatures non-intrusively through *in-situ* Fourier transform infrared (FT-IR) spectroscopy. Similar diagnostic methods have been used previously in combustion systems.[1] Figure 5.4 shows a schematic of the prototype system. The apparatus is based on a Nicolet Magna-IR 550 spectrometer with DGTS-A and liquid nitrogen cooled MCT-A detectors. This unit has been modified so as to pass the source radiation through an external reactor before it reaches the detector. A detailed view of the reactor section used for infrared access is included in Figure 5.5. The cylindrical reactor is water-cooled to stabilize the wall temperature; an uncooled or heated reactor could be substituted to decrease heat losses. Calcium fluoride (CaF_2) windows are used (Ealing Electro-Optics 36-1790, 50.8 mm diameter x 4 mm) which have a peak transmission in the infrared of greater than 90 percent over the wavelength range 0.3 - 7 μm. A slight flow of nitrogen gas (BOC Gases, Grade 2.0) is passed over the inner window surfaces to prevent damage by water in the reacting mixture and to insulate from thermal shock when the plasma is ignited. The aperture allows optical access to a section of the cylindrical reactor 3.5 cm in length; the entire width of the reactor can be observed. The optics associated with this reactor allow the infrared beam to be located at any axial and radial position within the optically accessible area; the beam position can be moved at any time during an experiment. Spatial resolution is adjustable by means of an iris, at the expense of signal throughput.

Initial results with the FT-IR diagnostics are promising; frequency resolution of 2 cm^{-1} has been achieved in experimental measurements. Portions of two experimental spectra are included in Figure 5.6, showing the ν_3 absorption band of methane in cold flow and during plasma-driven reforming. Concentration measurements are obtained from the integrated area under bands such as this one, and temperature is obtained from the relative intensities of the lines contained in the band, which correspond to different rotational transitions of the molecule. Temperature resolutions of ± 50 K have been achieved with related *in-situ* FT-IR systems, and the initial results suggest similar resolution for this apparatus.[2]

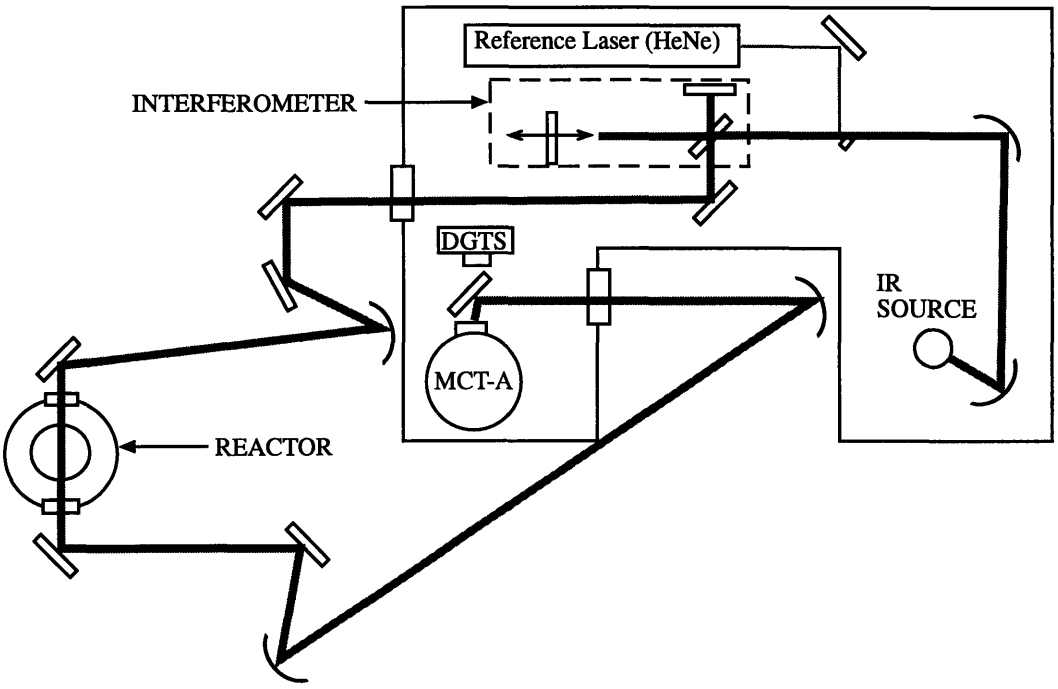

Figure 5.4. Schematic diagram of *in-situ* FT-IR spectroscopy system.

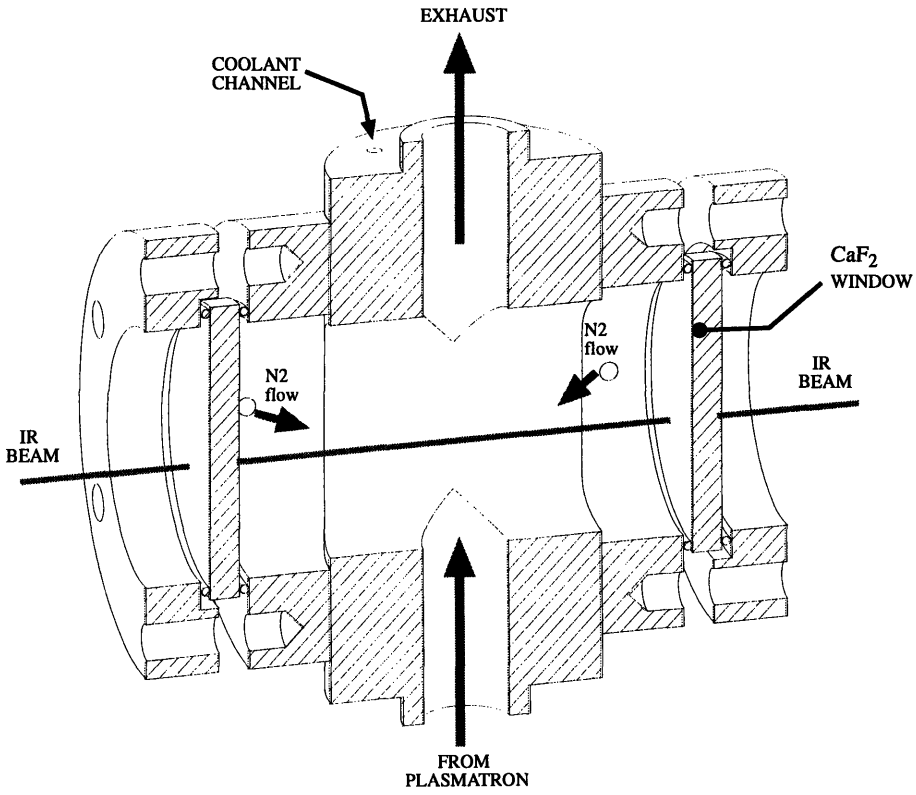

Figure 5.5. Cross-section view of reactor section for infrared access.

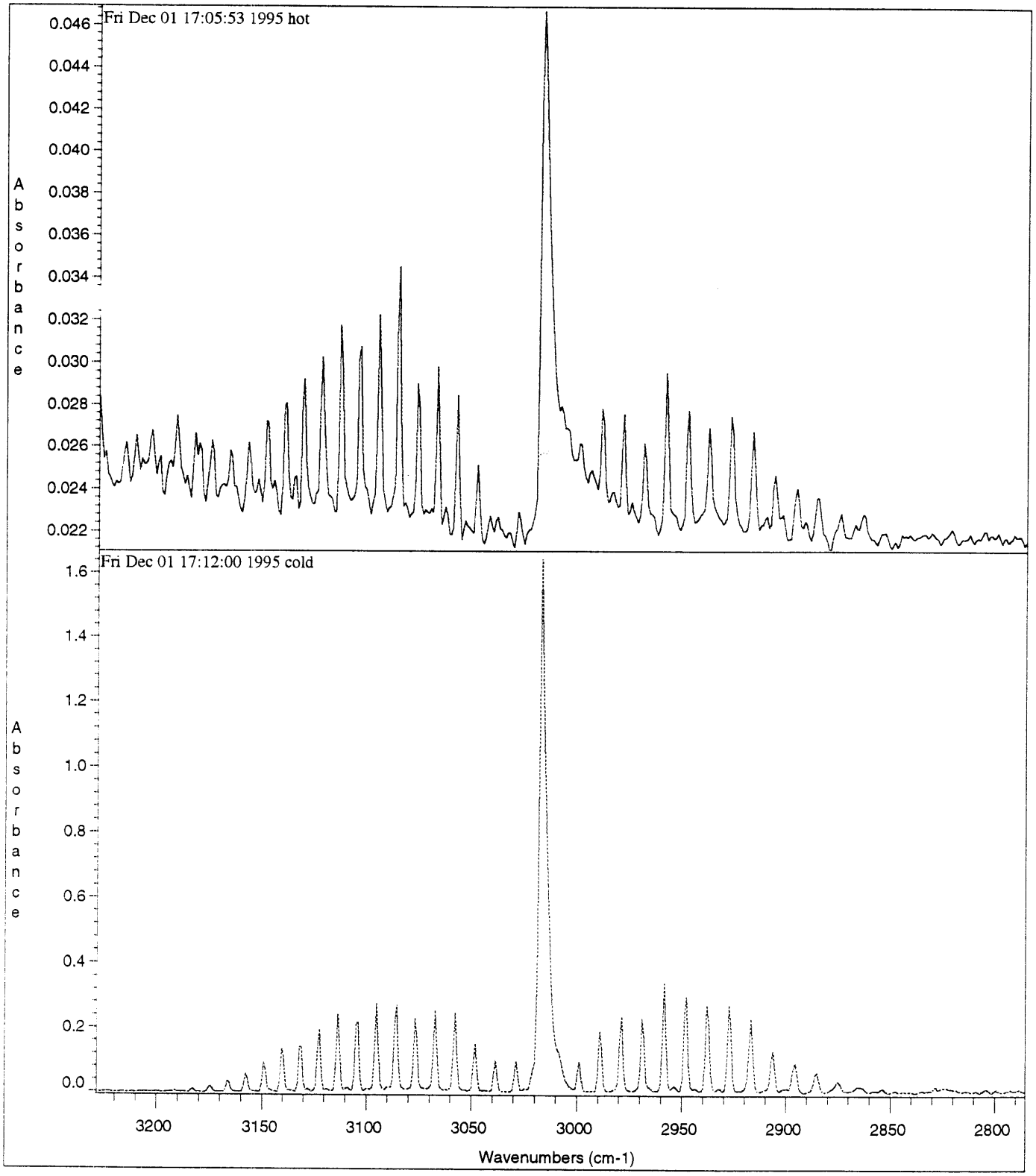

Figure 5.6. Spectra of the ν_3 absorption band of CH_4, taken using the apparatus from Figures 5.4 and 5.5. Upper spectrum was taken during plasma-driven reforming (T > 1000 K); lower spectrum shows cold flow for the same input flow rates (no plasma).

5.6 REFERENCES

[1] P.R. Solomon, P.E. Best, R.M. Carangelo, J.R. Markham, P.L. Chien, R.J. Santoro, and H.G. Semerjian, *Twenty-First Symposium (International) on Combustion*, The Combustion Institute, Pittsburgh, p. 1763 (1987).

[2] P.E. Best, P.L. Chien, R.M. Carangelo, P.R. Solomon, M. Danchak, and I. Ilovici, *Combustion and Flame* **85** 309 (1991).

CHAPTER 6

Analysis of Experimental Results

6.1 PLASMATRON CHARACTERISTICS

The first experimental priority was to quantify the performance characteristics of the plasmatron itself. These include ranges of operation in electrical power and total gas flow rate, heat loss rates, and the efficiency of transfer of input electrical power to output gas enthalpy. Although several plasmatron models are currently under development, only one has been used in the experiments to be presented herein; all the data presented below on plasmatron performance correspond to this particular unit.

6.1.1 Power and flow ranges

The accessible flow and power ranges for a given plasmatron are determined by the limitations of the plasmatron unit itself and those of the power supply. The design of the plasmatron and the gas supplies place an upper bound on the flow of the working gas. The dimensions of the gap between electrodes, along with the pressure range of the working gas supply and the physical properties of the working gas itself, determine the range of flow rates that are available. In the current experimental device, air flow rates up to 0.6 g/s can be achieved with a supply pressure of 7 atm (see Chapter 5). However, the establishment of a stable electrical arc depends on the interaction between this flow and the current and voltage imposed by the power supply. Figure 6.1 shows the relation between flow rate of air through the plasmatron and arc voltage for several arc currents, indicating that the arc voltage tends to increase with flow rate.[i] As the flow rate increases, the air flow carries the stream of ionized gas originating at the cathode further in the axial direction before it meets the anode wall. This "arc stretching" effect limits the flow rates at which an arc can be established for a given current to those for which the associated voltage can be provided by the power supply. The design of the research plasmatron incorporates a step in the diameter of the central channel in order to reduce the magnitude of the arc stretching. The sudden increase in diameter creates a recirculation zone that brings the ionized gas to the anode wall quickly, keeping the arc length relatively constant over a wide range of flow rates; the total variation in voltage with a doubling in air flow rate at a given current is less than 19 percent. Hence, the upper bound on flow rate is imposed either by the flow limit imposed by the plasmatron and gas supply or by the highest

[i] It should be noted that the current-voltage relation for an electric arc is not linear.

voltage that the power supply can provide at a given current. Due to the arc stabilization in the current arrangement, the former is the practical limitation. A lower limit on the flow rate is imposed by the loss of swirl that accompanies decreased flow speeds. Heat losses to the anode are dependent upon the amount of time that the root of the arc spends in any one region; the swirling flow of working gas causes the arc root to move rapidly across the anode surface. If the amount of swirl is insufficient, the power consumption due to heat losses can overcome the capabilities of the power supply. With increasing currents, the swirl-based lower flow limit is approximately constant.

Given the above constraints, the operating range of the research plasmatron is shown in Figure 6.2. Flow rates range from 0.26 to 0.53 g/s of air, and power can be varied from 1.5 to 2.4 kW.

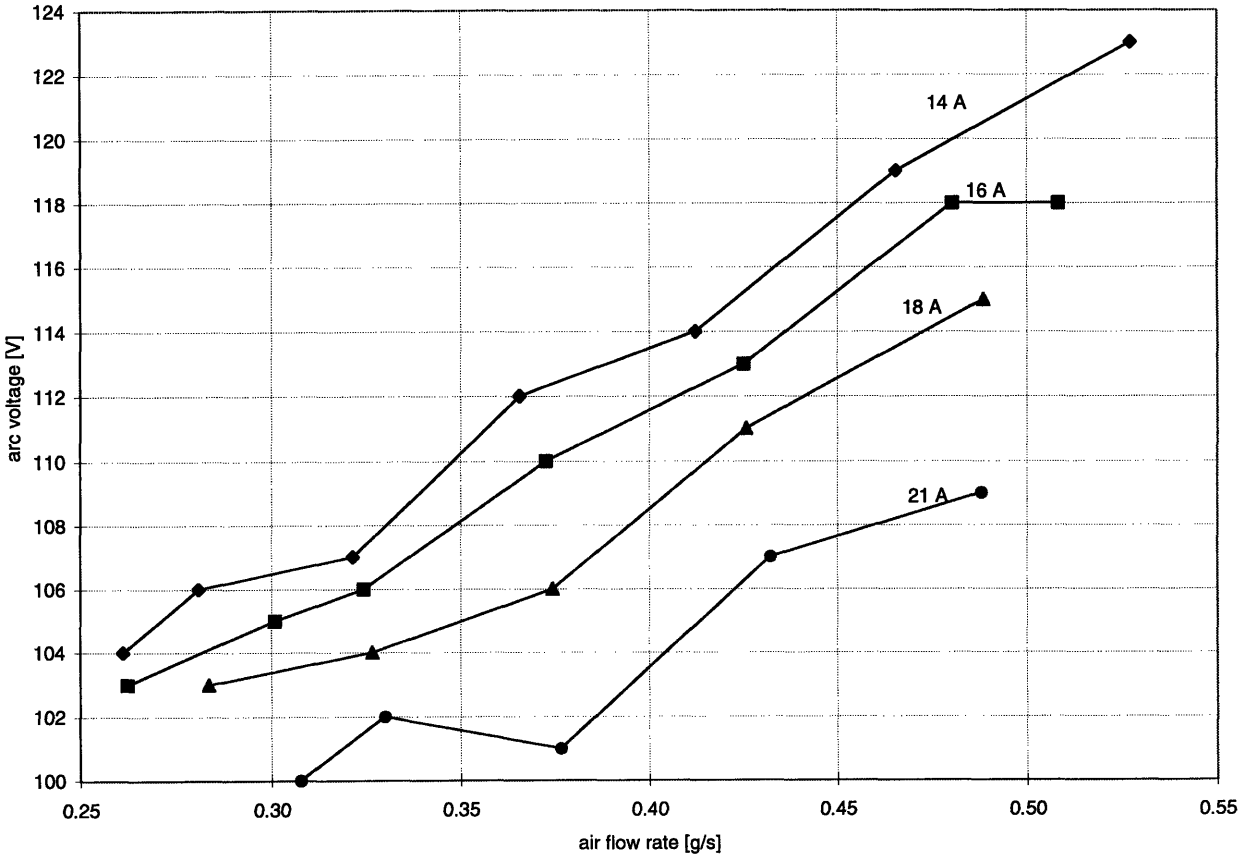

Figure 6.1. Arc voltage versus air flow rate for the research plasmatron at several currents.

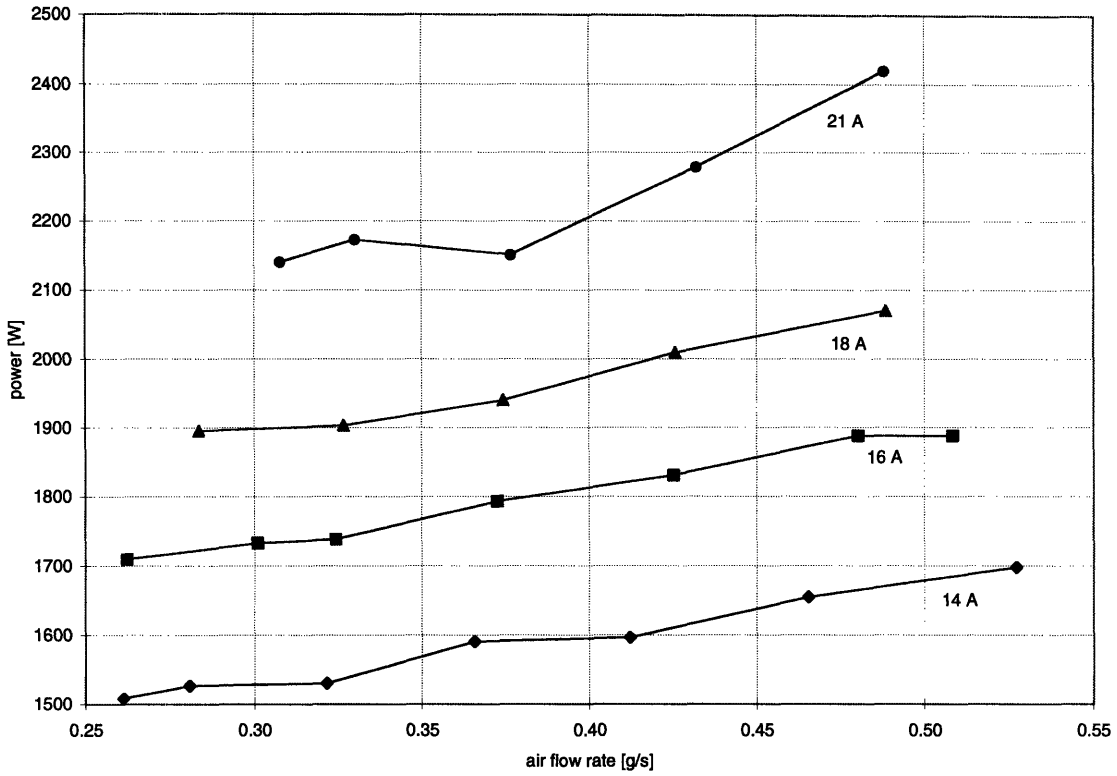

Figure 6.2. Power versus air flow rate over the accessible range of the research plasmatron.

6.1.2 Heat losses and thermal efficiency

Heat losses from the plasmatron were monitored through the temperature increase of the anode cooling water (see Chapter 5 for a description of the plasmatron diagnostics). All data were taken with the plasmatron in steady state operation. At these conditions, the outside of the anode is at room temperature, and there are no appreciable radiation losses; hence, the only two significant means for energy flow out of the plasmatron are the enthalpies of the gas stream and the cooling water. The rate of energy loss to the coolant for a given flow rate and temperature increase (assuming that the water is incompressible and that its specific heat is approximately constant over the temperature interval) is given by

$$P_l = \dot{m}_{H_2O} c_{v,H_2O} \Delta T$$

where c_{v,H_2O} is the specific heat at constant volume of liquid water in J/kg.K (taken at 298 K), $\dot{m}_{H_2O}$ is the mass flow rate of water through the anode in kg/s, and ΔT is the temperature difference between the outlet and the inlet in kelvin.

During steady state operation, the power flowing into the plasmatron must equal the power flowing out; hence, the input electrical power P is equal to the sum of the power loss to

the coolant P_l and the power flowing to the gas stream P_g. The thermal efficiency of the plasmatron η can then be defined as

$$\eta = \frac{P_g}{P} = \frac{P - P_l}{P}$$

It should be noted that this definition of efficiency does *not* correspond to the efficiency of gas heating by the arc itself. The heat losses measured are those that occur along the entire length of the anode, whereas the end of the arc and the fuel injection point both are located significantly before the end of the anode. The efficiency η as measured is thus smaller than the arc gas heating efficiency.[ii] The importance of η is that the enthalpy added to the total gas flow (air and fuel) between its entry to the plasmatron and the end of the anode is given by ηP.

Figure 6.3 shows the variation of thermal efficiency with the air flow rate through the plasmatron over the operating range of the device. The efficiency is observed to increase slightly with flow rate, due both to increased swirl and lower residence times in the plasmatron. The efficiency and power data in Figures 6.2 and 6.3 allow calculation of the air temperature at the plasmatron outlet; over the operating range of the plasmatron, this temperature varies from 2100 to 3900 K.

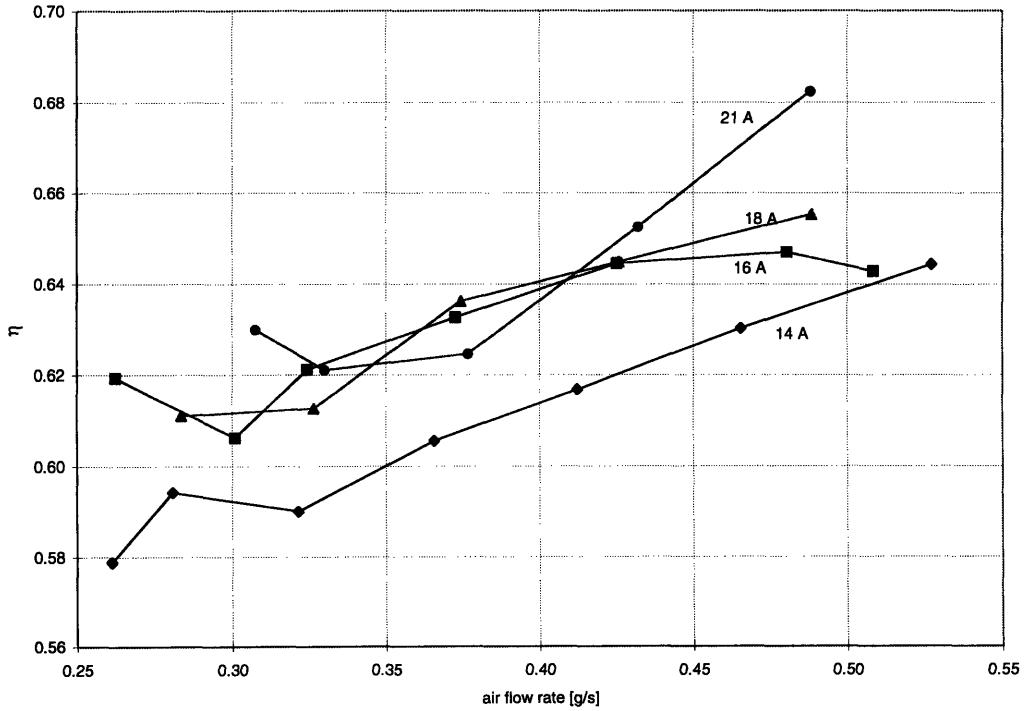

Figure 6.3. Thermal efficiency η as a function of air flow rate at several operating currents.

[ii] A more accurate measurement of the gas heating efficiency has been accomplished with an alternate plasmatron design. Over the range of flow rates of this device, the efficiency varied from 70 to 83 percent.

6.2 OUTPUT SPECIES CONCENTRATIONS

Species concentrations at the reformer outlet have been measured via gas chromatography. The experiments that have been performed to date do not represent an organized examination of a parameter space; rather, they consist of data taken during a period of validation and refinement of the initial plasma reformer design. Hence, the plasmatron behavior varied slightly from experiment to experiment, and the full ranges of power and flow capabilities of the reformer have yet to be explored. Nevertheless, as will be seen below, the data collected on the output species concentrations of the reformer during this series of experiments, along with the kinetic and equilibrium models discussed previously, allow a relatively clear interpretation of the effects of major system parameters on the reformer output, and give strong indications of the key directions to pursue in the detailed experiments that are to follow in the next phase of the project.

6.2.1 Data reduction and definition of the parameter space

Several parameters are of key importance to the behavior of the reformer (see Chapters 3 and 4), and these can be used as a basis for examining the experimental results. The air-to-fuel ratio λ affects both the equilibrium composition of the gas mixture and the kinetics of the system. A second key element is the energy input to the mixture per unit mass of methane ζ, which controls the reacting temperature T_r, and thus the extent of reforming and progress toward equilibrium. Since T_r cannot be measured directly in the current experimental arrangement, ζ is a useful measure of the initial system energy. Another variable is the residence time τ_r, which determines the extent of reaction within the reformer and the volumetric heat loss from the mixture during reforming. The degree of mixing within the reformer is also of obvious importance. However, it is difficult to characterize this mixing with the current data. In future work, which will include spatially-resolved species concentration and temperature measurements within the reformer (see Chapter 5), the extent of mixing and turbulence intensities will be analyzed, whereas in this discussion no attempt will be made to determine mixing effects.

The data available for analysis from a given experiment include the input flow rates of air and methane, the rates of heat loss to cooling water in both the plasmatron and the reactor, the voltage and current of the arc, and the output mole fractions of the species H_2, CO, CO_2, CH_4, O_2 and N_2.

From the air and fuel flow rates it is possible to calculate λ:

$$\lambda = \frac{\frac{\dot{m}_{air}}{\dot{m}_{CH_4}}}{\left(\frac{\dot{m}_{air}}{\dot{m}_{CH_4}}\right)_{\substack{stoic.\\combustion}}} = \frac{\dot{m}_{air}}{17.16\dot{m}_{CH_4}}$$

With the plasmatron efficiency η calculated as described in 6.1.2, ζ is obtained from the experimental data by

$$\zeta = \frac{\eta P}{\dot{m}_{CH_4}}$$

It should be noted that incomplete mixing could cause the effective values of λ and ζ to differ from these calculated values, which correspond to a perfectly mixed situation.

Calculation of the residence time for a given experiment requires the temperature within the reactor T_r. Making the assumptions that the plasma heating occurs almost instantaneously, that thermal equilibrium is reached before reaction begins, and that the heat release due to reaction is small compared to the heat input from the plasma, T_r may be obtained as follows:

$$T_r = \int_0^{\zeta} \frac{1}{c_p} dh$$

where c_p is the mass average specific heat of the mixture per unit mass of methane. The above assumptions are reasonably accurate for the process under consideration, as was discussed in Chapter 4. The residence time is then given by

$$\tau_r = \frac{\left(\frac{PV_r}{RT_r}\right)}{\dot{n}_t}$$

where $\dot{n}_t$ is the total molar flow rate (fuel and air) and V_r is the reactor volume.

The gas chromatography analysis yields the mole fractions of species in the output mixture, as opposed to absolute molar amounts. Therefore, some normalization is required in order to compare the output species flow rates quantitatively to reactant flow rates. From the measured output mole fractions and known input flow rates, and assuming that nitrogen is largely unreactive, it is possible to express the molar flow rates (or moles) of output species relative to the input molar flow rate (or moles) of methane:

$$\frac{n_{S,out}}{n_{CH_4,in}} = \frac{n_{S,out}}{n_{N_2}} \frac{n_{N_2}}{n_{CH_4,in}} = \frac{n_{S,out}}{n_{N_2,out}} \frac{n_{N_2,in}}{n_{CH_4,in}} = \frac{X_{S,out}}{X_{N_2,out}} \frac{\dot{n}_{N_2,in}}{\dot{n}_{CH_4,in}}$$

where S represents an output species. In the results presented below all concentrations are reported with this normalization. Note that complete reforming at $\lambda = 0.25$ would correspond to a normalized H_2 concentration of 2, CO concentration of 1 and N_2 concentration of 1.88 in the output mixture.

Some important chemical species are not directly measured with the current experimental apparatus; these include water, acetylene and higher hydrocarbons. Under the assumption that the only major oxygen-containing species in the output gas are CO, CO_2, O_2, and H_2O, the water concentration can be found via an oxygen atom balance, since the input flow rate of oxygen and the output concentrations of the first three of the four listed compounds are known. This assumption is in accordance with the previous modeling results (see Chapters 3 and 4) and past experimental observations.[1] The unobserved hydrocarbons are a more difficult problem. The predominant species in this category should be acetylene (C_2H_2), but soot formation on the cold walls of the reactor and sampler could also account for a large portion of the unobserved carbon and hydrogen. Hence, the analysis of the data below will not rely on knowledge of the concentrations of these species. The planned FT-IR diagnostics will be able to resolve some of these difficulties (see Chapter 5).

Figures 6.4 - 6.6 show the location of the experiments in the λ-ζ-τ_r parameter space. These controlling parameters could not be varied completely independently in this series of experiments, due to the nature of the apparatus. Several correlations between parameters can be seen in these plots. The most noticeable is that of λ and ζ, as shown in Figure 6.4. The overall trend is that ζ increases with increasing λ; this is due to the fact that in most experiments all the air flow passed through the arc, and the methane was injected afterwards. In general, an increase in λ was obtained by decreasing methane flow for a given air flow rate and plasmatron power (all experiments reported here were performed at the lowest available plasmatron power); hence increasing the energy input per unit mass of methane. In those experiments in which premixed air and fuel were injected after the arc, these two parameters could be varied more independently. Figures 6.5 and 6.6 show that the residence time τ_r is reasonably well decoupled from λ and ζ, but the total variation in τ_r is quite small; all the experiments performed to date fall in the range $30 \text{ ms} < \tau_r < 60 \text{ ms}$.

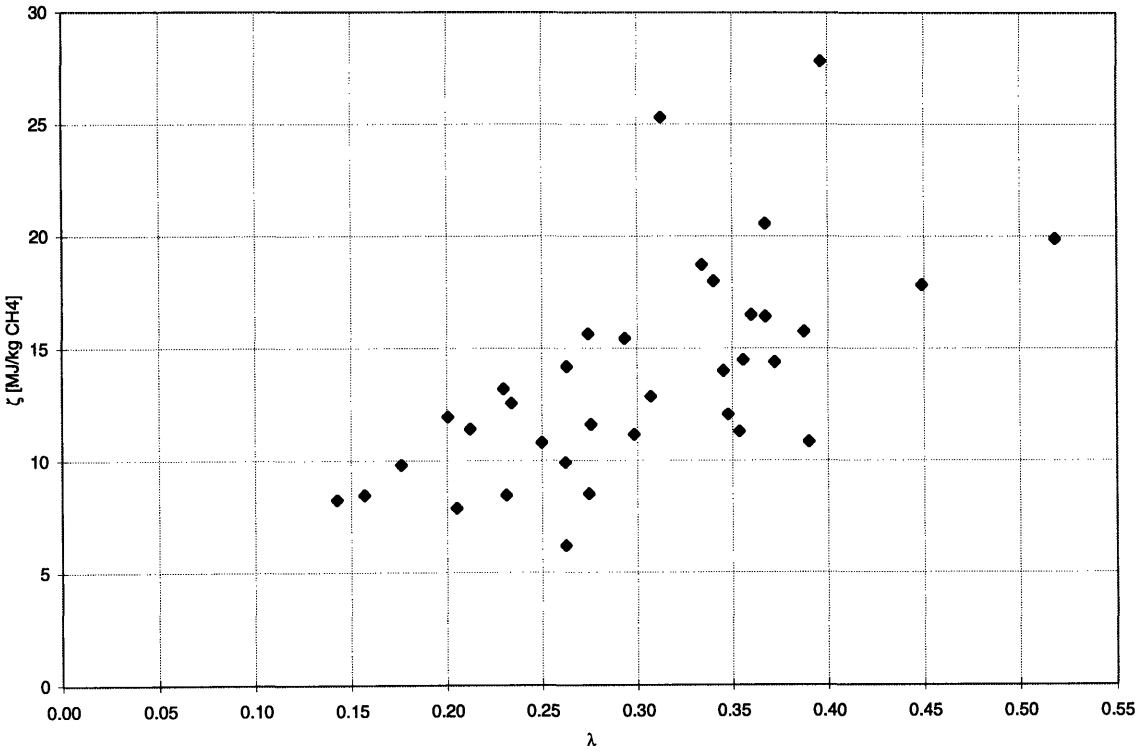

Figure 6.4. Experiments located in the λ-ζ plane.

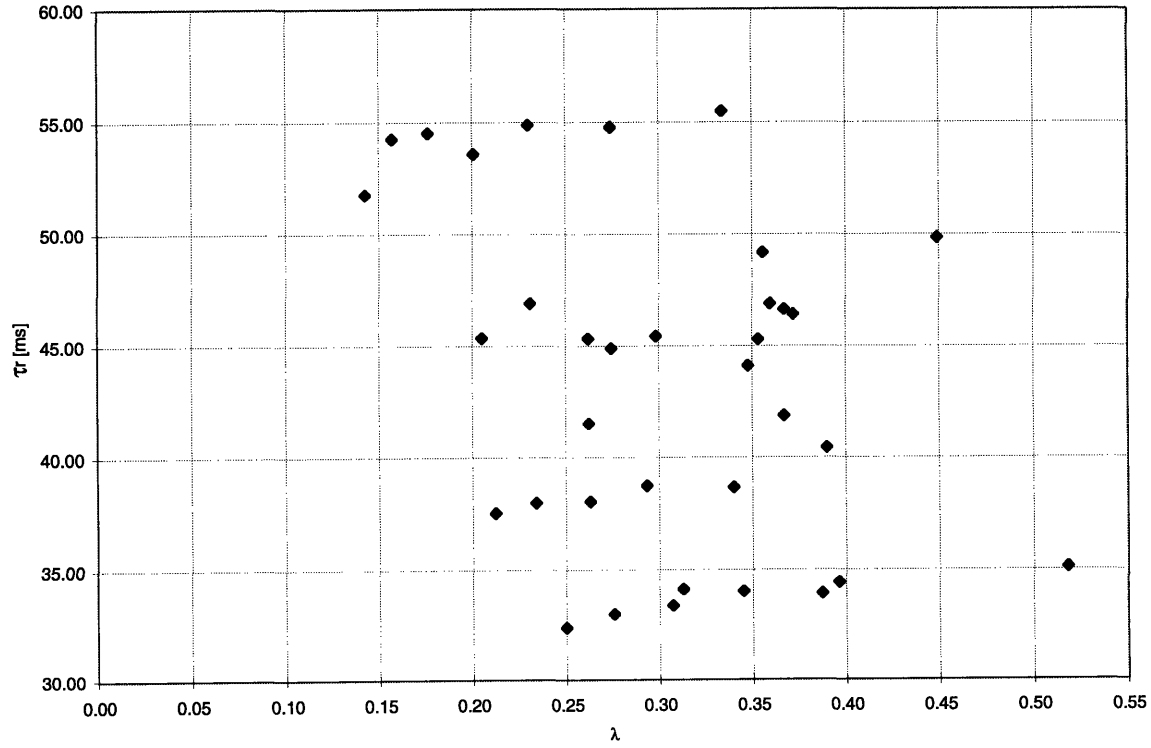

Figure 6.5. Experiments located in the λ-τ_r plane.

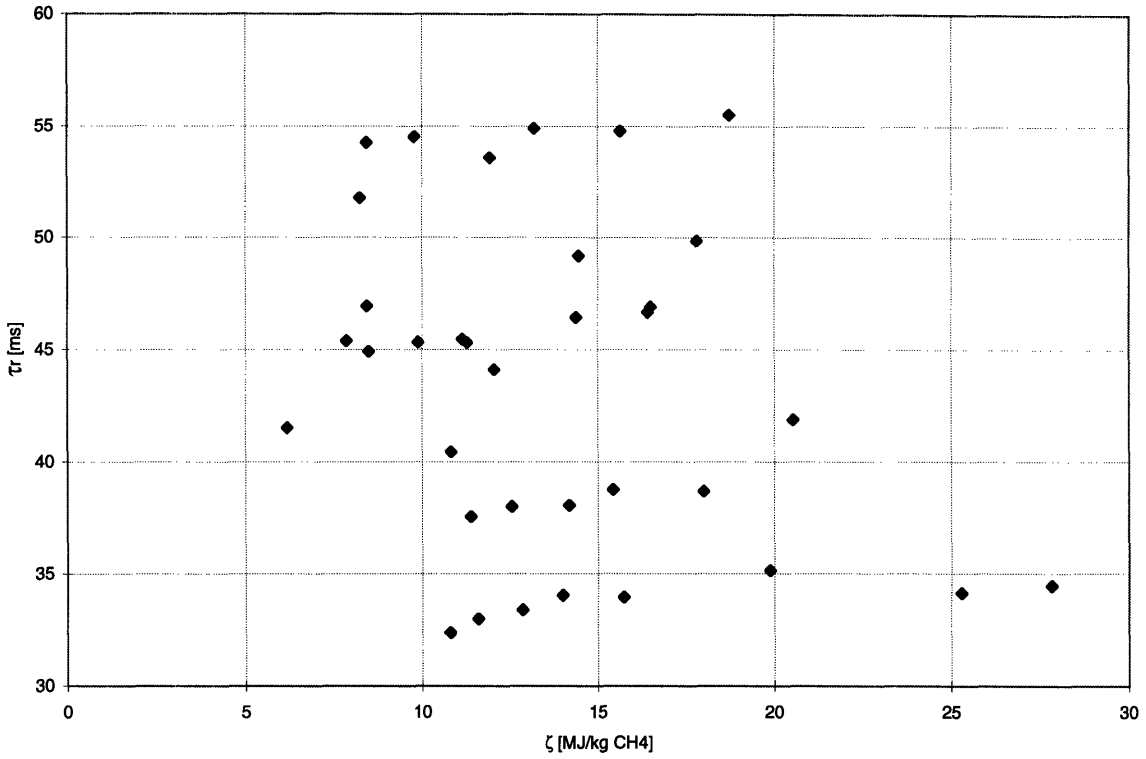

Figure 6.6. Experiments located in the ζ-τ_r plane.

Using the information in these figures as a guide, the experimental results can be organized in a useful way for the study of the λ-ζ-τ_r space. It was noted above that the observed range of residence times is very small; no clear trends in output concentrations are seen over this range. Hence, those trends that are observed result from a combination of the influences of λ and ζ. The following analysis allows these effects to be separated, using both experimental and modeling results.

6.2.2 Analysis of observed trends

The mechanism that has been suggested for the partial oxidation of methane both in the literature (see Chapter 2) and in the kinetics modeling herein (see Chapter 4) is an important guide to the interpretation of the experimental observations. While the precise details of this mechanism are somewhat uncertain, the major features are relatively undisputed: the reaction begins with a rapid partial combustion of methane with most of the available oxygen, producing a mixture of CH_4, H_2O, CO_2, H_2 and CO, followed by a much slower reforming of this mixture to the equilibrium composition, consisting almost entirely of H_2 and CO. A representative plot of the time evolutions of the species concentrations is shown in Figure 6.7. It will be seen

below that the observed trends in output concentrations can be explained by this model of the reaction mechanism; suggesting that chemical kinetics calculations made using this mechanism may be a useful guide in reformer optimization.

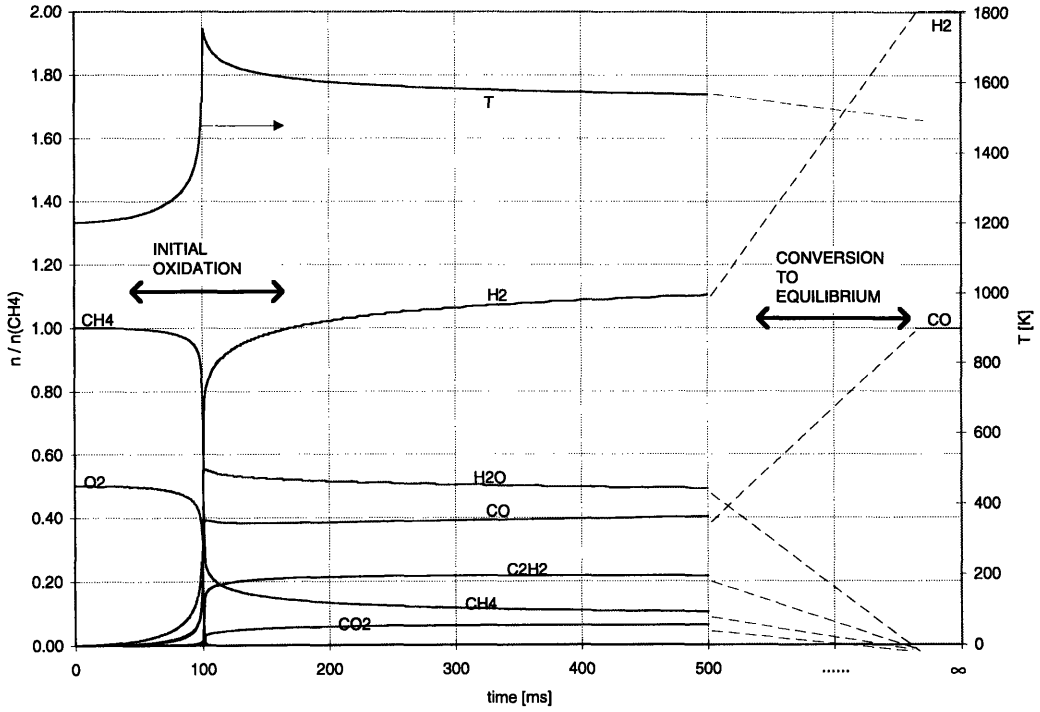

Figure 6.7. Representative plot of species time evolutions as calculated for a plug flow reactor (see Chapter 4).

Figure 6.8 shows the variation of H_2O and CO_2 output concentrations with λ over the entire set of experiments. Both species show a strong linear relationship to λ, which is consistent over variations in energy input and residence time. This indicates that the initial formation of H_2O and CO_2 is a very fast process compared to the residence time, even at lower energy input levels, and hence depends almost entirely on the mixture stoichiometry. The linear dependence on λ is consistent with the idea that the extent of initial combustion is controlled by the amount of O_2 in the feed gas. None of the other observed species shows such a clear dependence on λ in the presence of variations in other parameters, suggesting that the processes related to the production and consumption of these other species are in fact slow enough to depend significantly on ζ or τ_r.

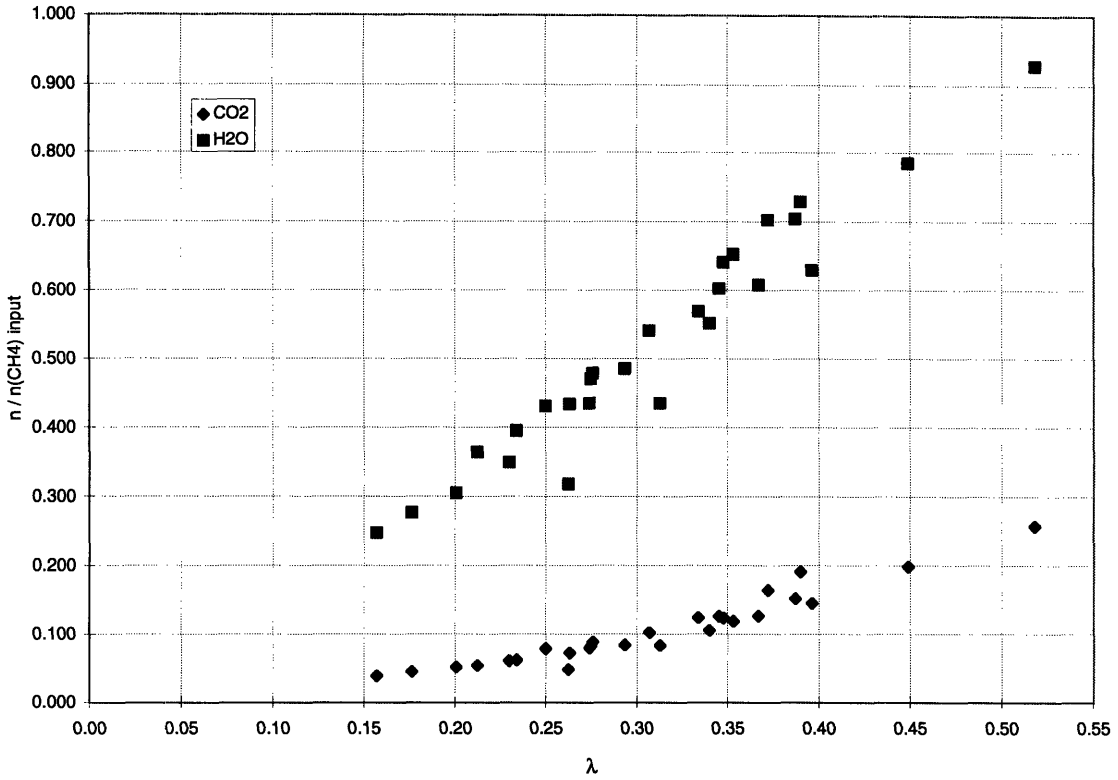

Figure 6.8. H_2O and CO_2 output concentrations per mole of CH_4 input versus λ for all experiments.

Figures 6.9 - 6.11 show the variation of CH_4, O_2, H_2, and CO with ζ, again over the entire set of experiments. In all cases, there is a very strong dependence of the species concentration on ζ for values of $\zeta < 15$ MJ/kg CH_4; for the "reactant" molecules CH_4 and O_2, the concentration drops with increasing ζ, while for the "product" molecules H_2 and CO, the concentration increases as ζ is increased. These trends show that up to $\zeta = 15$ MJ/kg CH_4, the consumption of CH_4 and O_2 and production of H_2 and CO within the reformer are predominantly controlled by the initial energy content (or equivalently, the initial temperature) of the mixture, indicating that the timescales for the evolution of these species concentrations towards their equilibrium values are long compared to the physical timescales imposed by the reformer. The variations with ζ become weaker for larger energy inputs; as ζ moves far enough from the critical region, the influences of λ and τ_r become more noticeable. The H_2O and CO_2 concentrations show no such trends with ζ for the same series of experiments, which is consistent with the assertion that their initial production is controlled by a fast process relative to τ_r.

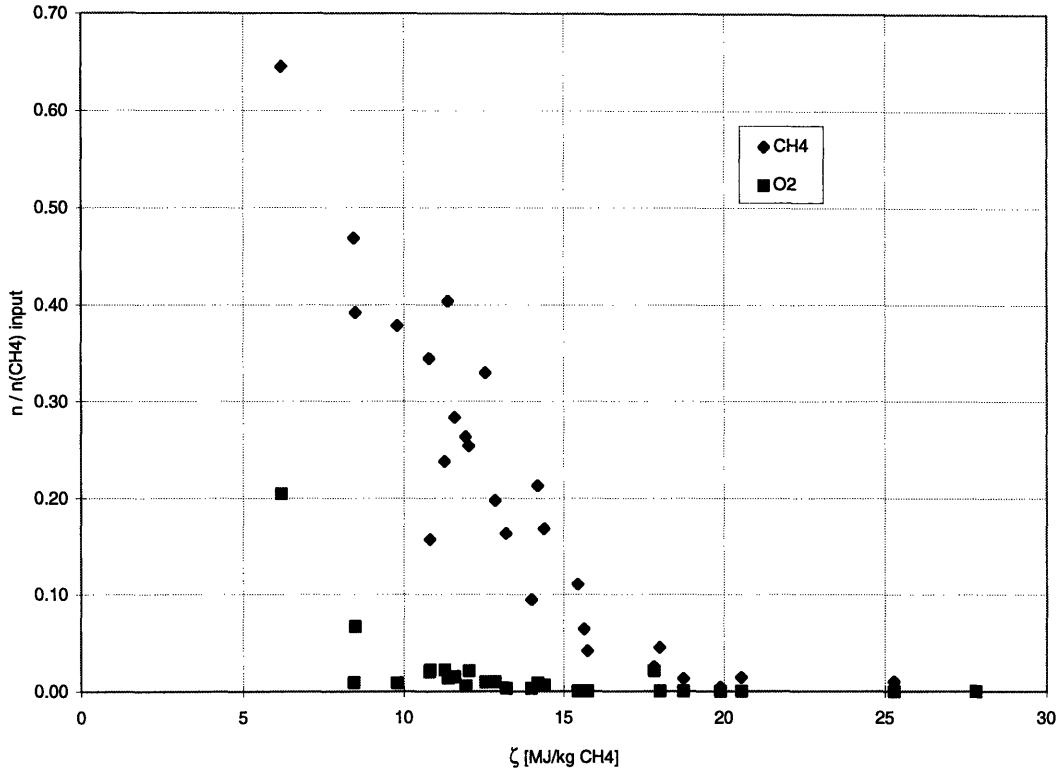

Figure 6.9. CH_4 and O_2 output concentrations per mole of CH_4 input versus ζ for all experiments.

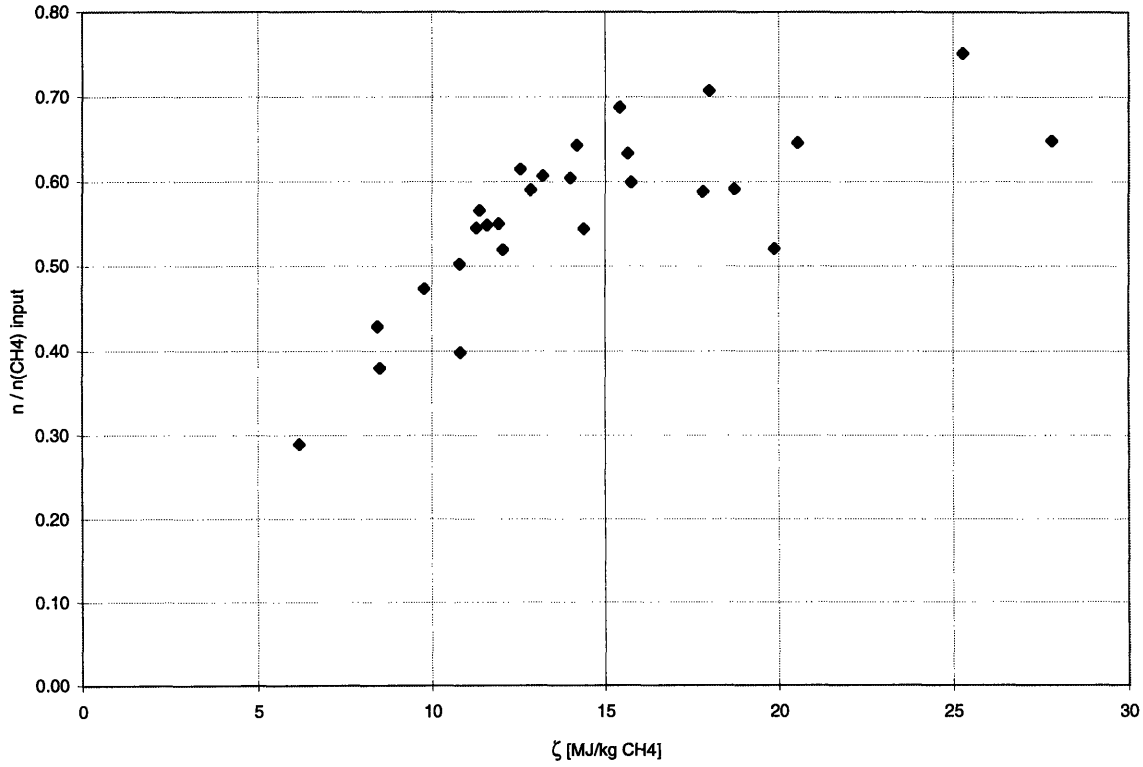

Figure 6.10. H_2 output concentration per mole of CH_4 input versus ζ for all experiments.

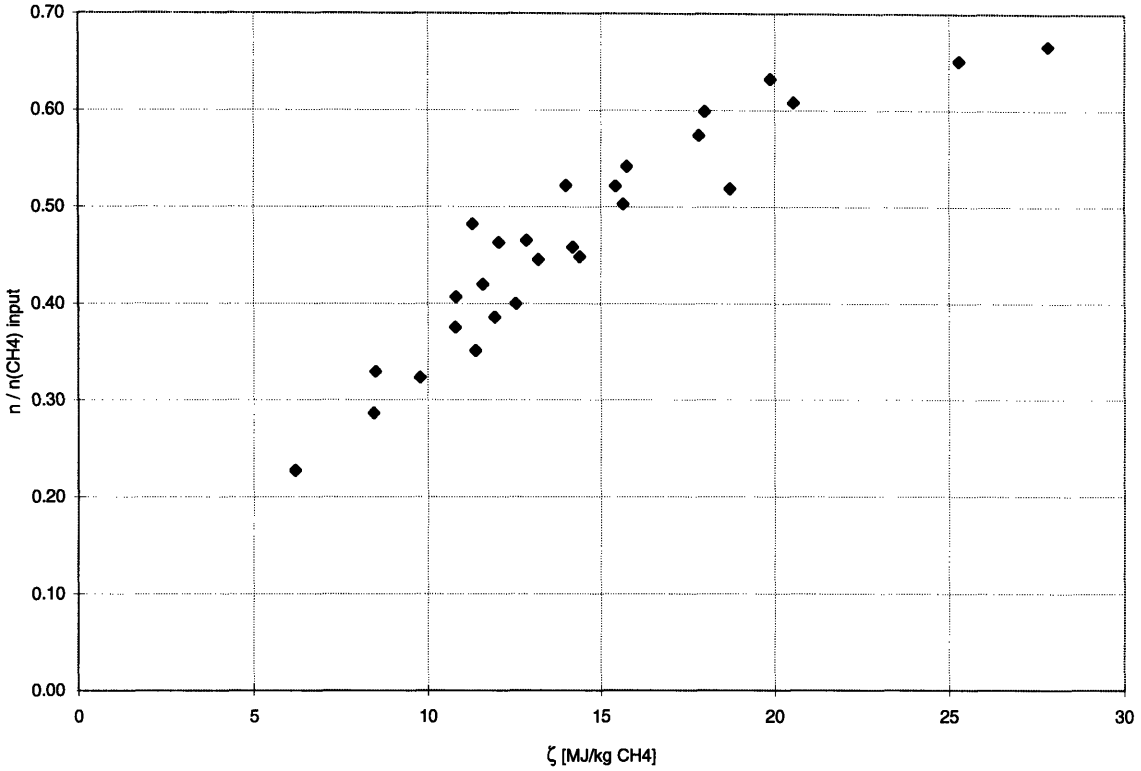

Figure 6.11. CO output concentration per mole of CH_4 input versus ζ for all experiments.

Weaker trends in the data are obscured due to the competing influences of λ and ζ. The effects of these two variables can be separated by examining the changes in output species concentrations with one of the parameters as the other is held fixed within a small range of values.

Figures 6.12 - 6.14 show the variation of output concentrations of CH_4, H_2, and CO with λ for several small ranges of ζ. For a given ζ range, CH_4 and H_2 output concentrations are seen to decrease with increasing λ, whereas CO tends to increase slightly. It has already been shown in Figure 6.8 that H_2O and CO_2 increase with λ independently of ζ. Figures 6.12 - 6.14 also show that for a given λ, H_2 and CO concentrations increase with ζ while the CH_4 concentration decreases with ζ. The trends with respect to ζ are the same as those discussed previously; the variations with λ for given ζ provide some new information. These results can again be explained by a balance between fast and slow kinetic processes in the reacting mixture. It is clear that as λ increases, more of the hydrogen from the input methane goes to water

instead of H_2. On first impression, it may seem that the increase in CO with increasing λ is contradictory to the proposed mechanism; however, the formation of CO_2 must pass through CO as an intermediate, so the rates of production of these species naturally are closely linked. A clearer picture of how the relationship between the carbon oxides changes as the mixture stoichiometry is varied is given by Figure 6.15, which shows the ratio of CO to CO_2 in the output mixture as a function of λ over the range of experiments. The downward trend in this figure indicates that larger air-to-fuel ratios favor carbon dioxide over carbon monoxide. The fact that CH_4 concentrations decrease with λ for a given ζ can be attributed to the increasing amount of initial combustion of CH_4 for larger λ values (i.e. the overall rate of CH_4 consumption increases, since combustion is a fast process).

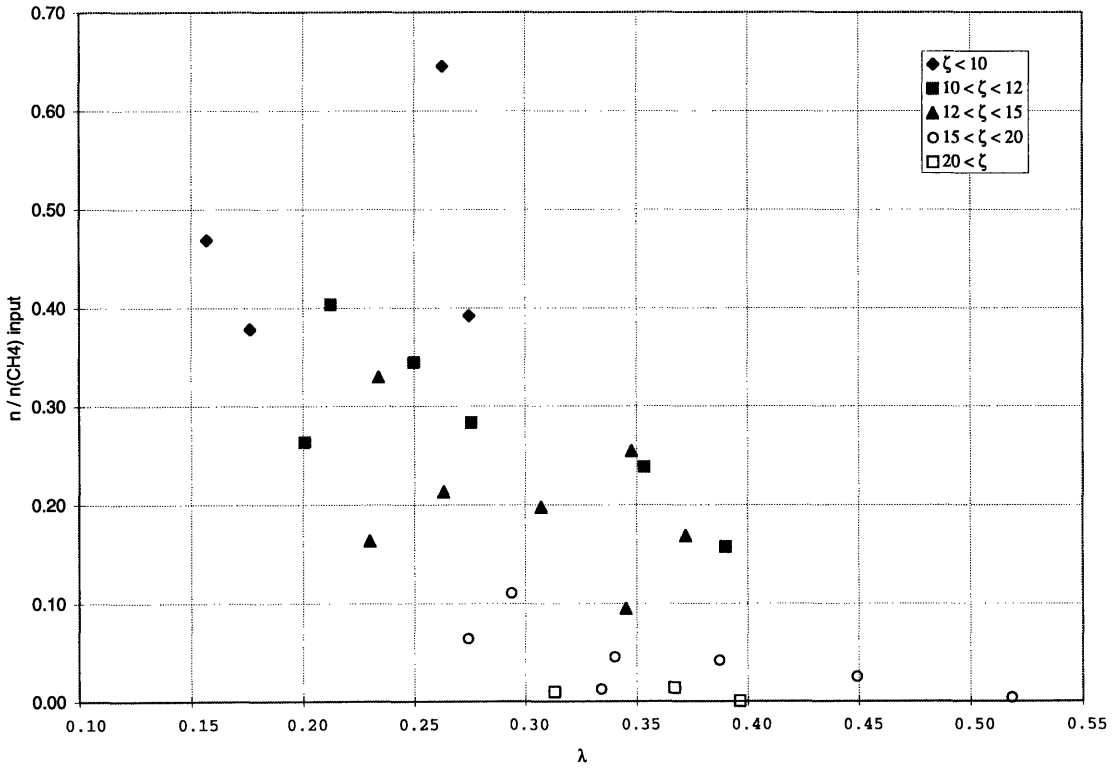

Figure 6.12. CH_4 output concentration per mole of CH_4 input versus λ for several ζ ranges.

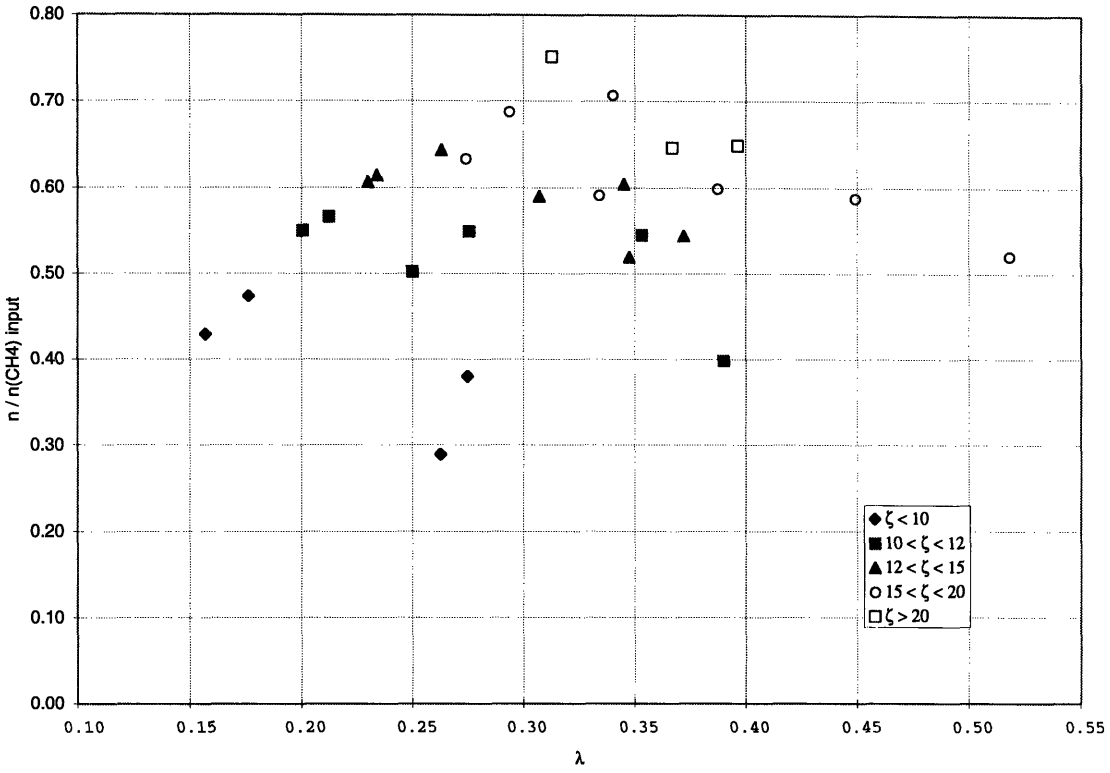

Figure 6.13. H_2 output concentration per mole of CH_4 input versus λ for several ζ ranges.

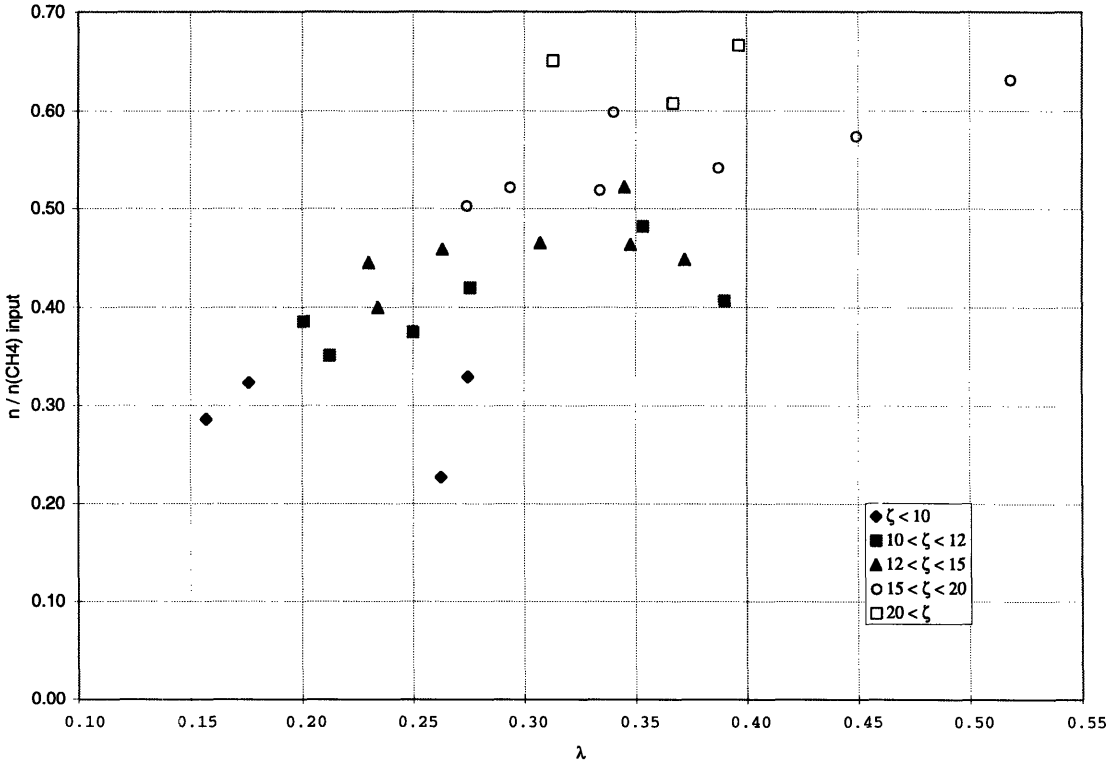

Figure 6.14. CO output concentration per mole of CH_4 input versus λ for several ζ ranges.

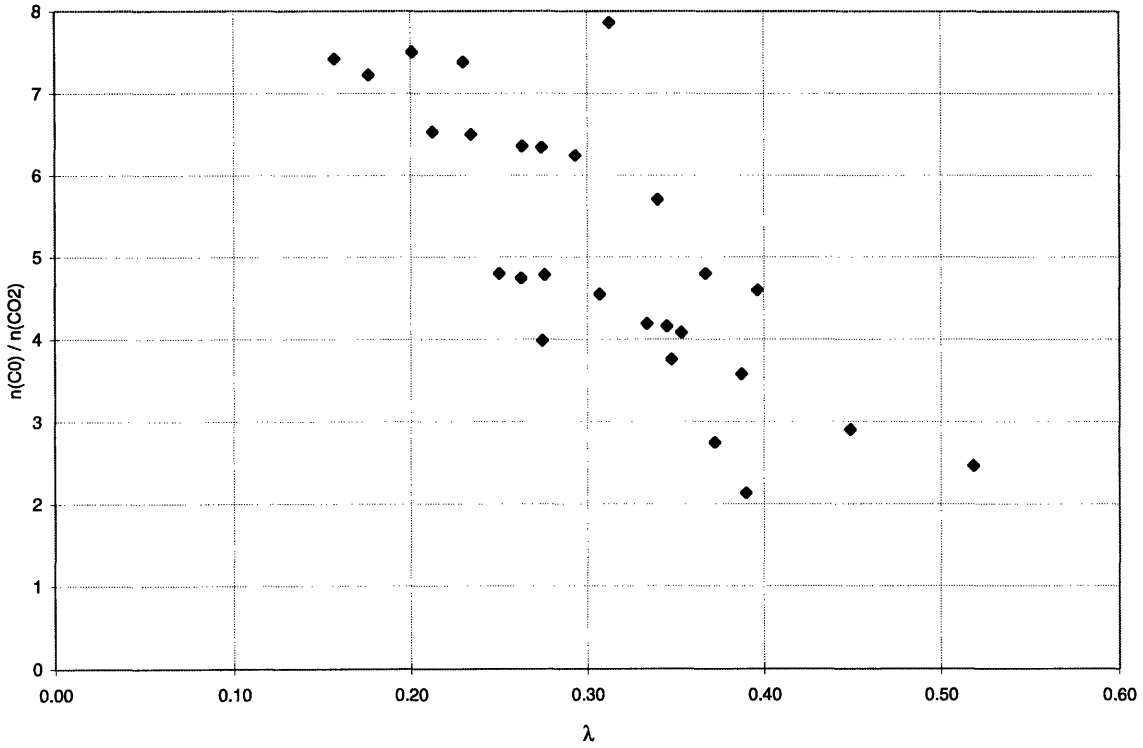

Figure 6.15. CO to CO_2 ratio as a function of λ.

6.3 COMPARISON OF EXPERIMENTAL RESULTS WITH MODEL PREDICTIONS

It has been shown in the preceding discussion that the experimental results are in agreement with the main qualitative features of the reaction mechanism model. A more quantitative comparison of the data with the results of the various models discussed in this work, which include features of the reforming system such as mixing characteristics and power requirements, will help to validate these models as design tools and provide further insight into profitable future research directions.

The models that we have to compare to these results include the equilibrium analysis of Chapter 3 and the plug flow reactor and perfectly stirred reactor chemical kinetic models of Chapter 4. The assumptions and constraints embedded in these models dictate that each of them may only be compared usefully to certain aspects of the observations described above. The results of the equilibrium analysis may be used to aid in the examination of the observed variations with λ; however, it must be considered that the strong effect of ζ on the output species distribution indicates that the current system does not reach equilibrium within the residence time, which limits the applicability of this model. The plug flow reactor calculations, which use a realistic chemical mechanism, will be useful for examining the changes in species

distributions with ζ, whereas the perfectly stirred reactor model with one-step chemistry is insufficient for this purpose. The results of both of the kinetic models can be compared to the observed effects of ζ on the consumption of methane within the reformer. While neither of these models is likely to be an extremely accurate physical representation of the reformer, they represent limiting cases, so that the real system behavior can be expected to fall within the bounds set by the results of the two models.

The analysis of the variation of equilibrium species distributions with H:C and O:C ratios (see Chapter 3) shows several obvious trends that should be apparent in a methane-air system, presuming that the system reaches equilibrium within the residence time. For gas mixtures in equilibrium at high temperature (greater than 1000 K) with H:C = 4, the analysis showed that both CO and H_2 concentrations should show maxima at $\lambda = 0.25$, whereas H_2O and CO_2 should increase for all $\lambda < 1$. In the experiments, no maximum is observed for CO, H_2 shows only a weak trend (see figures 6.13 and 6.14), and the magnitudes of the H_2O and CO_2 concentrations are significantly greater than those predicted by the equilibrium calculations. This comparison strongly suggests that the gas mixture does not reach equilibrium within the reformer.

The results of the plug flow reactor model predict detailed species time evolutions which can be very useful for examination of the observed trends in species concentrations with ζ. As noted above, the overall structure of the predicted time evolution of the mixture is consistent with the observations; it consists of a rapid first phase (partial combustion or ignition) which produces H_2, CO, H_2O, and CO_2 while consuming most of the methane and oxygen, followed by a much slower conversion of H_2O, CO_2 and the remaining CH_4 to H_2 and CO as the system progresses towards the eventual equilibrium product distribution. The time evolutions shown in figures 4.1 - 4.3 indicate that for residence times in the experimental range of 30 to 60 ms and ζ values between 7.5 and 15 MJ/kg CH_4, the output mixture should be in the beginning of the second process; that is, ignition always occurs within the reformer for this series of experiments, but the post-ignition mixture does not progress very far towards equilibrium before reaching the sample probe. This interpretation is consistent with the observation that the output concentrations of H_2O and CO_2 are independent of ζ in the range covered by these experiments. Immediately after the ignition, the concentrations of these species are at high levels, which change very slowly thereafter; hence, it is reasonable that the output concentrations would be relatively constant over small ranges of ζ and τ_r such as those observed

here. Figure 6.16 shows the predicted variation of CH_4 and H_2 output concentrations with ζ for a residence time of 45 ms in comparison to the observed values. Clearly, the PFR model does not quantitatively predict the output concentrations. There are several possible reasons for this; most important is the variation of λ for the experimental points listed. In general, the experiments with higher ζ values also had higher λ values, which would lead to more water and less H_2 in the output. Other factors that may contribute to the lack of correspondence between model and experiment include poor mixing, soot formation, and heat losses in the reactor. Although soot formation has been observed in some cases, it was only to a small extent, and concentration measurements taken at different radial positions show no strong variations to indicate poor mixing. Hence, heat losses from the reactor are the most likely cause for the discrepancy between predicted and observed concentrations. Although this model suggests that near equilibrium species distributions may be reached within the residence times examined so far, the comparison with experiment suggests that considerably longer residence times may be required.

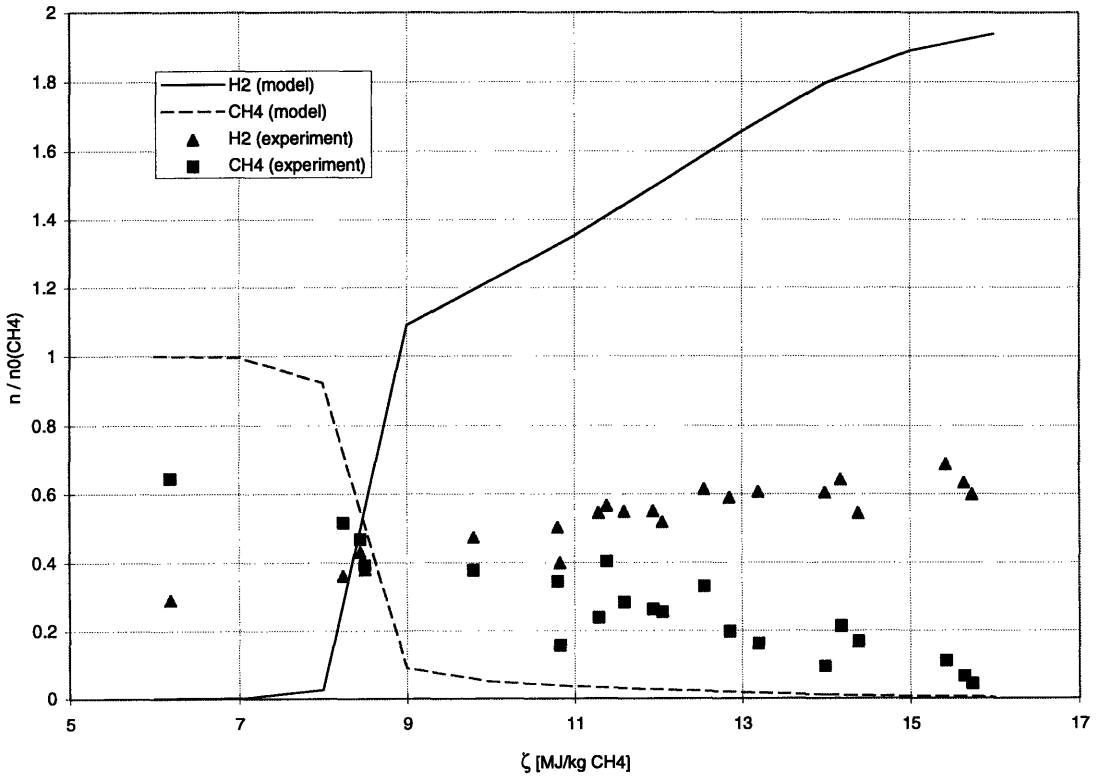

Figure 6.16 CH_4 and H_2 output concentrations predicted by the PFR model of Chapter 4 for 45 ms residence time (lines) and experimentally observed levels (points) versus ζ.

The main result of the perfectly stirred reactor model that can be compared with the experimental observations is the decrease in CH_4 conversion as ζ decreases. Figure 6.17 compares the model prediction for residual CH_4 as a fraction of the input amount to the measured values. While the predicted rate of decrease of methane concentration is much greater that the observed rate, the region of the ζ axis in which the drop occurs is predicted accurately. The difference in the rates of decrease may be attributed to the one-step chemistry included in the model; future modeling in this area will include a full chemical mechanism. However, the PFR model shows a similar disagreement, indicating that the problem may instead be related to the basic assumptions made regarding mixing and heat transfer. Nevertheless, accurate prediction of the critical values of ζ for conversion based on a physically realistic reformer model can be a useful design tool.

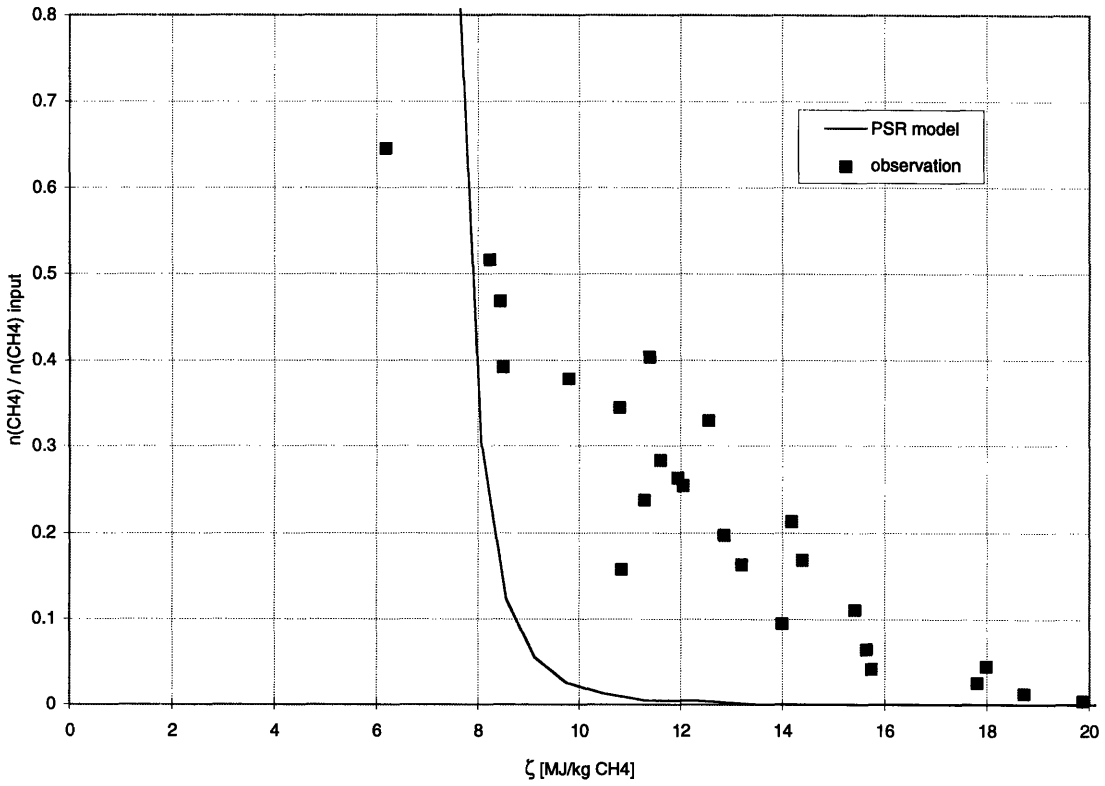

Figure 6.17. Residual CH_4 concentrations versus ζ as predicted by the PSR model (solid line) and observed experimentally (individual points)

In summary, the two kinetic models developed in this work are sufficient to explain overall trends in the experimental results, and show quantitative agreement in broad features such as the critical value of ζ for conversion. However, further work is needed in order to

make these models into useful predictive tools, including the addition of heat losses, more careful consideration (or experimental control) of mixing, and investigation of soot formation.

6.4 Conclusions and directions indicated by results to date

Despite the scattered nature of the available data from the validation phase of this project, some strong conclusions may be drawn regarding the current experimental system and numerical simulations. First, we can see that the efficiency of the plasmatron is limited by the cooling requirements of the anode; in a system designed to produce the highest possible reacting temperatures, the anode should be as short as possible and followed by an insulated reactor. Secondly, it is clear that the output gas mixture is either far from equilibrium or at a much lower temperature than desired, resulting in the presence of water and carbon dioxide in relatively high concentrations. Hence, either a higher reactor temperature or longer residence time will be required in order to optimize H_2 production. Thirdly, the comparison of two adiabatic numerical models of the system, with different mixing assumptions, results in overprediction of the extent of conversion and output H_2 levels. This is consistent with the hypothesis that the reacting temperatures are lower than predicted due to heat losses.

These few conclusions give very strong indications of the most profitable areas for investigation in the ensuing phases of this project. Along with a more organized examination of the parameter space discussed here, there is a clear need to increase the range of τ_r in the experiments. This will necessitate more careful control of heat losses from the reactor in order to maintain a high reacting temperature; suggesting a change from the water-cooled copper reactor adopted for simplicity in the initial experiments to a refractory ceramic or other highly insulating material. A larger range of ζ values (i.e. higher arc currents) should also be examined in order to determine the feasibility of accelerating the kinetics to the point where equilibrium can be reached within the current range of residence times. Extended measurements at different axial locations in the reformer will also be useful to further clarify the details of and interactions between the two main kinetic processes involved in partial oxidation. Another important direction for future work is the measurement of temperatures within the reactor, which will allow more detailed comparisons of experimental data with the model results.

6.5 References

[1] D. Eastman, *Industrial and Engineering Chemistry* **48**(7) p. 1118 (1956).

CHAPTER 7

Conclusions

The models and experimental results presented in this thesis represent only the initial, exploratory phase of this research. As such, their main function is to suggest the field of possibilities that should be examined in future work. The information provided by this work can help to focus the project on those areas where progress may be made most rapidly.

Before consideration of the detailed results, it is important to note one conclusion from this research that is of a much larger scope, and has many implications: a small, highly efficient plasmatron *can* drive reforming reactions on short timescales without a catalyst. This result alone opens up an entire range of applications for this technology that could be significant additions to future energy and power systems, due to the intrinsic properties of the plasmatron itself. For example, the device has essentially no warm-up time, and the response to changes in power or flow rates is very fast; this creates the possibility of a true load-following inline reformer, a key element in the application of fuel cells to transportation systems.[i] Plasmatrons have been operated at power levels ranging from hundreds of watts to several megawatts; plasma reformers could feasibly be scaled to any part of this range. Whereas catalytic reformers are extremely fuel-specific, the thermal processes utilized in plasma reformers have a much greater fuel flexibility. The initial phase of this research has in effect demonstrated the basic utility of thermal plasma devices as components of efficient power systems; what is left is the detailed engineering of specific applications.

The beginning of that engineering process for the application of hydrogen production systems is embodied in the work presented herein. The key results are the following: complete conversion of methane has been achieved with the current apparatus; however, the hydrogen production levels are lower than the predicted equilibrium values. Given that the computational models employed covered a range of mixing conditions, it is more likely that this deficiency in hydrogen production is caused by heat losses from the reacting gas than by mixing effects. Detailed analysis of the species concentrations confirms that the qualitative features of the reaction mechanism are consistent with the computational model and the mechanisms suggested by past workers; the specific characteristics of the mechanism, especially during the initial combustion phase, have yet to be determined.

---

[i] Wow!

These results suggest several directions for this project. Few of these directions have to do with alterations of the plasmatron itself; rather, they involve incorporation of the plasma technology into a reactor that is optimized for a given purpose.

Some of the parameters that need to be optimized in order to meet the goal of increased hydrogen production have been determined by this research. The disagreement between the (adiabatic) numerical models and experimental data indicates that heat losses may be an important factor in the current reaction system. These can be minimized by using an insulated or heated reactor. Another possible method of managing the heat transfer in the system is related to the two-stage nature of the chemical reaction mechanism. The heat release from this reaction occurs very early on in the process; in the experimental reactor used now, this heat release may even occur within the plasmatron itself. In a plug flow situation, this energy could be lost from the system early in the evolution of the reaction, resulting in lower temperatures for the entire second phase of the reaction. If the reactor is redesigned to better approximate a perfectly-stirred reactor, the heat release from the initial combustion will increase the temperature of the entire mixture, in effect accelerating all parts of the reaction. In such a configuration, the jet created by expansion of the heated gas in the arc could be utilized to improve the mixing further. Both the experiments and the numerical models indicate that the residence time in the reactor should be increased to improve the hydrogen output levels.

Another important task that is made evident by these experiments is the need to improve the agreement between the numerical predictions and observed results. This will involve the inclusion of heat losses in the current models and the addition of a detailed reaction mechanism to the PSR model. A more thorough experimental investigation of the parameter space in question will also be an important part of this effort. The experimental facilities for model validation are now in place, allowing for spatially-resolved measurement of species concentrations and temperatures. This data, along with the current models, will provide the basis for a physical model of the reformer that is quantitatively predictive; such a model is an essential tool for the investigation of scaling of the reforming apparatus, which could be prohibitively difficult to accomplish experimentally.

In summary, the initial phase of this project had shown very promising results for the application of thermal plasmas to fuel reforming systems; the potential for replacing a catalyst by a plasmatron, especially in cases where fast startup or response times are required, has been clearly demonstrated. Although some work has been focused on similar systems in the past, a large number of essentially unexplored possible applications for this technology exist, and many more may be created in the transition to a future energy and power economy, based increasingly on renewable resources and on electricity. This situation offers the chance not only to address

known needs for energy and fuel conversion and processing, but to develop a relatively untapped technology, perhaps resulting in applications that take as yet unknown directions towards future power systems.

APPENDIX A

Chemical Equilibrium Calculations

A.1 ELEMENT POTENTIAL METHOD

The chemical equilibrium calculations presented in this thesis were performed by the element potential method, using the STANJAN equilibrium code.[1] A full description of the theory and numerical solution method is found in reference [1]; the basic points and the specific details of this set of calculations are included here.

The equilibrium state of a thermodynamic system corresponds to the minimization of the Gibbs function of that system under the relevant constraints (i.e. temperature and pressure, entropy and volume, etc.). The Gibbs function for a system containing S species can be expressed as

$$G = \sum_{j=1}^{S} g_j N_j$$

where g_j is the molar Gibbs function of species j, and N_j is the number of moles of the species. The molar Gibbs function of a particular species (assuming a perfect gas mixture) is expressed as

$$g_j = H_j - TS_j + RT \ln X_j$$

where H_j and S_j are the molar enthalpy and entropy of species j, respectively (see Chapter 3), and X_j is the mole fraction of j.

To find the equilibrium state, G must be minimized under the constraints imposed by the atomic population of the system:

$$\sum_{j=1}^{S} n_{ij} N_j = P_i \quad i = 1,2,...,A$$

where n_{ij} is the number of atoms of element i in a molecule of species j, P_i is the total molar population of i atoms in the system, and A is the total number of elements. The problem of minimization subject to constraints is solved by the method of Lagrange multipliers. The main result of this method is the expression

$$X_j = e^{\left(-\frac{g_j}{RT} + \sum_{i=1}^{A} \lambda_i n_{ij}\right)}$$

which applies to all species j, in which the undetermined Lagrange multipliers λ_i are referred to as the element potentials. Physically, these element potentials are system properties, and represent G/RT per mole of i atoms. The problem is thus reduced to solving a set of A

equations (for a single-phase system) for the A unknown element potentials. The mechanics of the solution process are discussed in detail in reference [1].

A.2 Species and Thermodynamic Data

In order to solve an equilibrium problem as described in the preceding section, a set of species must be provided, and the atomic composition and thermodynamic properties (i.e. H_j and S_j) of each species must be known. For the calculations presented in this work, the thermodynamic properties were calculated by the NASA polynomial approximations, using coefficients provided by the CHEMKIN thermodynamic database.[2,3]

The elements and species used in the calculations are specified in the following listing; choosing a set of species is a somewhat arbitrary process, relying in general on intuition or previous calculations concerning the system under consideration. This list includes species that are likely gas-phase equilibrium products of rich fuel-air mixtures. Thermodynamic property coefficients for many of the species, taken from the GRI-MECH thermodynamic database for consistency with the chemical kinetic calculations, are also included.[4] The CHEMKIN database was used for all other thermodynamic data.

Chemical species and thermodynamic data for equilibrium calculations:

```
ELEMENTS
H C O N
END
SPECIES
H H2
OH HO2 H2O H2O2
C CH CH2 CH2* CH3 CH4
C2H2 C2H3 C2H4 C2H5 C2H6
C3H3 C3H6 C3H8 NC3H7
C4H C4H2 C4H3 C4H6 C4H7
CH2CO C2H4O CH3CHO C3H6O
CH2O CH2OH C2H HCO CH3O CH3OH
HCCO HCCOH
CO CO2
O O2
N N2
NO NO2 N2O
HNO HCN
END
THERMO
300.      5000.     1000.
HCN              XXXX96H   1C   1N   1     G   300.000  5000.000  1000.00     1
 3.65007700E+00 3.46099800E-03-1.27427880E-06 2.21765500E-10-1.47717740E-14    2
 1.49839160E+04 2.39322000E+00 2.49046200E+00 8.61128000E-03-1.03103420E-05    3
 7.48149800E-09-2.22910900E-12 1.52083440E+04 7.90498100E+00                   4
```

```
! GRI-MECH version 1.1 Thermodynamics released 3/15/94
! NASA Polynomial format for CHEMKIN-II
O                 L 1/90O   1   00   00   00G   200.000  3500.000  1000.000    1
 2.56942078E+00-8.59741137E-05 4.19484589E-08-1.00177799E-11 1.22833691E-15    2
 2.92175791E+04 4.78433864E+00 3.16826710E+00-3.27931884E-03 6.64306396E-06    3
-6.12806624E-09 2.11265971E-12 2.91222592E+04 2.05193346E+00 6.72540300E+03    4
O2                TPIS89O   2   00   00   00G   200.000  3500.000  1000.000    1
 3.28253784E+00 1.48308754E-03-7.57966669E-07 2.09470555E-10-2.16717794E-14    2
-1.08845772E+03 5.45323129E+00 3.78245636E+00-2.99673416E-03 9.84730201E-06    3
-9.68129509E-09 3.24372837E-12-1.06394356E+03 3.65767573E+00 8.68010400E+03    4
H                 L 7/88H   1   00   00   00G   200.000  3500.000   1000.00    1
 2.50000001E+00-2.30842973E-11 1.61561948E-14-4.73515235E-18 4.98197357E-22    2
 2.54736599E+04-4.46682914E-01 2.50000000E+00 7.05332819E-13-1.99591964E-15    3
 2.30081632E-18-9.27732332E-22 2.54736599E+04-4.46682853E-01 6.19742800E+03    4
H2                TPIS78H   2   00   00   00G   200.000  3500.000   1000.00    1
 3.33727920E+00-4.94024731E-05 4.99456778E-07-1.79566394E-10 2.00255376E-14    2
-9.50158922E+02-3.20502331E+00 2.34433112E+00 7.98052075E-03-1.94781510E-05    3
 2.01572094E-08-7.37611761E-12-9.17935173E+02 6.83010238E-01 8.46810200E+03    4
OH                RUS 78O   1H   1   00   00G   200.000  3500.000  1000.000    1
 3.09288767E+00 5.48429716E-04 1.26505228E-07-8.79461556E-11 1.17412376E-14    2
 3.85865700E+03 4.47669610E+00 3.99201543E+00-2.40131752E-03 4.61793841E-06    3
-3.88113333E-09 1.36411470E-12 3.61508056E+03-1.03925458E-01 8.81310600E+03    4
H2O               L 8/89H   2O   1   00   00G   200.000  3500.000  1000.000    1
 3.03399249E+00 2.17691804E-03-1.64072518E-07-9.70419870E-11 1.68200992E-14    2
-3.00042971E+04 4.96677010E+00 4.19864056E+00-2.03643410E-03 6.52040211E-06    3
-5.48797062E-09 1.77197817E-12-3.02937267E+04-8.49032208E-01 9.90409200E+03    4
HO2               L 5/89H   1O   2   00   00G   200.000  3500.000  1000.000    1
 4.01721090E+00 2.23982013E-03-6.33658150E-07 1.14246370E-10-1.07908535E-14    2
 1.11856713E+02 3.78510215E+00 4.30179801E+00-4.74912051E-03 2.11582891E-05    3
-2.42763894E-08 9.29225124E-12 2.94808040E+02 3.71666245E+00 1.00021620E+04    4
H2O2              L 7/88H   2O   2   00   00G   200.000  3500.000  1000.000    1
 4.16500285E+00 4.90831694E-03-1.90139225E-06 3.71185986E-10-2.87908305E-14    2
-1.78617877E+04 2.91615662E+00 4.27611269E+00-5.42822417E-04 1.67335701E-05    3
-2.15770813E-08 8.62454363E-12-1.77025821E+04 3.43505074E+00 1.11588350E+04    4
C                 L11/88C   1   00   00   00G   200.000  3500.000  1000.000    1
 2.49266888E+00 4.79889284E-05-7.24335020E-08 3.74291029E-11-4.87277893E-15    2
 8.54512953E+04 4.80150373E+00 2.55423955E+00-3.21537724E-04 7.33792245E-07    3
-7.32234889E-10 2.66521446E-13 8.54438832E+04 4.53130848E+00 6.53589500E+03    4
CH                TPIS79C   1H   1   00   00G   200.000  3500.000  1000.000    1
 2.87846473E+00 9.70913681E-04 1.44445655E-07-1.30687849E-10 1.76079383E-14    2
 7.10124364E+04 5.48497999E+00 3.48981665E+00 3.23835541E-04-1.68899065E-06    3
 3.16217327E-09-1.40609067E-12 7.07972934E+04 2.08401108E+00 8.62500000E+03    4
CH2               L S/93C   1H   2   00   00G   200.000  3500.000  1000.000    1
 2.87410113E+00 3.65639292E-03-1.40894597E-06 2.60179549E-10-1.87727567E-14    2
 4.62636040E+04 6.17119324E+00 3.76267867E+00 9.68872143E-04 2.79489841E-06    3
-3.85091153E-09 1.68741719E-12 4.60040401E+04 1.56253185E+00 1.00274170E+04    4
CH2*              L S/93C   1H   2   00   00G   200.000  3500.000  1000.000    1
 2.29203842E+00 4.65588637E-03-2.01191947E-06 4.17906000E-10-3.39716365E-14    2
 5.09259997E+04 8.62650169E+00 4.19860411E+00-2.36661419E-03 8.23296220E-06    3
-6.68815981E-09 1.94314737E-12 5.04968163E+04-7.69118967E-01 9.93967200E+03    4
CH3               L11/89C   1H   3   00   00G   200.000  3500.000  1000.000    1
 2.28571772E+00 7.23990037E-03-2.98714348E-06 5.95684644E-10-4.67154394E-14    2
 1.67755843E+04 8.48007179E+00 3.67359040E+00 2.01095175E-03 5.73021856E-06    3
-6.87117425E-09 2.54385734E-12 1.64449988E+04 1.60456433E+00 1.03663400E+04    4
CH4               L 8/88C   1H   4   00   00G   200.000  3500.000  1000.000    1
 7.48514950E-02 1.33909467E-02-5.73285809E-06 1.22292535E-09-1.01815230E-13    2
-9.46834459E+03 1.84373180E+01 5.14987613E+00-1.36709788E-02 4.91800599E-05    3
-4.84743026E-08 1.66693956E-11-1.02466476E+04-4.64130376E+00 1.00161980E+04    4
```

```
CO                TPIS79C   1O   1   00   00G   200.000  3500.000  1000.000    1
 2.71518561E+00 2.06252743E-03-9.98825771E-07 2.30053008E-10-2.03647716E-14    2
-1.41518724E+04 7.81868772E+00 3.57953347E+00-6.10353680E-04 1.01681433E-06    3
 9.07005884E-10-9.04424499E-13-1.43440860E+04 3.50840928E+00 8.67100000E+03    4
CO2               L 7/88C   1O   2   00   00G   200.000  3500.000  1000.000    1
 3.85746029E+00 4.41437026E-03-2.21481404E-06 5.23490188E-10-4.72084164E-14    2
-4.87591660E+04 2.27163806E+00 2.35677352E+00 8.98459677E-03-7.12356269E-06    3
 2.45919022E-09-1.43699548E-13-4.83719697E+04 9.90105222E+00 9.36546900E+03    4
HCO               L12/89H   1C   1O   1   00G   200.000  3500.000  1000.000    1
 2.77217438E+00 4.95695526E-03-2.48445613E-06 5.89161778E-10-5.33508711E-14    2
 4.01191815E+03 9.79834492E+00 4.22118584E+00-3.24392532E-03 1.37799446E-05    3
-1.33144093E-08 4.33768865E-12 3.83956496E+03 3.39437243E+00 9.98945000E+03    4
CH2O              L 8/88H   2C   1O   1   00G   200.000  3500.000  1000.000    1
 1.76069008E+00 9.20000082E-03-4.42258813E-06 1.00641212E-09-8.83855640E-14    2
-1.39958323E+04 1.36563230E+01 4.79372315E+00-9.90833369E-03 3.73220008E-05    3
-3.79285261E-08 1.31772652E-11-1.43089567E+04 6.02812900E-01 1.00197170E+04    4
CH2OH             GUNL93C   1H   3O   1   00G   200.000  3500.000 1000.0      1
 3.69266569E+00 8.64576797E-03-3.75101120E-06 7.87234636E-10-6.48554201E-14    2
-3.24250627E+03 5.81043215E+00 3.86388918E+00 5.59672304E-03 5.93271791E-06    3
-1.04532012E-08 4.36967278E-12-3.19391367E+03 5.47302243E+00 1.18339080E+04    4
CH3O              121686C   1H   3O   1    G  0300.00   3000.00  1000.00     1
 0.03770799E+02 0.07871497E-01-0.02656384E-04 0.03944431E-08-0.02112616E-12    2
 0.12783252E+03 0.02929575E+02 0.02106204E+02 0.07216595E-01 0.05338472E-04    3
-0.07377636E-07 0.02075610E-10 0.09786011E+04 0.13152177E+02                  4
CH3OH             L 8/88C   1H   4O   1   00G   200.000  3500.000  1000.000    1
 1.78970791E+00 1.40938292E-02-6.36500835E-06 1.38171085E-09-1.17060220E-13    2
-2.53748747E+04 1.45023623E+01 5.71539582E+00-1.52309129E-02 6.52441155E-05    3
-7.10806889E-08 2.61352698E-11-2.56427656E+04-1.50409823E+00 1.14352770E+04    4
C2H               L 1/91C   2H   1   00   00G   200.000  3500.000  1000.000    1
 3.16780652E+00 4.75221902E-03-1.83787077E-06 3.04190252E-10-1.77232770E-14    2
 6.71210650E+04 6.63589475E+00 2.88965733E+00 1.34099611E-02-2.84769501E-05    3
 2.94791045E-08-1.09331511E-11 6.68393932E+04 6.22296438E+00 1.04544720E+04    4
C2H2              L 1/91C   2H   2   00   00G   200.000  3500.000  1000.000    1
 4.14756964E+00 5.96166664E-03-2.37294852E-06 4.67412171E-10-3.61235213E-14    2
 2.59359992E+04-1.23028121E+00 8.08681094E-01 2.33615629E-02-3.55171815E-05    3
 2.80152437E-08-8.50072974E-12 2.64289807E+04 1.39397051E+01 1.00058390E+04    4
C2H3              L 2/92C   2H   3   00   00G   200.000  3500.000  1000.000    1
 3.01672400E+00 1.03302292E-02-4.68082349E-06 1.01763288E-09-8.62607041E-14    2
 3.46128739E+04 7.78732378E+00 3.21246645E+00 1.51479162E-03 2.59209412E-05    3
-3.57657847E-08 1.47150873E-11 3.48598468E+04 8.51054025E+00 1.05750490E+04    4
C2H4              L 1/91C   2H   4   00   00G   200.000  3500.000  1000.000    1
 2.03611116E+00 1.46454151E-02-6.71077915E-06 1.47222923E-09-1.25706061E-13    2
 4.93988614E+03 1.03053693E+01 3.95920148E+00-7.57052247E-03 5.70990292E-05    3
-6.91588753E-08 2.69884373E-11 5.08977593E+03 4.09733096E+00 1.05186890E+04    4
C2H5              L12/92C   2H   5   00   00G   200.000  3500.000  1000.000    1
 1.95465642E+00 1.73972722E-02-7.98206668E-06 1.75217689E-09-1.49641576E-13    2
 1.28575200E+04 1.34624343E+01 4.30646568E+00-4.18658892E-03 4.97142807E-05    3
-5.99126606E-08 2.30509004E-11 1.28416265E+04 4.70720924E+00 1.21852440E+04    4
C2H6              L 8/88C   2H   6   00   00G   200.000  3500.000  1000.000    1
 1.07188150E+00 2.16852677E-02-1.00256067E-05 2.21412001E-09-1.90002890E-13    2
-1.14263932E+04 1.51156107E+01 4.29142492E+00-5.50154270E-03 5.99438288E-05    3
-7.08466285E-08 2.68685771E-11-1.15222055E+04 2.66682316E+00 1.18915940E+04    4
CH2CO             L 5/90C   2H   2O   1   00G   200.000  3500.000  1000.000    1
 4.51129732E+00 9.00359745E-03-4.16939635E-06 9.23345882E-10-7.94838201E-14    2
-7.55105311E+03 6.32247205E-01 2.13583630E+00 1.81188721E-02-1.73947474E-05    3
 9.34397568E-09-2.01457615E-12-7.04291804E+03 1.22156480E+01 1.17977430E+04    4
```

```
HCCO             SRIC91H   1C   2O   1     G  0300.00   4000.00  1000.00      1
 0.56282058E+01 0.40853401E-02-0.15934547E-05 0.28626052E-09-0.19407832E-13    2
 0.19327215E+05-0.39302595E+01 0.22517214E+01 0.17655021E-01-0.23729101E-04    3
 0.17275759E-07-0.50664811E-11 0.20059449E+05 0.12490417E+02                   4
HCCOH             SRI91C   2O   1H   20   0G   300.000  5000.000   1000.G     1
 0.59238291E+01 0.67923600E-02-0.25658564E-05 0.44987841E-09-0.29940101E-13    2
 0.72646260E+04-0.76017742E+01 0.12423733E+01 0.31072201E-01-0.50866864E-04    3
 0.43137131E-07-0.14014594E-10 0.80316143E+04 0.13874319E+02                   4
N2               121286N   2              G  0300.00   5000.00  1000.00      1
 0.02926640E+02 0.14879768E-02-0.05684760E-05 0.10097038E-09-0.06753351E-13    2
-0.09227977E+04 0.05980528E+02 0.03298677E+02 0.14082404E-02-0.03963222E-04    3
 0.05641515E-07-0.02444854E-10-0.10208999E+04 0.03950372E+02                   4
END
```

A.3 REFERENCES

[1] W.C. Reynolds, "The Element Potential Method for Chemical Equilibrium Analysis: Implementation in the Interactive Program STANJAN," Department of Mechanical Engineering, Stanford University (1986).

[2] A. Burcat, "Thermochemical Data for Combustion Calculations," in W.C. Gardiner, ed., Combustion Chemistry, (New York: Springer-Verlag, 1984).

[3] R.J. Kee, F.M. Rupley, J.A. Miller, "The CHEMKIN Thermodynamic Data Base," Sandia National Laboratories Report SAND87-8215B (1990).

[4] M. Frenklach, H. Wang, C.T. Bowman, R.K. Hansen, G.P. Smith, D. Golden, W. Gardiner, V. Lissianski, "GRI-MECH," Gas Research Institute report, in press (1995).